กรมอุตุนิยมวิทยา

4353 ถนน สุขุมวิท กรุงเทพฯ 10260

METEOROLOGICAL DEPARTMENT

4353 Sukhumvit Road, Bangkok 10260, THAILAND

เอกสารวิชาการ

การวิเคราะห์ระบบตรวจวัดแผ่นดินไหวของกรมอุตุนิยมวิทยา เดือน มกราคม - มิถุนายน 2565

นายสัณฑวัฒน์ สุขรังษี

Analysis of TMD seismic network during January - June 2022

Santawat Sukrungsri

เอกสารวิชาการเลขที่ ๕๕๐.๓๔-๑๐-๒๕๖๕

Technical Document No. 550.34-10-2022

การวิเคราะห์ระบบตรวจวัดแผ่นดินไหวของกรมอุตุนิยมวิทยา เดือน มกราคม - มิถุนายน 2565

Analysis of TMD seismic network during January - June 2022

นายสัณฑวัฒน์ สุขรังษี

ส่วนวิเคราะห์และพัฒนาระบบตรวจวัดแผ่นดินไหว

กองเฝ้าระวังแผ่นดินไหว

Santawat Sukrungsri

Earthquake Monitoring System Analysis and Development Sub-division

Earthquake Observation Division

เดือน กันยายน 2565

September 2022

ABSTRACT

This study aimed to analyze the seismic network of Thai Meteorological Department (TMD) for detecting and recording earthquake events in Thailand and adjacent areas during January - June 2022. The both of seismicity and waveform data (velocity and acceleration) recorded by TMD stations were utilized to carefully investigate capability of seismic network, i.e., accuracy, precision, limitation, and application of seismic network including background noise around the seismic stations by using the statistical approaches. The obtained results indicated i) the most accuracy of TMD seismic network for locating seismic events in Thailand was approximately 3.1 km from the seismic source, ii) the highest precision covered zone of the northern and western parts of Thailand with the comparatively least RMS residual of 0.4 seconds and the best azimuthal gap was less than 100 degrees covering in the northern part, particularly in Chiang Rai and Lampang provinces, iii) earthquakes with magnitudes below 2.8 cannot be detected and recorded completely in Thailand, iv) the most of seismic stations of TMD were not affected significantly from ambient noise that noise levels were within the boundary of the global noise model, v) the application of TMD seismic network for determining the earthquake parameters of M3.6 Uttaradit indicated that the epicenter was surrounded by seismic stations of TMD resulting the focal mechanism can be calculated effectively and the interpretation was reasonable. However, this event was located away from the accelerograph stations of TMD causing the ground shaking data were not detected and recorded within the epicentral distance of 40 km. According to the results obtained in this study, the significant earthquakes with M>4.0 were still detected and recorded effectively by the seismic network of TMD during January - June 2022 for monitoring earthquake hazard in Thailand.

ACKNOWLEDGEMENTS

I appreciate Thai Meteorological Department (TMD) for supporting seismic data used in this study. Great acknowledgement goes to staff of the Earthquake Observation Division of TMD for recording the earthquake events continuously. I am grateful to International Institute of Seismology and Earthquake Engineering, Building Research Institute (BRI) in Japan for the excellent training course that was applied theoretically in this study.

CONTENTS

LIST OF TABLES

page

LIST OF FIGURES

Page

Page

Page

Page

Page

Page

Page

CHAPTER I
INTRODUCTION

1.1 TMD seismic network

Historically, the seismic network of Thailand has been continuously developed over the last five decades. In 1963, the first analogue station of Thailand (CHG) was established at Chiang Mai province, northern Thailand encouraged by the US Geological Survey (USGS) as World-Wide Standardized Seismograph Network (WWSSN) for principally monitoring the seismic waves associated with nuclear test in Asia. At present, it has been upgraded and operated as part of a Global Seismic Network (GSN) known as CHTO. In 1965, one additional station was built at Songkla province by USGS (purposed as mentioned above). Then, during 1975 - 1997, Thai Meteorological Department (TMD) expanded a seismic network of Thailand by installation of 14 analogue stations with short-period seismometers in order to detect local earthquake within Thailand and adjacent areas. Later, a period from 1998 - 2008, the 5 Digital seismic stations (2 short-period and 3 broadband seismometers) were provided by TMD for real-time monitoring both local and distant earthquakes. After devastation of M9.0 Sumatra-Andaman earthquake on December 26, 2004, TMD seismic network was further strengthened and rapidly expanded covering the whole of Thailand while analogue system was gradually changed to digital system. Such network has the 8 short-period (Trillium-40) and 7 broadband (Trillium-120) seismometers that each station equipped with the accelerometer (TSA-100) and digitizer (Taurus), including 6 strong motion accelerometers of Nanometrics company, were installed from 2005 to 2006. Subsequently, TMD seismic network (2006-2009) was developed by increasing 15 short-period (S-13), 10 broadband (KS-2000), 1 borehole broadband (KS-2000) seismometers (these stations coupled with the accelerometers, PA-23), and 1 borehole accelerometer (PA-23) including 20 strong motion accelerometers (Smart-24) that connected to the digitizers (Smart-24) of Geotech company. After installation and improving (1963-2009), TMD network consists of 40 stations (23 short-period and 17 broadband seismometers, these stations together with accelerometers), and 2 borehole stations (1 broadband seismometer and 1 accelerometer) including the 26 strong motion accelerograph stations (Table 1.1).

Table 1.1. Installations of TMD seismic stations during 1963-2009.

Year	Instrument	Company	Model
1963	1 analog station [at Chiang Mai]	-	-
1965	1 analog station [at Songkhla]	-	-
1975-1997	14 analog stations	-	-
1998-2008	5 digital stations		
	- 2 short period seismometers	- Mark Product/ Terra Tech.	- L4C3D/ SSA-320
	- 3 broadband seismometers	- Guralp/ Terra Technology	- CMG-40/ SSA-320
2005-2006	21 digital stations		
	- 8 short period seismometers	- Nanometrics/ Metrozet	- Trillium-40/ TSA-100
	- 7 broadband seismometers	- Nanometrics/ Metrozet	- Trillum-120/ TSA-100
	- 6 accelerometers	- Metrozet	- TSA-100
	- Digitizers	- Nanometrics	- Taurus
2006-2009	47 digital stations		
	- 15short period seismometers	- Geotech	- S-13/ PA-23
	- 10 broadband seismometers	- Geotech	- KS-2000/ PA-23
	- 1 borehole seismometer	- Geotech	- KS-2000
	- 1 borehole accelerometer	- Geotech	- PA-23
	- 20 accelerometers	- Geotech	- PA-23
	- Digitizers	- Geotech	- Smart-24

In order to develop the capability of the local earthquake detection, ground shaking monitoring, and Tsunami watch that might impact along the western coast of Thailand, TMD installed spatially dense stations in the vicinity of the seismogenic fault zones across Thailand under Project of High Performance Seismic Network for Earthquake and Tsunami Observation System during 2017 - 2018. Additional stations consist of 15 short-period (CMG-3T-1) and 10 broadband (CMG-3T-120) borehole seismometers equipped with accelerometers (CMG-5T), 5 broadband surface seismometers (CMG-3T-120) linked to the digitizer (Affinity), including 30 accelerometers (CMG-5T/ CMG-5TCDE) with digitizers (Affinity/ CD24) of Guralp systems. Moreover, the 6 existing stations were also upgraded, i.e. 2 short-period (CMG-3ESP-1) and 4 broadband seismometers (CMG-3T-120) with digitizers (Affinity) as illustrated in Table 1.2.

Table 1.2. Improvement of TMD Seismic network during 2017-2018.

Instrument	Company	Model	Digitizer
25 borehole stations			
- 15 short period seismometers	- Guralp	- CMG-3T-1/ CMG-5T	- Affinity
- 10 broadband seismometers	- Guralp	- CMG-3T-120/ CMG-5T	- Affinity
35 surface stations			
- 5 broadband seismometers	- Guralp	- CMG-3T-120	- Affinity
- 30 accelerometers	- Guralp	- CMG-5T/ CMG-5TCDE	- Affinity/CD24
6 upgraded existing stations			
- 2 short period seismometers	- Guralp	- CMG-3ESP-1	- Affinity
- 4 broadband seismometers	- Guralp	- CMG-3T-120	- Affinity

Most of seismic stations of TMD have both the triaxial seismometer and accelerometer, which enable to record unclipped waveforms in case of the strong earthquake nearby whereas the strong motion accelerograph stations located closer to urban areas for engineering ground-motion observation. All of seismic stations have the permanent housing, where the posthole seismometers are placed at the bottom of concreate vaults around 1-3 meters below ground surface separated from recording rooms (Fig.1.1a), while borehole seismometers are about 30-meters depth and located on hard soil (Fig.1.1b). In contrast, the surface accelerometers are positioned on a concrete base approximately 0.5 meters above ground surface as shown in Fig.1.1c. Seismic systems of TMD are mainly composed of seismometer, accelerometer, digitizer, GPS receiver, surge protector, as well as battery (Fig. 1.2), which the strong-motion sensors (accelerometers) with 4 g full-scale sensitivity were installed at the seismic site where seismometer records may be clipped from a strong earthquake in the region. They measure seismic signals between DC and 200 Hz. Whereas, TMD short-period seismometers measure the signals from approximately 0.1 to 100 Hz, with a corner frequency at 1 Hz. They have the flat response to ground velocity for frequencies greater than this corner frequency while TMD broadband sensors (Guralp CMG-3T seismometer) have a frequency range from 0.03 to 50 Hz. Utilizing TMD seismic network, seismic waves are detected by sensor of seismometer or

accelerometer, the observed signals are then converted to a sequence of corresponding digital signals with a 100 samples-per-second (sps) basis by using digitizer and are stored in data logger at the site. These data are called SCREAM, which are in format of GCF (Guralp Compressed Format), are transmitted continuously in real-time with SeedLink protocol to TMD operation center (converted to Mini-SEED) via the internet communication. TMD systems store continuous seismic signals on average 3 Mb of data per day generated at each remote site.

Fig. 1.1. TMD sites showing a) surface seismometer station, b) borehole seismometer station, and c) strong motion accelerometer station situated within Thailand.

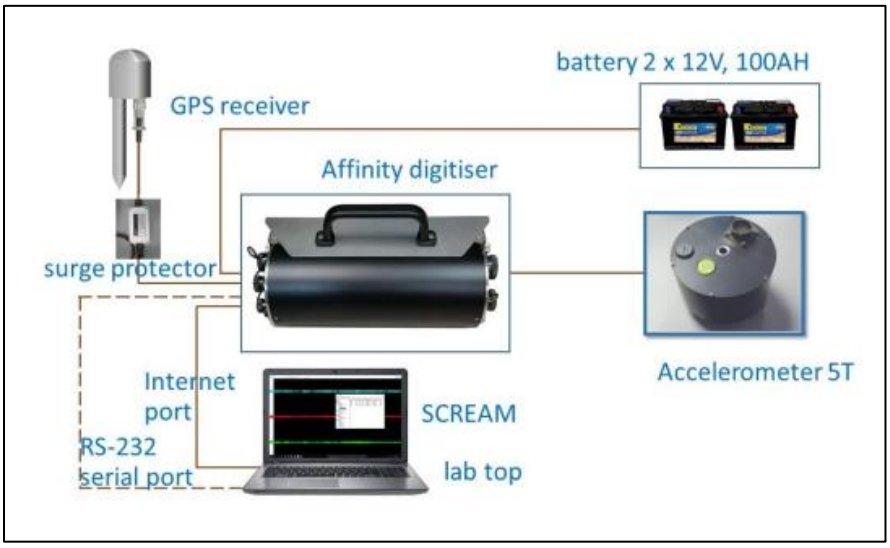

Fig. 1.2. TMD system showing instruments for detecting and recording seismic events.

During the last 10 years, the seismic network of TMD have been improved and altered significantly that 26 borehole seismic stations (15 short-period, 11 broadband seismometers), 45 surface seismic stations (21 short-period and 24 broadband seismometers), 1 borehole accelerograph station (TMDA), including 56 accelerograph stations are currently in operation throughout Thailand that the details are demonstrated in Table 1.3 and Fig. 1.3., respectively.

Table 1.3. TMD seismic stations are presently operated within Thailand.

Station	Instrument	Number of Station
Surface seismic stations	Seismometer/ Acc.	40
Borehole seismic stations	Seismometer/ Acc.	25
Surface seismic stations	Seismometer	5
Borehole seismic station [TMDB]	Seismometer	1
Strong motion accelerograph stations	Accelerometer	56
Borehole accelerograph station [TMDA]	Accelerometer	1
	Total	**128**

According to the communication of TMD seismic network, during 2005 - 2006, the observed seismic data transferred to TMD operation center via IPSTAR and ADSL. The NAQS Server (Nanometrics Acquisition System) was then applied for the data processing and the acquisition which earthquakes were calculated automatically and manually by EARLYBIRD and ATLAS software, respectively. Later, the Smart server (Geotechs) was deployed together with NAQS Server proposed previously whereas locations and magnitudes of the earthquakes (2006 - 2009) were calculated automatically and manually by SMARTQUAKE and SEISPLUS software, respectively. Presently (2019), SeiscomP3 software (Weber et al., 2007) developed by gempa GMbH (Potsdam, Germany) has been utilized for both the automatic and manual earthquake location with SeedLink as main protocol for real-time data acquisition connected by internet communication. The ratio of short-time average to long-time average (STA/LTA) of seismic signal (Trnkoczy et al., 2002) with adjustable band-pass filter is deployed for weak-motion triggering in TMD seismic network, which the short-time window (STA) is sensitive to seismic events, while the long-time window (LTA) provides the information about the temporal

amplitude variation of seismic noise at the site. When this ratio exceeds a preset value (usually set between 4 and 8), an event is alarmed. However, the STA/LTA algorithm is less effective in situations where man-made seismic noise is present. This is particularly important with BB seismometers where the small earthquake signals are often buried in dominant 0.2-0.3 Hz seismic noise. When at least five TMD seismic stations detect an event, a triggering system with STA/LTA algorithm is activated and calculate automatically the earthquake location and magnitude. Regarding the present-day TMD seismic network, the station spacing varies from 35 to 125 km, with closer spacing in area. The spatial distribution of the stations in a seismic network is very important for the network's capabilities of event determination. The geometry of the network will determine the accuracy of location in different directions, and a reasonably regular grid will give most uniform location accuracy. Furthermore, focal depths are generally more accurate for earthquakes within the seismic network where distance from the epicenter to the closest station is less than calculated focal depth. The seismic stations of TMD network are located on varied geological formations including sandstone, basalt, shale, limestone, and hard soil. All the stations are 5 to 15 km from main cities. The rocks in northern part are more compact in comparison to western part, which is a sedimentary basin with soft rocks. Also, the stations on hard soil show relatively high noise levels at higher frequencies (above 1.0 Hz). This may due to the fact that predominant frequencies at these stations are between 2 and 4 Hz which the long-period ambient noise levels were less than the short-period noise levels. These stations are good for recording teleseismic earthquakes as compared to local earthquakes. In case of the earthquake events outside the TMD seismic network, expect large errors in determining earthquake epicenters. Generally, do not expect reliable determination of the events, unless the azimuthal gap (the largest of all angles among the lines connecting a potential epicenter with all the stations in the network that recorded the event) is less than 180 degrees. Therefore, to increase the accuracy of epicenter determinations, especially for the events outside the seismic network of TMD, one needs to include data in the analysis from seismic stations in neighboring countries, as well as from any other available national (DMR, EGAT) or international sources (USGS, GEOFON). Acquiring this wider database is necessary for determining reliable event locations on the border or outside the seismic network of TMD.

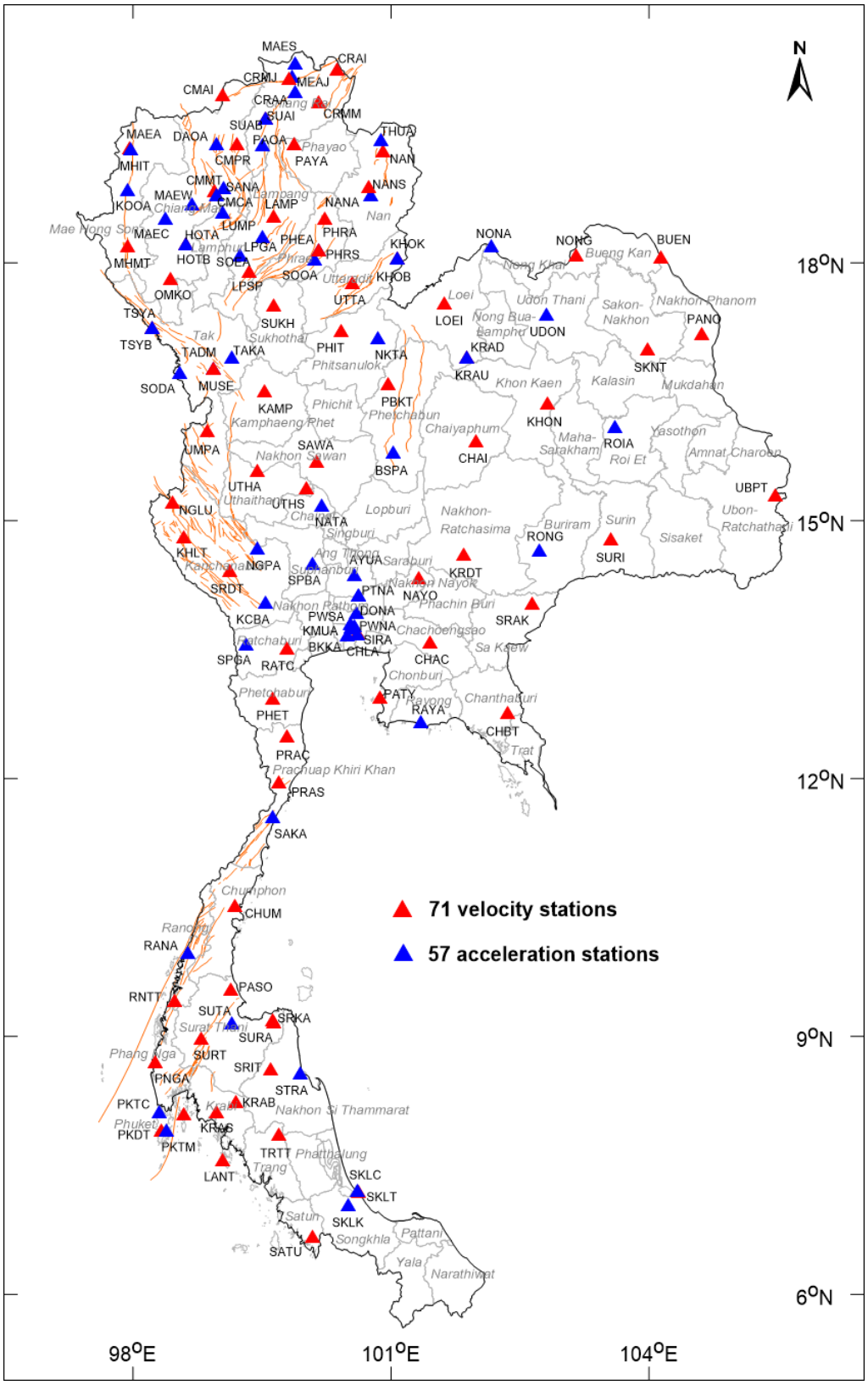

Fig. 1.3. Map showing the locations of seismic stations presently operated by TMD

1.2 Tectonic setting of South-East Asia

The present-day tectonic setting of SE Asia is dominated by interaction of three major lithospheric plates, i.e. (i) continental-oceanic Indo-Australian plate in the west and the south, (ii) the continental Eurasian plate in the middle, and (iii) the oceanic West Pacific plate in the east. The Indo-Australian and Eurasian boundary zone comprises the convergent margins, including the Burma oblique subduction zone, Andaman thrust and Sunda arc, to the north-west, west and south, respectively. Based on Charusiri et al. (2007), deformation rates across these plate boundaries are variable. The convergence rate of 65-70 mm/year as a result of Australia moving toward South East Asia (SEA). As India drove into the southern margin of Eurasia, The Indochina was rotated clockwise about 25° and extruded to the southeast by approximately 800 km along the Red river and Three Pagoda fault zones during the first 20-30 million years of the collision as demonstrated in Fig.1.4. The present tectonic stress regime in Thailand is one of transtension, with opening along north-south oriented basins and right-lateral and left-lateral slip on northwest- and northeast-striking faults, respectively. The Indian-Eurasian plate collision causes the high levels of seismic activity, not only along the Sumatra-Andaman Subduction Zone, but also as widespread the intraplate activity where the inland seismogenic faults are dominant. In addition, Indo-Australian plate was subducting obliquely beneath the Eurasian plate in the Andaman Sea, led to the movement along the large-scale strike-slip faults with the associated development of basins in northern Thailand. Thailand is part of the Eurasian plate whose boundary is presented by an active east-dipping subduction zone extending from north India, passing to west Myanmar and west of Andaman-Nicobar Island, and swinging eastward to southward along Sumatra-Java trench. So, the tectonics of Thailand related to the interactions among Indo-Australian, Eurasian, Philippine and Pacific plates combining with an opening of Andaman Sea. Thailand is surrounded by the convergent margins of Andaman subduction zone in the west, the Sunda and Java trenches in the south and Philippine trench in the east. Major changes in tectonics of Thailand may have occurred at the end of Mesozoic and are likely to have coincided with or be related to the north to north-eastward progressive collision of the Indian plate with the Eurasian plate. The occurrence of a major southeastward displacement of Indochina relative to South China along the Red River

fault zone by the Indian-Eurasian collision during Eocene possibly marks the major tectonic evolution of east and southeast Asia. A collision of the continental India with Asia could have caused the extrusion to southeast and the clockwise rotation of Indochina and Sunda shelf during Oligocene-Miocene. The phenomenon eventually accounted for sinistral displacement along the large-scale strike-slip faults in SE-Asia. Such displacement may have led to opening of South China, Gulf of Thailand, and Andaman seas and is thought still active. The collision of the Indian plate with southern Asia and the collision of the Indo-Burma block with Eastern Burma block, led to the movement along the large-scale strike-slip faults with the associated development of S-shaped basins in northern Thailand and Z-shaped basin in the Gulf.

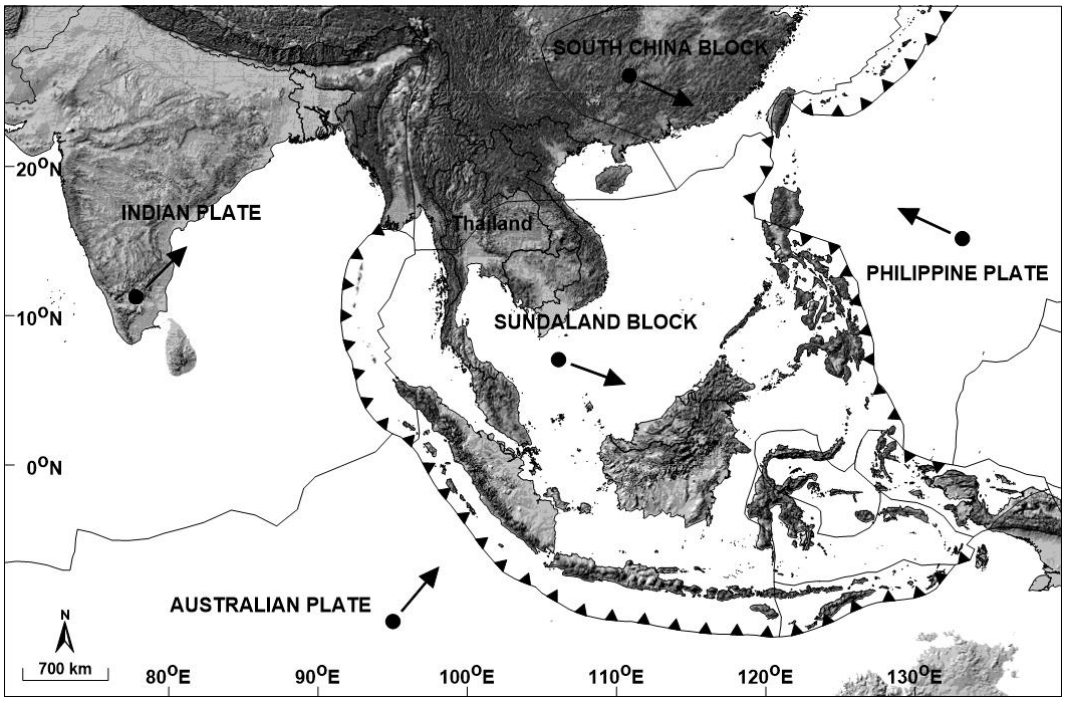

Fig. 1.4. Map showing relative movements (black arrows) of crustal block and tectonic plate in South-East Asia

The active plate margin of the Indian-Australian Plate is well defined along the north- and NE-dipping oceanic subduction zone and trench system that lies south and SW of Java and Sumatra. The trench continues northwards towards Burma, west of the Andaman and Nicobar Islands. Convergence across Sumatra-Java-Andaman Trench becomes increasingly more oblique to the north. Subduction beneath Andaman Island is ongoing with earthquake

recorded to depths of 150-200 km in a narrow east-dipping zone. Plate convergence rates between the Indian-Australian Plate oceanic crust and the Sunda Shelf are 5.7-3.8 cm/year. Convergence along this plate boundary has been responsible for a number of recent mega-earthquake approximately 1400 km of plate boundary ruptured from Sumatra north as far as Burmese coast. Tectonically, Thailand consists of two major intraplate regimes, namely Shan-Thai to the west, and the Indochina to the east, that were separated along the Nan-Uttaradit boundary. Effect of continental collision between the Shan-Thai, then as a part of the Eurasia, and the Western Burma tectonic plates, had greatly enhanced a complexity of the geological structures in this region with development of extensional Tertiary basins in northern Thailand. More than 70% of the basins in northern Thailand are related to strike-slip tectonics and their formation was initiated by a movement of NW-trending dextral faults and NE-trending sinistral faults associated with N-S compression and E-W extension as demonstrated in Fig.1.5.

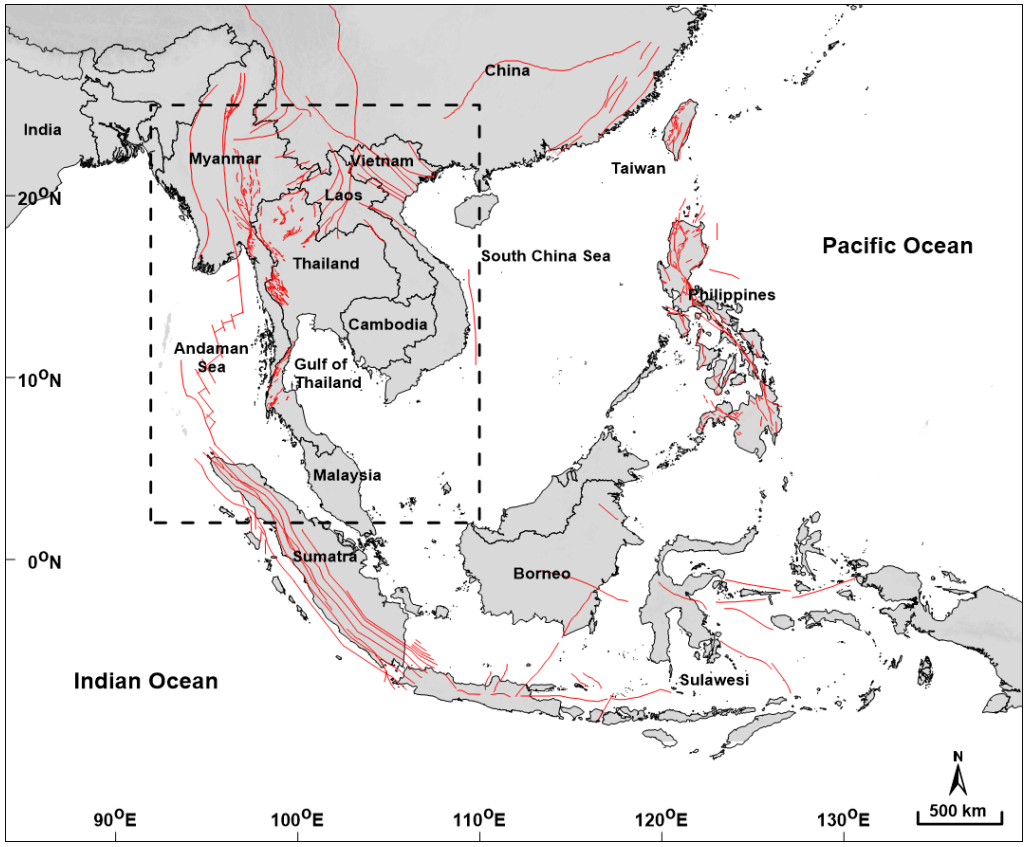

Fig. 1.5. Map showing the active faults (red lines) in South-East Asia and earthquake monitoring zone of TMD (dashed lines).

The tectonic activities as well as epicentral distribution define three distinct seismic source zones in Thailand, i.e. (1) the central-western Thailand dominated by the NW-trending Three-Pagoda, NNW-trending Sri Sawat, and NW-trending Mae Ping Faults, (2) the northern Thailand influenced by the N-trending Mae Hong Son, and NE-trending Mae Tha and Phrae Faults. At present, the most up-to-date active fault map in Thailand was proposed by the Department of Mineral Resources. The map was contributed by a knowledge integration of all updated relevant data. Furthermore, in many fault zones, the detailed paleo-seismological studies were partly clarified following empirical methodology (Pailoplee et al. 2009) Finally, DMR delineated the 16 seismogenic active fault zones of Thailand as demonstrated in Fig.1.6.

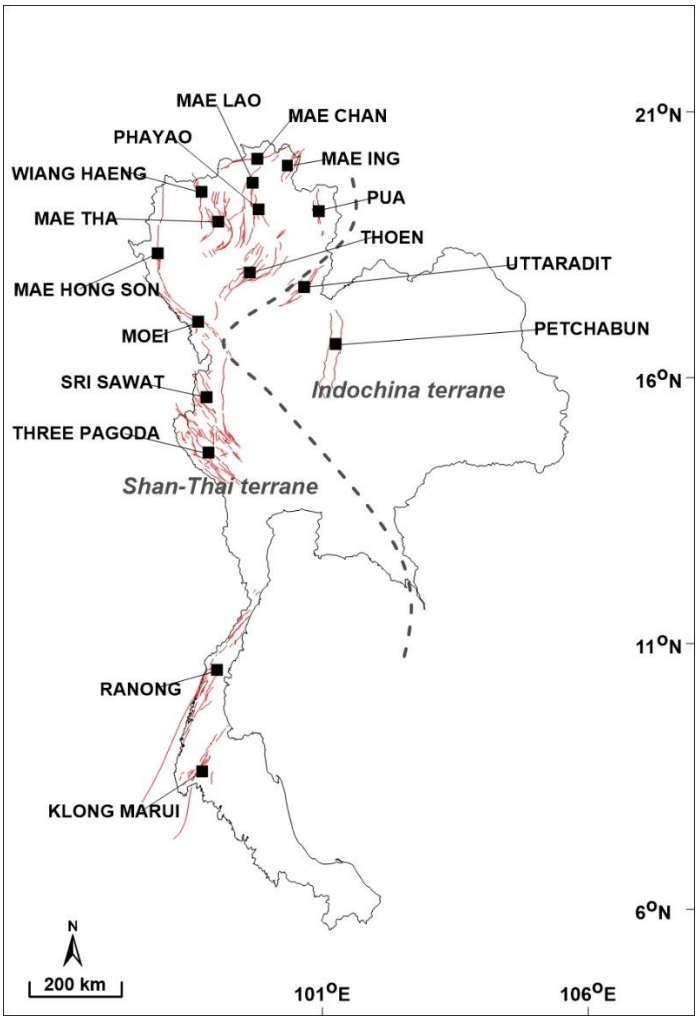

Fig. 1.6. Map showing the 16 active faults (red lines) and boundary of terrane (dashed line) in Thailand obtained from Department of Mineral Resources.

The high seismicity zones of Thailand are located in northern, western, and southern parts. Beside the active faults in Thailand, the active faults located outside Thailand are also recognized. According to Pailoplee et al (2009), the almost active fault zones were reported abundantly in central Myanmar, Laos-southern China border, northern Vietnam and Sumatra Island, Indonesia. Major active fault zone in Myanmar is the strike-slip Sagaing Fault Zone. This fault zone traverses central part of Myanmar from north to south. The Sagaing fault zone (SFZ), is one of the major continental fault zones in southeast Asia that strikes a N-S direction passing through the central part of Myanmar. This 1400-km long fault is active with a dextral slip rate of approximately 23mm/yr. In addition, for eastern Myanmar, three fault zones spread in northwest-southeast direction from Sagaing Fault Zone and extend to northern and western Thailand. In Laos-southern China border, there are a large number of faults and shear zones caused by the collision of Indian and Eurasian tectonic plates. Although People's Democratic Republic Laos (hereafter called Laos) is far away from the major tectonic plate boundary (the Sumatra-Andaman Subduction Zone), the tectonic stress caused by the present-day Indian-Eurasian plate collision influences areas within the plate. As a result, Laos and adjacent areas are dominated by the inland seismogenic fault zones, such as Dien Bien Phu, Mae Ing, Nam Ma. In northern Vietnam, the longest fault zone is the Red River Fault Zone. All of these fault zones have a NW–SE orientation and mainly follow the regional deformational structures. The present-day earthquake records in this area show that several moderate to large earthquakes are commonly associated with these seismogenic fault zones. Based mainly on paleoseismic investigation, the active faults in northern and western Thailand are characterized by the low slip rates, long recurrence intervals, and large magnitude paleoearthquake. The geomorphic indicators of active faulting of six major faults in Northern Thailand show the sense of the slip along these active faults as predominantly normal dip-slip. The western Thailand is dissected by number of northwest- and north-northwest-striking, right-lateral strike-slip faults related to the Sagaing Fault in Myanmar. Although showing much less activity than faults in neighboring Myanmar, these faults display abundant evidences for late Quaternary movement, including shutter ridges, sag ponds, and laterally offset streams. The three seismic-source zone can be differentiated on the basis of distinct patterns of the faults. These faults are considered to

be active. In western Thailand, there are the two large-scale strike-slip faults that probably control this seismic source zone, namely NW-trending Three-pagoda Fault and NNW-trending Si Sawat Fault. For tectonic setting in southern Thailand, the Ranong-Klong Marui Fault Zone illustrates obviously tectonic geomorphology (according to the remote sensing interpretation) indicating seismogenic faults such as the series of fault scarps, triangular facets, shutter ridges, including the offset streams. The Ranong fault extends from Gulf of Thailand toward Andaman Sea, strikes NE-SW direction along the southern peninsular of Thailand whereas the Klong Marui fault is more southern and parallel to the Ranong fault in the NE-SW direction.

1.3 Seismicity in Thailand and adjacent areas

Thailand is located within the area of low seismicity as it's not along the plate boundary. There were small to strong earthquakes that mainly occurred in northern and western parts of Thailand (Table 1.4 and Fig. 1.7). However, there are several seismic source zones surrounding Thailand that are able to generate large earthquakes such as Myanmar, Laos, and Sumatra Andaman Subduction Zone (SASZ). In 2014, there was strong earthquake of M6.3 occurred in Chiang Rai province. It's the largest earthquake in Thailand. This earthquake was generated by left-lateral strike-slip faulting of Mae-Lao fault. The earthquake ground shaking affected at least 7 provinces in the northern part of Thailand, at least 9000 building were damaged and followed by more than 1000 aftershocks.

Table 1.4. List of historical earthquakes with magnitudes ≥ 4.9 located within Thailand.

Mag (ML)	Date	Region	Active Fault
6.3	07 May 2014	Mae Lao, Chiang Rai	Mae-Lao Fault
5.9	22 Apr 1983	Sri Sawat, Kanchanaburi	Sri-Sawat Fault
5.6	17 Feb 1975	Thai- Myanmar (Tak)	Moei Fault
5.2	21 Dec 1995	Phrao, Chiang Mai	Mae-Tha Fault
5.1	11 Sep 1994	Mae Suai, Chiang Rai	Phayao Fault
5.1	09 Dec 1995	Rong Kwang, Phrae	Thoen Fault
5.1	13 Dec 2006	Mae Lim, Chiang Mai	Mae-Tha Fault
4.9	30 Dec 2018	Sri Sawat, Kanchanaburi	Sri-Sawat Fault
4.9	20 Feb 2019	Wang Nua, Lampang	Phayao Fault

In 1983, there was moderate earthquake of M5.9 occurred in Kanchanaburi province near the large dam. This event was regarded as the man-made activity because of it occurred after the large dam was built with the water level above 100 meters that may activate the fault nearby resulting the earthquake occurred. In 1975, the M5.6 earthquake occurred in Thailand-Myanmar border near the Tak province. It was generated by strike-slip faulting of Moei fault. The location of this event is not clear because of the limitation of instruments for detecting earthquake in the past. This earthquake is far away from Bangkok, the capital city of Thailand approximately 500 kilometers that long period ground motion affected particularly in Bangkok with the vibration of tall building resulting many people can be felt the ground shaking and were panic about the earthquake effect.

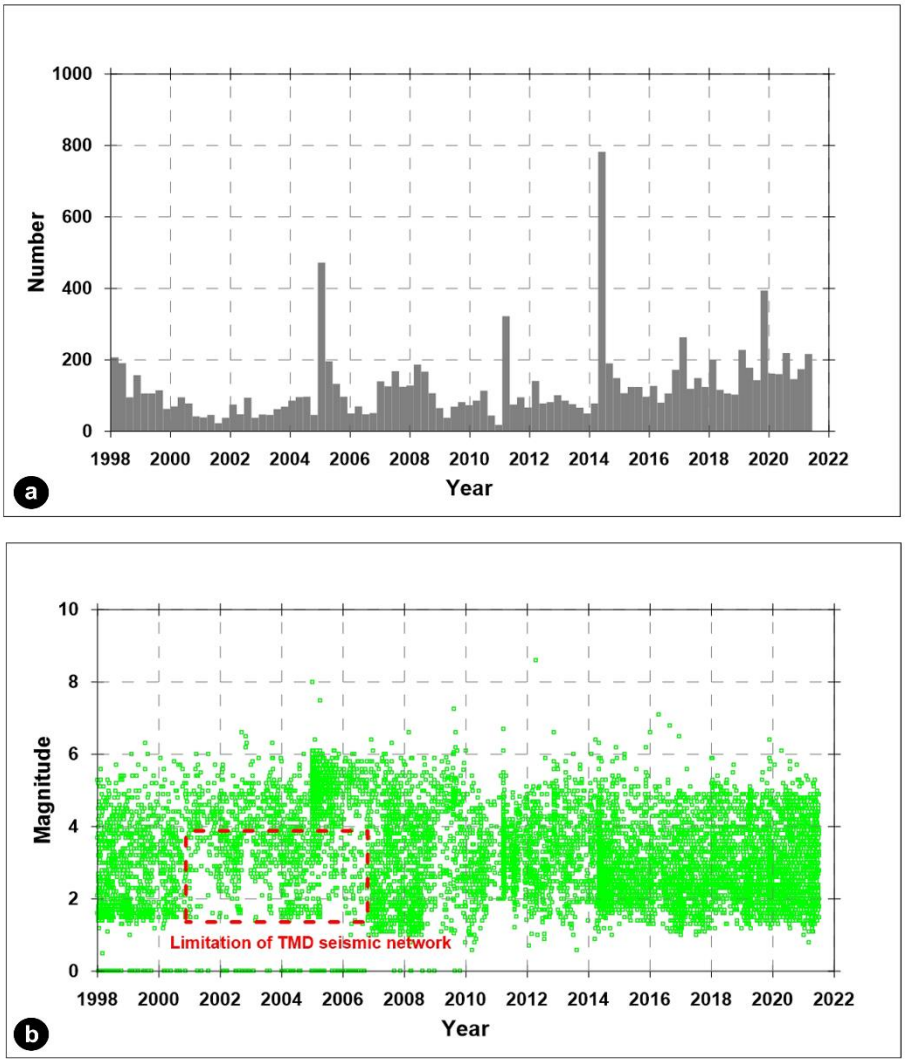

Fig. 1.7. Graphs showing a) the number of earthquakes and b) earthquake magnitudes over time during 1998-2021 recorded by TMD seismic network.

In addition, there were moderate earthquakes occurred in Phrae, Chiang Mai, and Chiang Rai during 1994-1995 that slightly damaged around the earthquake source. In the last few years, M4.9 earthquake occurred in Kanchanaburi province in 2018. It was generated by Si-Sawat fault that the ground shaking can be widely felt around the earthquake source with there was no damage. Then, in 2019, earthquake of M4.9 occurred in Lampang province generated by strike-slip faulting of Payao fault. It caused the ground shaking can be felt in several areas and followed by a lot of small aftershocks. Although most of earthquakes in Thailand have small magnitudes and did not damage significantly the buildings, many people can be felt the ground shaking and were panic about the earthquake effects. Moreover, during 5 years ago, there were at least 9 small earthquakes with magnitude less than 4.0 occurred in Thailand. In 2015, M4.8 and M4.5 earthquakes occurred in Kanchanaburi province generated by Three-pagoda fault. They were located away from the community. So, the ground shaking was weak and did not damage building. In 2017, there were 5 small earthquakes of M4.0-4.2 occurred in the northern part of Thailand, i.e. Chiang Rai, Chiang Mai, Nan, and Tak provinces. Most of these earth quakes can be felt the ground shaking but there were no damages. In 2019, earthquake of M4.0 occurred in Loei province that can be felt the ground shaking around the earthquake source. at present, there is no active fault that was published in this area.

According to the earthquakes outside Thailand during the last century, there were at least 54 large earthquakes of M7.0-9.1 occurred in SASZ including M9.1 earthquake in 2004 that was regarded as the third largest earthquake in the world. First and second largest earthquakes are M9.6 in Chile and M9.4 in Alaska, respectively. The 2004 M9.1 Sumatra earthquake occurred from the collision of Indo-Australian and Eurasian plates that generated large tsunami striking the western coast of Thailand. This event damaged a large number of buildings along the coast especially the areas surrounding Indian Ocean and caused approximately 230,000 casualties. Then, in 2005, the M8.6 earthquake was generated off west coast of northern Sumatra, Indonesia along the SAAZ that produced tsunami and at least 915 people were killed in this event. The ground shaking from this event can be felt in the distant areas up to 1000 kilometers from the epicenter including Bangkok, the capital city of Thailand. In 2007, there were 3 large earthquakes occurred at Sunda trench, off coast of southern Sumatra that M8.4 occurred before and followed by M7.9 and M7.0 within the same day and next day, respectively. This large earthquake sequence was located in the sea leading to the tsunami warning was alerted about 4 times within 24 hours. surrounding the earthquake source that the tsunami with 1 meter-heigh was found in this event. The details as shown in Table 1.5.

Table 1.5. List of large earthquakes ($M \geq 7.0$) within the earthquake monitoring zone of TMD during 2000-2021 obtained from USGS earthquake catalogue.

Mag (USGS)	Date	Depth (km)	Region
9.1	26-12-2004	30	Sumatra-Andaman Islands
8.6	11-04-2012	20	Off the west coast of northern Sumatra
8.6	28-03-2005	30	Northern Sumatra, Indonesia
7.8	06-04-2010	31	Northern Sumatra, Indonesia
7.5	10-08-2009	24	Andaman Island, India
7.4	20-02-2008	26	Simeulue, Indonesia
7.4	02-11-2002	30	Simeulue, Indonesia
7.2	10-01-2012	19	Off the west coast of northern Sumatra
7.2	09-05-2010	38	Northern Sumatra, Indonesia
7.2	24-07-2005	16	Nicobar Island, India
7.2	26-12-2004	39	Nicobar Island, India

In 2012, there were 2 great earthquakes occurred within a day that a M8.6 was generated off west coast of Sumatra and followed by M8.2 aftershock. There was tsunami warning and was canceled in the next time. Although these events occurred in the sea, they were located within the plate as the intraplate earthquake with strike-slip faulting. There was no vertical movement obviously. So, Tsunami cannot be generated in these events. However, the strong ground shaking can be felt in several areas including Thailand. Based on research papers, these events were referred as the subsequent earthquakes of M9.1 Sumatra earthquake in 2004. After that during 2013 to present, there were no large earthquake was found in SASZ. Not only SASZ that is the significant earthquake source affecting Thailand but also there is the Sagaing fault in Myanmar that is able to generate large earthquake and affect Thailand. This fault is very long and has mainly right-lateral strike-slip faulting. During 1429-1991, there were at least 70 large earthquakes occurred along the Sagaing fault and approximately 20 events that can be identified location, time, and magnitude clearly. Most of these events were located at south of Sagaing fault close to the Thailand-Myanmar border that the ground shaking can be felt in Northern Thailand. Based on historical earthquake record, the largest earthquake generated by Sagaing fault was M8.0 earthquake at Mandalay city in 1912. Moreover, there were also other active faults in Myanmar that generated large earthquake in the past. For example, at least 11

large earthquakes that occurred in Myanmar during 1908-1991. However, within the latest 30 years, there were no large earthquake located at Sagaing fault and in Myanmar. Based on the earthquake catalog of TMD covering 2-25N and 92-110E, the earthquakes were recorded continuously since 1998 that the amount of the earthquakes recorded before 2004, were small especially earthquake with magnitude less than 4.0 as the limitation of instruments in the past. After M9.1 Sumatra earthquake in 2004 that followed by a large number of aftershocks, the earthquake events were increased obviously during 2005-2006. Then in 2014, there was strong earthquake of M6.3 occurred in Chiang Rai province in northern Thailand. This event generated more than 1000 aftershocks in the region as well as the development of seismic network in Thailand resulting the recorded earthquakes were increased significantly in 2014. For earthquake events increased in 2011 and 2019, most of these events were aftershocks of M6.7 Myanmar in 2011 and M6.4 Laos in 2019, respectively. At present, the earthquakes detected and recorded by seismic network of TMD, are collected in the pattern of seismicity data in earthquake catalogue of TMD during 1998 to 2021 covering the area of latitude 2-25N and longitude 92-110E and the pattern of waveform data in both local and distant earthquakes during 2007 to 2021.

With respect to the distribution of earthquake data obtained from the earthquake catalogue of TMD, most of these data were located within the plate that called intraplate earthquake covering the major areas of northern Thailand and Myanmar including some areas in Laos, Vietnam and southern China. In Thailand, the earthquakes were located mainly in the northern and western parts along the active faults while the southern part has a small number of earthquake events. This was due to there are 12 active faults located in the northern part whereas there are only 2 active faults located in western and southern parts of Thailand. Moreover, moderate to strong earthquakes mainly occurred in the northern part that they generated a large number of aftershock events resulting high seismicity in the northern part as shown in Fig. 1.8. For the earthquake distribution along the SASZ, the number of earthquake events are small and their epicenters are far away from each other. This was due to locations of these earthquakes were far away from the seismic network of TMD resulting they cannot be detected and recorded completely. Therefore, the earthquake data in this area cannot actually represent the tectonic activity in the SASZ. However, the significant earthquakes with magnitudes of larger than 5 located along the SASZ, can be detected effectively by the seismic network of TMD that encourage for monitoring and warning tsunami generated from the large earthquake in SASZ.

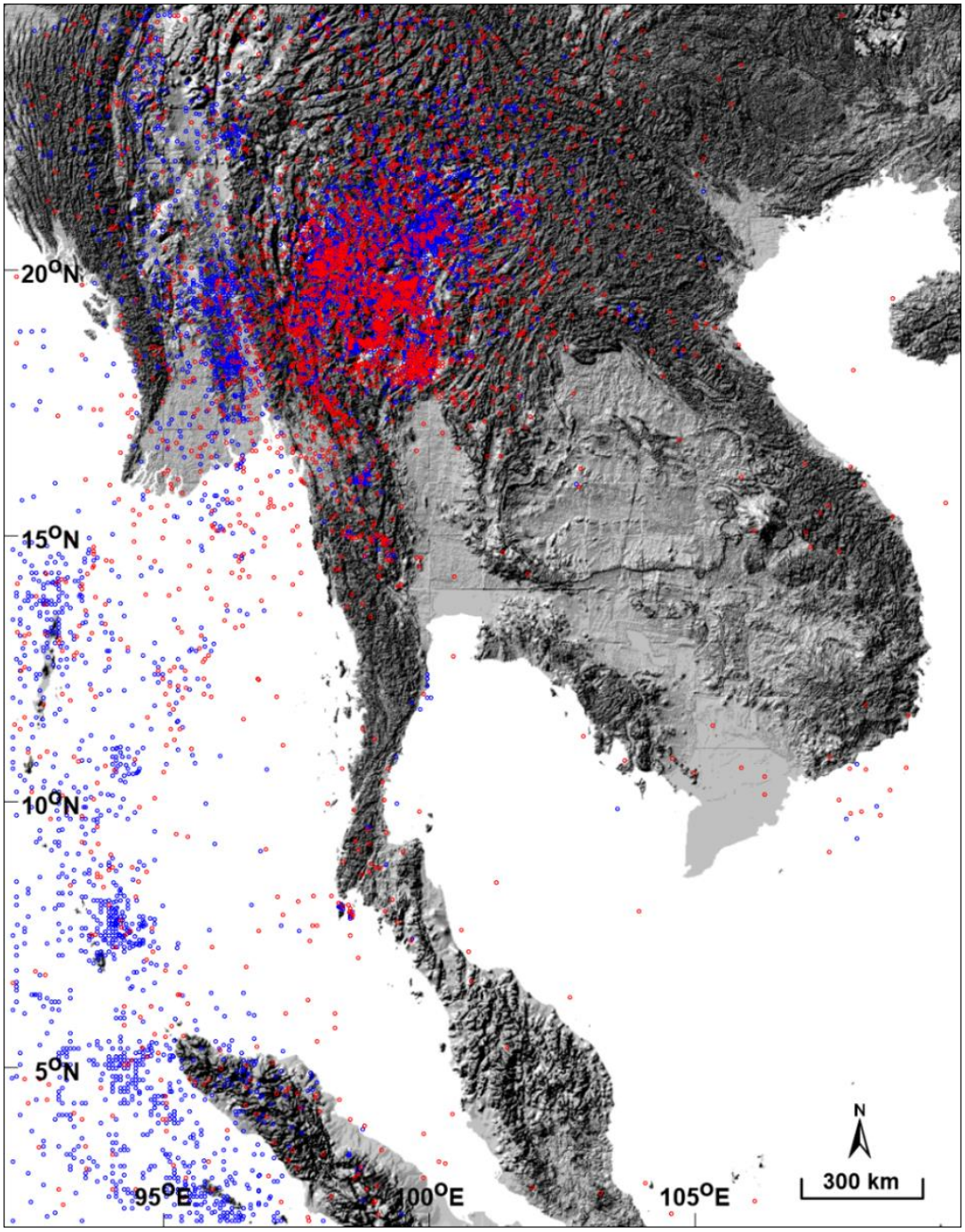

Fig. 1.8. Map showing the distribution of main shocks (red circles) and aftershocks (blue circles) in Thailand and adjacent areas recorded by TMD seismic network

1.4 Study Area and Scope of Study

The study area is located between the latitudes 2°-25°N and longitudes 92°-110°E covering the seismic stations of TMD in Thailand and significant earthquake sources in the region, for instance, the Sumatra- Andaman subduction zone, Sagaing fault zone, Andaman basin including seismogenic fault zones in Thailand and adjacent area as shown in Fig. 1.9. In order to investigate capability of TMD seismic network, the earthquake catalogue (Table. 1.6) and waveform data were statistically analyzed indicating accuracy, precision, limitation of TMD seismic network, and the seismic noises around the sites as well as the application of TMD network for determining earthquake parameters in January - June 2022.

Table 1.6. Example of TMD earthquake catalogue that was used in this study.

Date	Mag	Latitude	Longitude	Depth	Region
05-03-2022	5.6	4.563°N	95.187°E	10	North of Sumatra Island
03-04-2022	3.3	17.512°N	100.055°E	1	Laplae, Uttaradit
04-04-2022	3.6	17.512°N	100.048°E	2	Laplae, Uttaradit
14-04-2022	3.2	18.581°N	98.342°E	1	Mae Chaem, Chiang Mai
17-04-2022	3.2	18.967°N	98.546°E	1	Mae Ramat, Tak
28-04-2022	3.2	19.450°N	99.298°E	1	Som Prap, Lampang
08-06-2022	5.0	22.424°N	99.866°E	2	Myanmar
29-06-2022	5.4	21.119°N	99.883 °E	3	Myanmar

1.5 Objective

The purpose of this study is,

- To investigate the seismic network of TMD for detecting and recording earthquakes in Thailand and adjacent areas (Fig. 1.9) during January - June 2022.

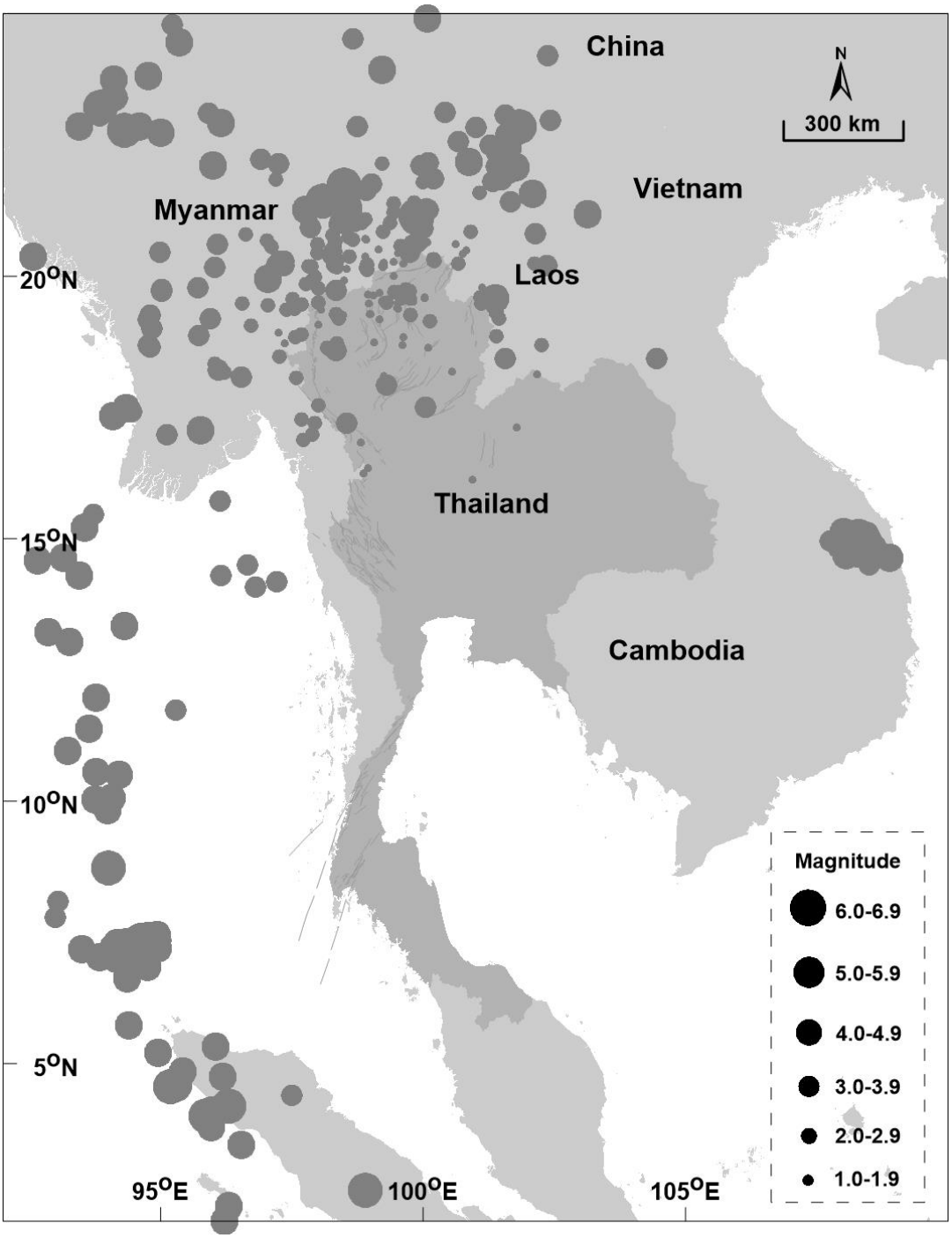

Fig. 1.9. Map showing the study area and earthquake events (gray circles) recorded by TMD seismic network during January - June 2022 that were used in this study.

CHAPTER II
THEORY AND LITERATURE REVIEW

2.1 Theory

Theoretically, the earthquakes can be located using different techniques ranging from standard linearized techniques to probabilistic techniques employing direct-searches of the solution space, from the single-event locations to the joint multiple-event locations, from the absolute locations to the relative locations. An earthquake location is usually determined by the match or misfit between observed arrival times of seismic phases at seismic stations, and predictions of these arrival times for different source locations using a given model of seismic velocities. The location that yields the smallest misfit between observed and predicted arrival times defines the hypocenter location. The earliest, formal earthquake locations using arrival time information from seismic phases applied direct-search procedures such as graphical methods (Milne, 1886) or simple grid-searches (Reid, 1910). The graphical methods using the circles based on the S-P arrival times, in which the radii of the circles are given by the corresponding S-P arrival time. In the 1970s digital computers allowed the use of linearized, iterative methods of Geiger (1912). Increasing a computing power over the last decades has made large-scale, grid and stochastic direct searches feasible for earthquake locations.

2.1.1 Accuracy of seismic network

Accuracy of seismic network and uncertainties in earthquake locations are dominated by three factor, i.e. measurement errors of seismic arrival times, modeling errors of calculated travel times, and a nonlinearity of earthquake location problem (Pavlis, 1986). The waveforms detected by seismic network with errors of arrival times are always present depending on a signal-to-noise ratio and a dominant frequency of the arriving phase. The arrival of seismic phase at a station is usually automatically marked by a change in amplitude and frequency content of the waveform obtained from seismic network which errors of arrival time lead to a relative location scatter of earthquake events around the actual seismic source indicating low accuracy of the seismic network in the region. An accuracy of the seismic network is able to investigate using the epicenter calculated by network compare with the location of known

seismic source. In this study, the epicenters of probable mining events calculated by TMD seismic network were compared with the location of mine in the region. The probable mining events are discriminated from the earthquake events using statistical method, i.e. Complexity (C) and Spectral ratio (Sr) that are able to distinguish the characteristic of amplitude and frequency of seismic events in the region. In the definitions, Complexity (C) is the ratio of the seismogram's integrated powers $s^2(t)$ in the selected time windows (t_1-t_2 and t_0-t_1) (Arai and Yosida, 2004) that the limits of the integral of C were determined by a trial-and error approach to find the best representative C values for both blasts and earthquake as shown in Eq. (2.1).

$$C = \int_{t_1}^{t_2} S^2(t)dt \,/\, \int_{t_0}^{t_1} S^2(t)dt \tag{2.1}$$

Generally, the complexity has the smaller C-values for the blast events because of the P-wave amplitudes of the blast events are obviously dominant (Compared to the earthquake event). Based on Sr method, Sr is the ratio of seismogram's integrated spectral amplitudes a(f) in the selected frequency bands (high-frequency band, h1-h2, and low-frequency band, l1-l2), that the limits of the integrals of Sr were selected by comparing the low and high energy in the spectra of mining blasts and earthquake (Gitterman and Shapira, 1993) as given by Eq. (2.2).

$$Sr = \int_{h_1}^{h_2} a(f)df \,/\, \int_{l_1}^{l_2} a(f)df \tag{2.2}$$

Theoretically, the P wave energy of a quarry blast is greater than that of the S wave, whereas the S wave energy of earthquakes is larger than that of the P wave. The frequencies and phases of the seismic waves generating from the earthquakes and explosions are different. Earthquakes have a wider bandwidth, than quarry blast. P waves generating from explosions contain higher frequencies and more impulses that Fourier analysis is able to convert a signal from the time domain to the frequency domain. Based on characteristic of seismic wave, the discriminant criterion is obtained from the plot of complexity (C) versus the spectral ratio of the seismogram (Sr) for the selected probable mining events and earthquakes events in the study region. The classification was carried out by using the linear discriminant function (LDF) to create discrimination line for classifying of seismic events in the region (Fisher, 1936).

2.1.2 Precision of seismic network

At present, the earthquake locations provide the uncertainty estimates under certain assumptions indicating the reliability of earthquake location using criteria derived from the geometry of the seismic network, i.e. number of observations (P- and S-wave arrival times), greatest azimuthal angle without observation, distance to the closest station, and root mean square of the travel time residuals for a final earthquake location. The earthquake location is able to basically be determined by comparison between observed and calculated arrival time of seismic wave from given location of earthquake to each seismic station that the differences of observed and calculated arrival times (R) were statistically evaluated in the term of the root mean square (RMS) residual as illustrated in Eq. (2.3). The spatial distributions of RMS values of the earthquake events along the seismic source zones indicate the precision of seismic network in the region. Given location with the lowest RMS represented the possible epicenter.

$$RMS = \sqrt{\frac{\sum_{i=1}^{N} R_i^2}{N-1}} \tag{2.3}$$

The RMS values of earthquake events also associated with the precision of seismic network in the region that the RMS values of earthquake events were lower (compared to the other areas) indicating better precision of seismic network in the region. A reliable seismic network will be able to clearly detect waveforms of the earthquake that observed arrival times of P-wave are analyzed precisely resulting the RMS values of the earthquake events are small and close to zero. However, the velocity model of seismic wave travelling in the crustal layers of the earth related to calculated arrival time of P-wave also influences RMS value of earthquake event. Furthermore, azimuthal gap of seismic stations surrounding an earthquake epicenter (Fig. 2.1) is able to represent the precision of seismic network in the region, which is defined by primary and secondary azimuthal gap measurements. The primary azimuthal gap is the largest gap between a network's event-station azimuths and secondary azimuthal gap is the largest gap that results when any given station is removed from the network. The primary azimuthal gap is directly linked to the seismic network geometry and represents a quantitative

measure of how well the epicenter is surrounded by the seismic stations. However, this metric is sensitive to reading errors, thus the use of the secondary azimuthal gap is more standardly accepted. The secondary azimuthal gap is the more robust measure of the network geometry, as it reduces the vulnerability to phase picking and travel time prediction errors, and implicitly invokes the constrains on the primary azimuthal gap and the minimum number of stations. To provide the best azimuthal coverage for the event location, intuitively, the stations in a local network should be uniformly distributed among the azimuths as demonstrated in Fig. 2.1.

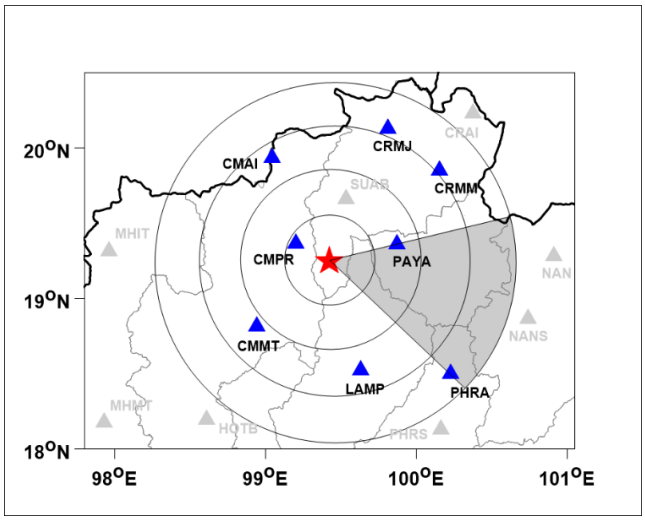

Fig. 2.1. Map showing azimuthal gaps (shaded area) of seismic network with the seismic stations (blue triangles) and earthquake epicenter (red star) in Thailand.

In general, the less azimuthal gap of the seismic network will encourage to precisely calculate earthquake epicenter that the earthquake event with a primary azimuthal gap of less than 110° and a secondary azimuthal gap of less than 160° was located at 5 km accuracy or better according to Monte Carlo simulation while an increase in azimuthal gap to more than 180° commonly influence on precision of seismic network for earthquake location (Kissling, 1988). The reliable precision of seismic network typically requires at least eight travel time arrivals, of which at least one is an S-wave arrival, and at least one was reported from a station within a focal depth's distance from the epicenter for a well constrained location (Chatelain et al., 1980) while the largest constraint on the location precision is given by the errors that result from the picking seismic phases by the automatic system and the manual routine analysis.

2.1.3 Limitation of seismic network

Up to the present, it is widely accepted that although instrumental earthquake records cover a much shorter time period than the paleo-seismological data, the instrumental seismic records, i.e., earthquake catalogue, are a valuable for seismicity, seismotectonic, seismic risk and hazard investigations. However, the earthquake events detected by seismic network are normally incomplete in term of representing the seismotectonic activities of any time span and site specific of interest. This is because earthquake data recorded by the seismic network that change in time and space with varying operational practices and procedures. Therefore, in order to obtain reliable results from the statistical analysis, the critical issue to be addressed is to assess quantity, quality, and consistency of those earthquake data including limitation of seismic network in the region. Empirically, earthquakes detected by seismic network are normally contaminated by the varying operational procedures. As a result, the biases and heterogeneity in the rate of reporting different magnitude earthquakes is present, which may distort the earthquake catalogue. To avoid these artifacts in reporting procedure, the GENAS algorithm (Habermann, 1987), which relies on comparisons of the changes in the significant seismicity rates at the different time intervals, was applied throughout period of earthquake catalogue. The significant breaks in the slope of the reporting rate were searched for at the individual magnitude level in order to view affected magnitude range in individual time span.

Theoretically, in order to evaluate the location, time and magnitude of an individual earthquake, the range of an earthquake signal must cover an area with at least four seismic recording stations. However, in practice, it lies in the nature of earthquake reporting that small earthquakes are more difficult to detect. Signals of small earthquakes do not travel far. The energy is quickly lost and the signal recorded by stations at a certain distance is weak. As a result, for every seismic recording network, there exists a level above which all earthquakes that occur in the region, i.e. 100%, are actually reported. This limit is called the magnitude of completeness, Mc, which indicates the smallest magnitude earthquake that can be detected reliably by the existent seismic recording stations across that time period and so forms a complete record in both space and time (Taylor et al., 1990; Wiemer and Wyss, 2000). For a certain space and time, a power-law can approximate the frequency-magnitude distribution

(FMD). The FMD describes the relationship between frequency of occurrence and magnitude of earthquakes, as shown in Eq. (2.4) (Gutenberg and Richter, 1944; Ishimoto and Iida, 1939). In order to investigate limitation of seismic network and earthquake detecting capabilities, the distribution of Mc-value was calculated for 0.25^{o} x 0.25^{o} grid cells covering an area of 150 km buffering from the seismogenic fault zones (Pailoplee et al., 2009). From each individual grid node, the earthquake within a radius of 300 km (Gupta, 2002) were used to plot the FMD and evaluate the Mc. The obtained results were then contoured showing the limitation of seismic network and the capability of earthquake detection in each area that the areas with the low Mc-value represent high efficiency of seismic network for detecting earthquake in the region.

$$Log(N) = a - bM \tag{2.4}$$

where N is the cumulative number of earthquakes having magnitudes larger than M and a, b are constant values depending on seismotectonic activity in the region. FMD follows a straight line on a log-normal-diagram for the magnitude range in which all earthquakes are reported as shown in Fig. 2.2. Below a certain magnitude, the line flattens. For magnitudes smaller than the start of the curvature, not all earthquakes are reported. This point of flexing is Mc. Below Mc-value, the reporting homogeneity often varies and produces the changes of seismicity rate, are not of a natural origin that incompletely reported earthquakes are simply ignored.

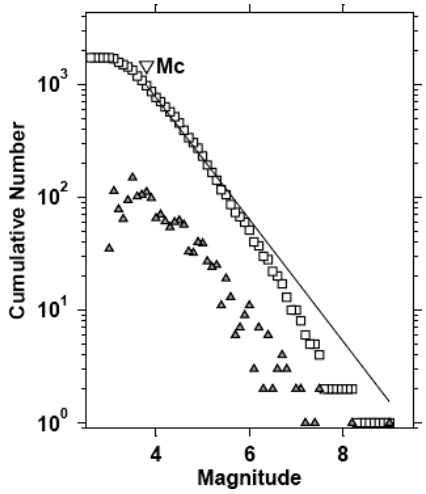

Fig. 2.2. The FMD plot of the seismicity data. The solid line is the line of best fit according to Woessner and Wiemer (2005). Mc is defined as a magnitude of completeness.

2.1.4 Ambient noise in seismic network

The efficiency of seismic network commonly related to the ambient noises around the site that consist of short-period and long-period seismic noise. The short-period seismic noise may be generated by human activities or have natural causes such as wind or rushing waters. Wind-generated noise is broadband, ranging from approximately 0.5 Hz up to about 15 to 60 Hz (Young et al., 1996). The particle motion of short-period noise is more erratic than for long-period noise. At long periods, horizontal noise power may be significantly larger than vertical noise power. The ratio increases with the period and may reach a factor of up to 300 (about 50 dB). The site can be considered as still favorable when the horizontal noise at about 100 to 300 s is within 20 dB. This is mainly due to tilt, which gravity into the horizontal components but not into vertical. Tile may be caused by the traffic, wind or local fluctuations of barometric pressure. Theoretically, oscillatory ground motion of noise can be approximated by sine-waves $x(t) = a_d \sin \omega t$ with a_d as the displacement amplitude. Therefore, when converting displacements into the related velocities or accelerations, will be able to calculate respective values of velocity or acceleration power spectral density as shown in Eq. 2.5. (Willmore, 1979)

$$P_a(\omega) = 16\pi^4 f^4 P_d \tag{2.5}$$

The new global noise model was employed as the upper- and lower-bound envelopes of the cumulative compilation of representative ground acceleration power spectral densities for noisy and quiet periods at the 75 digital station world-wide (Peterson, 1993). The models are commonly referred to as the New High Noise Model (NHNM) and the New Low Noise Model (NLNM) and represent the currently accepted standard for expected limits of seismic noise that NLNM and NHNM are useful in the intercomparison of noise fields from the different sites. Physically, a waveform detected by seismic network at frequency below 0.5 Hz (microseisms) indicated the ambient noise generated by oceanic and large-scale meteorological sources, a waveform with frequency at 1 Hz are wind effects and local meteorological condition while a waveform with frequencies above 1 Hz (microtremors) represents human activities around the seismic site (Bard et al., 2003) that microtremor and microseism are weak ground motion influenced by a subsurface structure. The published previous studies are shown in Table 2.1.

Table 2.1. Synthesis of noise sources according to frequency.

Noise sources	Gutenberg (1958)	Asten and Henstridge (1984)
Wave striking the coast	0.05 - 0.1 Hz	0.5 - 1.2 Hz
Monsoon/ metrological perturbations	0.1 - 0.25 Hz	0.16 - 0.5 Hz
Cyclones over the ocean	0.3 - 1 Hz	0.5 - 3 Hz
Local meteorological conditions	1.4 - 5 Hz	-
Volcanic tremor	2 - 10 Hz	-
Urban	1 - 100 Hz	1.4 - 3.0 Hz

Furthermore, the efficiency of a seismic network may be dominated by the spatial and temporal variations of the ambient noise in the region. Based on Burtin et al. (2008), seismic stations located in a densely populated area and installed on soft sediments, is the noisiest station over the entire frequency band. Horizontal components display energy amplitudes systemically larger by 20 dB, the microseismic peak at 0.2 Hz is more pronounced. The main seasonal noise variation is in the high-frequency band (>1 Hz) with an average increase of 15 dB during summer. The noise amplitudes on seismograms are then 6 time larger at high frequency during the monsoon period than during the dry season. Diurnal variation in seismic noise at remote locations typically is weather related. Wilson et al. (2002) compared midday and midnight noise levels measured at seismic stations. At low frequencies (0.01–0.06 Hz), the midday noise levels were 2 dB higher (vertical components) and more than 7 dB higher (horizontal components). The larger variation in horizontal noise components was attributed to diurnal variations of wind, barometric pressure, and temperature, which interact with vault geometry and/or soil conditions to cause tilting of the slab on which a seismic sensor is mounted. At microseismic frequencies (0.06–0.3 Hz), day/night variations were less than 1 dB. At high frequencies (0.3–8.5 Hz), the average midday noise levels were as much as 8 dB higher than midnight noise levels. The ambient noise can interfere with a seismic detection of personnel in two ways. Current seismic sensors trigger on a perturbation to the background level of ground motion. The strong seismic noise can mask a weaker disturbance caused by a moving person in the region, resulting in either non-detection or reduced detection range.

2.1.5 Application of seismic network

Besides the accuracy, precision, and limitation of seismic network, the capability of application for determining the earthquake parameters, i.e. the focal mechanism and strong ground-motion attenuation are important indicating efficiency of seismic network in the region. A focal mechanism solution (FMS) is the result of an analysis of waveforms generated by an earthquake and detected by seismic network. It usually takes at least 10 records to produce a reasonable FMS, and then only if seismic stations are well distributed geographically around the epicenter. The FMS provides the orientation of a fault plane, the direction of hanging-wall slip, and hence the type of fault involved in the earthquake strike-slip, reverse, normal, oblique as shown in Fig. 2.3. And all of this information can be obtained within seconds by a structural geologist who knows how to interpret a graphic depiction of the FMS, known as a "beachball" diagram. Analysis of several FMS in a main shock-aftershock sequence allows us to map the patch along the fault that slipped, and evaluate whether more than the one fault generated earthquakes during the sequence. More sophisticated quantitative analysis of the earthquake source mechanics can sometimes identify the direction of fault propagation. The P-wave first motion polarity technique is one of the most wildly used method for determining FMS utilizing polarities of first P-waves recorded by seismic stations surrounding an epicenter together with the azimuth and take-off angle of each station plotting beachball diagram (Snoke et al. 1984).

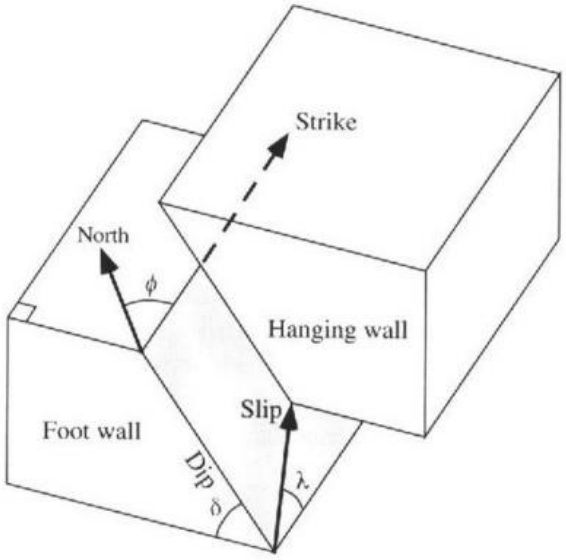

Fig. 2.3. Diagram showing fault displacement obtained from a focal mechanism solution.

The strong motion accelerations (SMA) recorded by seismic network were applied for developing attenuation model in the region. Theoretically, the SMA should be observed close to the earthquake epicenter in order to represent the actual ground shaking generated by the earthquake. A number of seismic stations in the vicinity of the earthquake epicenter that can detected the SMA from the earthquake event indicating efficiency of a seismic network in the region. The ground-motion prediction equations (GMPEs) are utilized in the seismic hazard applications to specify the expected levels of shaking as a function of the predictor variables. GMPEs for the active crustal regions are typically developed from the empirical regression of observed amplitudes against available set of predictor variables as shown in Eq. (2.6). First group is Next Generation Attenuation Models (NGA), is to improve information of earthquake from the original equations. NGA composed of the Abrahamson and Silva (2008) and Idriss (2008). The second group is Stable Continental Region, that divided by type of earthquake is a stable movement, listed of Toro et al. (2002), Hwang and Huo (1997) and Dahle et al. (1995).

$$ln(PGA) = f_{base} + f_{fault+AS} + f_{site} + f_{TOR} + f_{dist} \quad (2.6)$$

Where: PGA is calculated peak ground acceleration, f_{base} is function of base model, $f_{fault+AS}$ is a function of fault and aftershock model, f_{site} is a function of site response model, f_{TOR} is a function of depth-to-top of rupture model and f_{dist} is a function of large distance model, respectively. A focal mechanism mentioned above was employed to calculate together with strong-motion attenuation model that the obtained PGA values were then analyzed spatially showing the distribution of ground shaking in the region known as Shake Map. The ground shaking obtained from both the model and seismic network will be strong in the direction of fault slip related to the focal mechanism that the significant damages and felt reports were mainly found along the fault rupture of the earthquake event. Practically, the earthquake ground shaking was empirically converted to the earthquake intensity on the Modified Mercalli Intensity (MMI) scale in order to estimate the severity of earthquake in the region. Moreover, the comparison of the ground motion obtained from the model and the PGA values recorded by the seismic network represent the accuracy of attenuation model and efficiency of seismic network that can be utilized for developing the suitable attenuation model in the further study.

2.2 Literature review

Regarding to a section of literature review, previous works, in particular for the theory aspect, were viewed. The main aim of this procedure is to summarize the methodology for investigating seismic network including accuracy, precision, limitation, ambient noise as well as application of seismic network. In earlier studies, the efficiencies of seismic networks were analyzed using the various method with suitable parameters depending on characteristic of seismic network and seismotectonic activities in the region. The difference of tectonic setting in each study area influenced seismicity in the region associated with the selection of suitable methodology and parameters representing the capability of the earthquake detection of the seismic network. Therefore, the results obtained from the reviews of previous publications in this study, are the guideline for analyzing and investigating the seismic network in Thailand.

2.2.1 Accuracy of seismic network

Sukrungsri et al. (2019) discriminated microaftershocks generated by M4.9 Lampang earthquake from the quarry blasts within Lampang province using Complexity (C) technique that is regard as an effective statistical approach for seismic discrimination. This technique based on the quarry blast typically generated larger P-wave energy than that of earthquakes in the specific time window. They used 30 short period seismograms with local magnitudes of 1.0-1.9, recorded in February 2019 by the Thai Meteorological Department (TMD). These events posed in vicinity of both the quarry and the fault rupture zone which associated with the main shock event of M4.9 in Lampang province. The suitable parameters that were used in this study obtained from the retrospective tests revealing the time windows of t1 = 3s and t2 = 6s were appropriate for classifying the seismic events in Lampang province. The results showing all of seismic events that located in mining area have C-values lower than 1.0 (in the range of 0.23-0.95) while the events with C-values higher than 1.0 (varies from 1,12 to 4.31) were located only within the aftershock zone of M4.9 main shock. The proposed criteria in this study were the seismic events with C-values were lower than 1.0 and higher than 1.0 be identified as quarry blast and earthquake, respectively. However, the plot of C-value versus focal depth indicates some earthquake events were placed below a discrimination line of C-value of 1.0 as shown in Fig. 2.4 representing limitation of Complexity technique in this study.

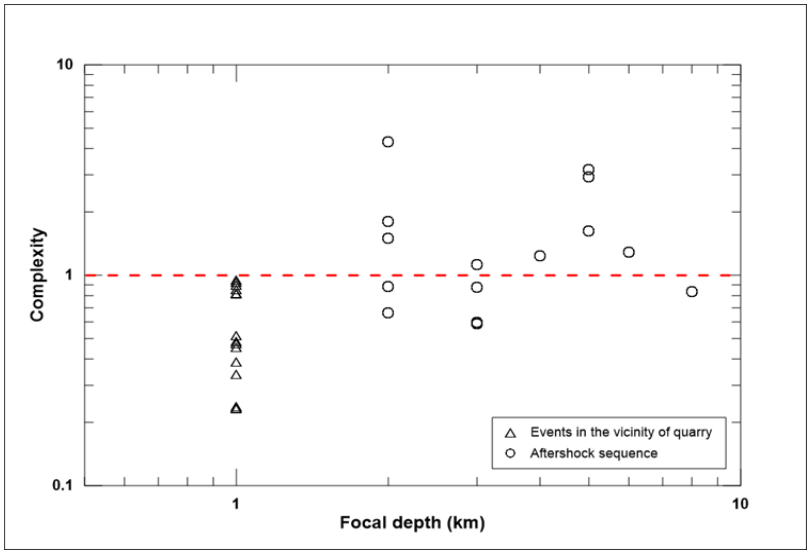

Fig. 2.4. Distribution of Complexity for the seismic events in Lampang province with the discrimination line (dashed line) obtained from this study.

Yilmaz et al. (2012) classified seismic events in the eastern Black Sea region of Turkey due to a large number of quarry blasts have been detonated in a region. They were recorded by seismic network that caused the contamination of the regional earthquake catalog. In this study, earthquakes and quarry blasts can be separated through the different methods consist of calculating the maximum ratio of S to P wave (S/P), complexity (C), spectral ratio, and time frequency analysis. They used the 186 seismic events recorded by the Karadeniz Technical University and the Bogazici University between 2002 and 2010. As a result, 68% of examined events were determined to be the blasts and 32% to be the earthquake that blasts were made in daytime and concentrated in quarries and about 60% of earthquakes occurred on land.

Kekovali et al. (2012) develop time and frequency techniques to characterize quarry blasts. They used methods consist of S/P wave amplitude peak ratio, complexity, and spectral ratio to analyze a set of known earthquake and mining blasts seismograms of 520 seismic events with the magnitude in the range of 2.3 - 3.0 from the Kandilli Observatory Earthquake Research Institute and National Earthquake Monitoring Center (KOERI-NEMC) seismic catalog between 2009 to 2011. Out of a total 520 records, 344 are related to probable mining blasts and 176 to earthquake. They developed a new approach namely Pe (power of event) value that can classify quarry blast from the earthquake with acceptable high results of 99.6%.

2.2.2 Precision of seismic network

Belinic et al. (2017) presented criteria (called as GT criteria) for estimating epicentral location precision of seismic events recorded at network stations within 400 km around the city of Zagreb. The criteria were based only on the network coverage metrics and GT5 level represents absolute location error lower than 5 km developed using a bootstrap resampling method that the same earthquakes were relocated many times but with different, randomly selected seismic stations. They used the 330 reference events from ISC showing the location accuracy is most affected by the distance to the farthest station in the seismic network, while not at all influenced by the distance to the nearest. The developed GT criteria for GT5 level of accuracy require 10 or more network stations, all within 125 km from an earthquake epicenter, and the secondary azimuthal gap (the largest gap when any given station is removed from the network) less than 200°, or the network quality metric that the deviation between optimal uniformly distributed network and the actual network less than 0.41 (Fig. 2.5). The obtained results revealed that the global criteria were too restrictive and unsuitable for the study area since they require more regular networks. With criteria obtained from this study, they achieved higher accuracy with a bigger secondary azimuthal gap or greater network quality metric.

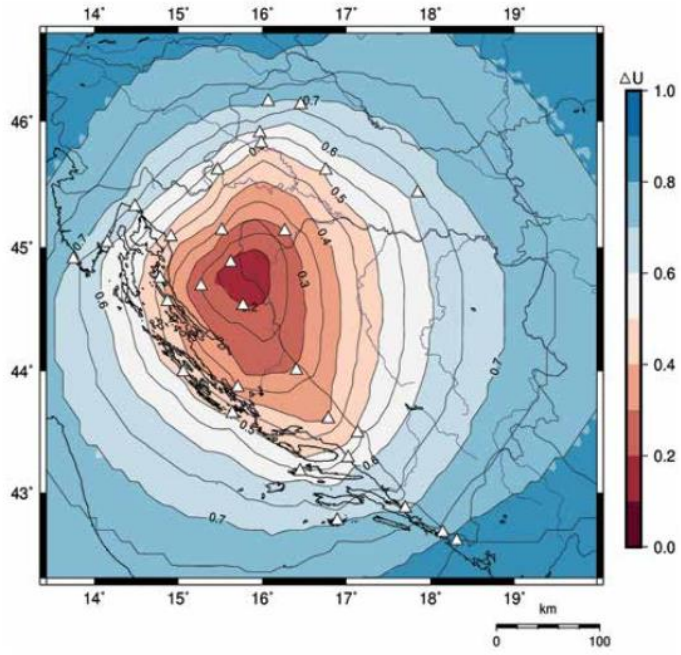

Fig. 2.5. Map of calculated network quality metric for Croatian seismological network that the seismic stations are represented by white triangles.

Hsiao et al. (2013) analyzed the precision of seismic network for locating earthquake and monitoring tsunami along the northeastern offshore of Taiwan after additional installation of seismometers in the region. According to observations from January 2012 to June 2013, They found that a total of 15,168 earthquakes recorded by the upgraded seismic network and the number of relocated earthquakes with an azimuth gap less than 180 degrees substantially increase about 34% (Fig. 2.6). Meanwhile, the root-mean-square of time residual, the error in epicenter, and the error in depth of the earthquake locations decrease. So, implementation of upgraded network has the advantage of extending the coverage of existing Taiwan network to offshore, providing more accurate and real-time data for offshore earthquake monitoring.

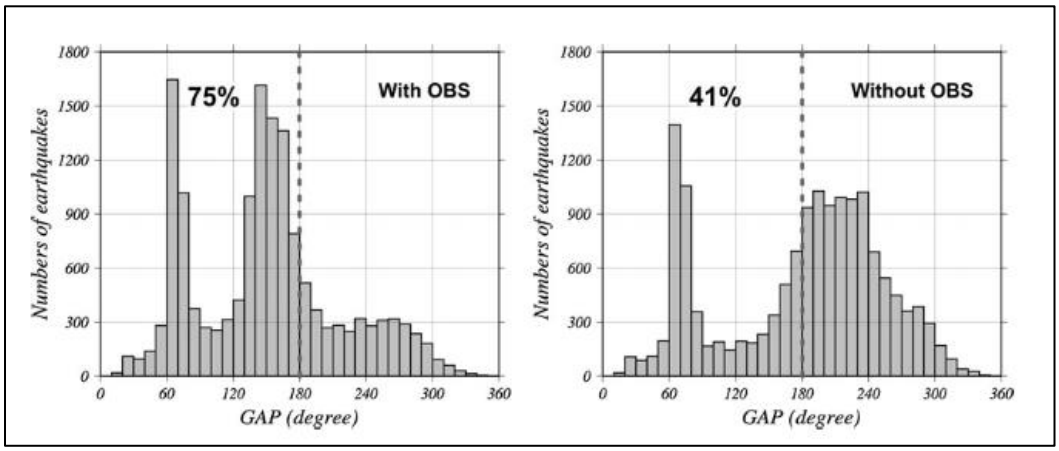

Fig. 2.6. Statistical charts of earthquake number with respect to gap angle, showing the results obtained with OBS data (left) and without OBS data (right).

Bondar et al. (2003) analyzed the epicenter location precision using data available in published seismic bulletins. The location precision is most reliably estimated by the station geometry. They used two explosions with exactly known epicenter to develop local network location accuracy criteria. According to Monte Carlo simulations of network geometry, found that local network locations are accurate to within 5 km with 95 percent confidence level when the network followed by the criteria: 1) there are 10 or more stations, all within 250 km, 2) an azimuthal gap of less than 110°, 3) a secondary azimuthal gap of less than 160° and 4) at least one station within 30 km. When stations coverage with azimuthal gap of less than 120°, regional and teleseismic networks provide 25 km accuracy at 90 percent confidence level.

2.2.3 Limitation of seismic network

Sukrungsri and Pailoplee (2016) investigated limitation of earthquake detection along Sumatra-Andaman subduction zone (SASZ) using the compilation of earthquake catalogues reported by four agencies, i.e. ISC, NEIC, GCMT, and TMD in 1980-2015. After earthquake compilation, they classified statistically the main shock from the aftershock in the region using assumption of Gardner and Knopoff (1974) that 1,958 clusters of 102,017 earthquakes were screened and 2,763 events were defined as main shocks represented actual seismotectonic activities in the region. The obtained main shocks were then analyzed frequency-magnitude distribution (FMD). A slope of FMD plot known as magnitude of completeness (Mc) indicated the limitation of seismic network for detecting the earthquake events in the region (Fig. 2.7)

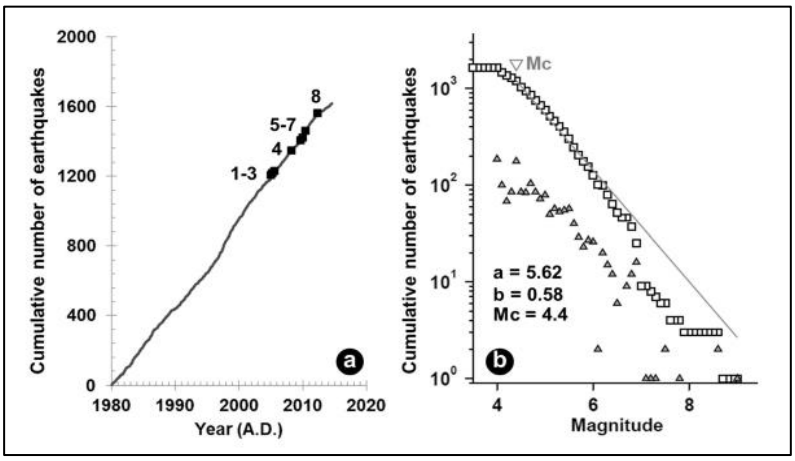

Fig. 2.7. a) Cumulative number of seismicity data with major earthquakes (black squares). b) FMD plot showing the Mc detected by seismic network.

In this study, found that earthquake magnitudes along SASZ that can be detected completely by seismic network, are magnitude larger than 4.4. These main shocks were investigated both temporal and spatial seismicity rate changes in order to determine the precursor of large earthquake along the SASZ. They mainly found that the rate of seismicity data significantly decreases at the Z-value higher than 6.0 prior to occur the major earthquakes along the SASZ. Furthermore, they proposed three prospective areas of the upcoming major earthquakes with the decrease of seismicity rate at Z-value over 6.7, i.e. Nicobar Island, western offshore of Sumatra Island and western Myanmar where effective mitigation plans should be contributed.

Woessner and Wiemer (2005) introduced a new method to determine the magnitude of completeness (Mc) and its uncertainty representing the limitation of seismic network. Their method models the entire magnitude range (EMR method). They compare EMR method with three existing techniques, found that EMR showing a superior performance when applied to synthetic test cases or real data from regional and global earthquake catalogues. By explicitly computing uncertainties in Magnitude of completeness by using a bootstrap approach, they revealed that uncertainties in b-values are larger than traditionally assumed, especially when considering the small sample sizes. They also demonstrated that the EMR method is the most favorable choice to determine Mc because 1) a method is stable under most conditions, 2) a comprehensive seismicity model is computed, and 3) a model fit can be tested. According to automated mapping purposes, the mean value of the N Bootstrapped Mc determinations is a suitable estimate of Magnitude of completeness because it avoids outliers and smooths results and bootstrap approach to determine uncertainties in Mc is a reliable method.

Marsan (2003) introduced a method computing the b-value and the log-likelihood of completeness for earthquake events above a certain cutoff magnitude. The log-likelihood of completeness is defined as the logarithmic probability that the Gutenberg-Richter law fitted to the data above the cutoff magnitude can predict the number of the earthquakes in the magnitude bin just below the cutoff magnitude. A magnitude of completeness (Mc) is chosen so that (1) the b-value drops for the earthquake magnitudes smaller than Mc, and (2) the log-likelihood drops at Mc-value that the two criteria are difficult to combine for automatic Mc value calculations. Moreover, calculating the log-likelihood for only one magnitude bin bears instabilities, as frequencies of the earthquake in the magnitude bins varies strongly.

Rydelek and Sacks (1989) introduce method to estimate Magnitude of completeness (Mc) applying the random walk simulation (Schuster's method) that the test assumes (1) that earthquakes, at any magnitude level, follow a Poisson distribution; and (2) that due to higher, man-made noise-levels during daytime, Mc value is higher at this time. The method requires that other nonrandom features in the earthquake catalogues, such as swarms, aftershock sequences, or mining blasts, are removed in advance, implying that it is not useful for the determination of Mc if such features are present, that strong limitations on applicability.

2.2.4 Ambient noise in seismic network

Peterson (1993) generated noise power spectral density plots over frequencies up to 10 Hz for each of 75 stations worldwide. All of the data used in this study were extracted from digital data archive at U.S. Geological Survey's Albuquerque Seismological Laboratory (ASL). This archive dates from 1972 when the ASL first began deploying digital seismograph system and collecting and distributing digital data. The obtained data were generated by a variety of data acquisition systems representing technology that has evolved steadily over past twenty years. By assembling a composite of background noise from a large network of stations, many of the local station variables are masked, create generalized spectral plots of earth seismic noise for hypothetical quiet and noisy stations as demonstrated in Fig. 2.8.

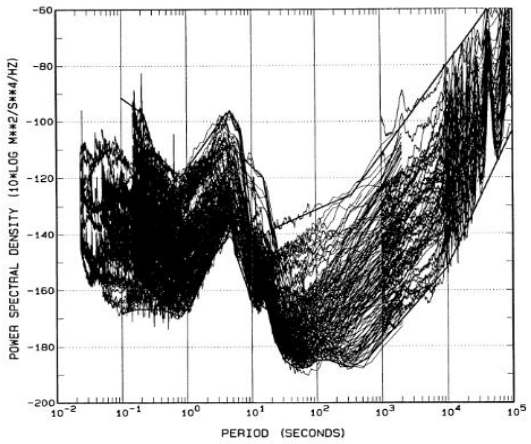

Fig. 2.8. An overlay of network spectra with straight-line segments fitted to the high-noise and low-noise envelopes of the overlay.

According to the combined curves, he defined two parameters comprising a new low noise model (NLNM) and a new high noise model (NHNM) as the spectrum of average low and high background noise power in the network, replaced earlier low and high noise models, respectively (Peterson 1980). Neither the NLNM nor the NHNM was ever likely to represent the actual noise spectrum at a specific site, the former because it is a composite of curves that individually are influenced by instrumentation, geology, and geography, latter because it is an average over the network. McNamara and Buland (2004) pointed out that NLNM has become less representative over time for the seismic stations within the network that have

been encroached upon by urban sprawl and now experience stronger cultural noise. As standards in seismology community, however, the NLNM and NHNM are useful in the intercomparison of noise fields from the different seismic sites as shown in Fig. 2.8.

Wilson et al. (2002) generated noise acceleration power spectral density estimates between 0.01 and 8.5 Hz from measurements with seismometers at stations along 951-km network transecting Utah, New Mexico, and Texas. The seismometers were surface mounted in dirt-covered vaults. At frequencies of 0.01-0.06 Hz, horizontal components of noise differed more from the NLNM and borehole noise than did vertical components. This was attributed to sensitivity of surface-mounted broadband seismometers to dynamic tilting caused by thermal and barometric induced surface displacements. (Borehole noise measurements were available from a site within 55 km of the midpoint of the Utah-Texas network.) Noise levels varied by as much as 15 dB across the network, which was indicative of local nature of noise at these frequencies and attributed to the influences of surface site conditions such as slope, diurnal shading conditions, soil type, soil moisture, and vault design. At the microseismic frequencies in the range of approximately 0.06–0.3 Hz, the seismic noise components were indistinguishable from seismic noise of the borehole station. At high frequencies in the range of approximately 0.3–8.5 Hz, noise levels were higher than borehole noise and depended on proximity to population centers, transportation corridors, and oil or gas production sites.

McNamara and Buland (2004) presented a new approach to effectively characterize the background seismic noise across the continental United States. They used power spectral density (PSD) estimating at broadband seismic stations for frequencies ranging from 0.01 to 16 Hz. They selected a large number of 1-hr waveform segments during a 3-yr period, from 2001 to 2003, from a continuous data. They proposed two examples of the seasonal variation in seismic noise in the continental United States. The microseismic noise at the frequency of approximately 0.12 Hz increased by ~15-20 dB in power and decreased slightly in frequency during winter months, which was attributed to increase in the intensity of Atlantic and Pacific storms during fall and winter. Furthermore, the seismic noise at the frequencies in the range of approximately 0.01-0.02 Hz was stronger in spring and summer, which was attributed to the larger amplitude of the daily thermal variations that compared to winter months.

2.2.5 Application of seismic network

Rocca and Galluzzo (2019) analyzed the volcano tectonic earthquakes that occurred in caldera of Campi Flegrei, Italy from 2000 to 2009 in order to compute the focal mechanisms. They used data from a large number of the seismic stations to estimate the reliable fault plane solutions for 71 events ranging between $0.5 \leq M \leq 2.5$. They found that most solutions were of a normal type and were rake-angle negative focal mechanisms in 86% of the cases. Only a few earthquakes occurred normal dip-slip fault; the majority occurred on varying degrees of the oblique slip. Only one event had a pure reverse-mechanism, and it was located far from the caldera center. A spatial distribution of computed mechanisms exhibited a remarkable mix of the fault orientations without any relationship to the location area or source depth. The predominance of normal kinematics on high-angle and nearly vertical faults and the very shallow source depth exhibited good agreement with the fact that seismicity at Campi Flegrei occurred during periods of ground uplift. In fact, ground uplift elongated the shallowest crust, thus reducing the normal stress on existing locked faults; this facilitated earthquakes, particularly characterized by the normal, dip-slip, and strike-slip mechanisms. In contrast, ground subsidence produced a horizontal shortening of the upper crust, that increased normal stress on high-angle faults and reduced earthquake occurrence as shown in Fig. 2.9.

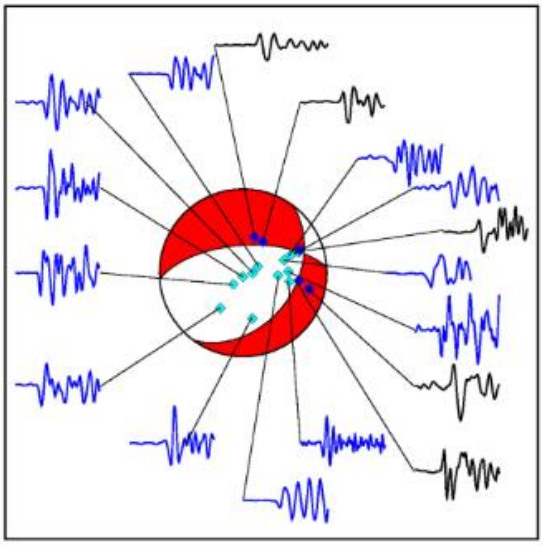

Fig. 2.9. P-wave of earthquake recorded at 17 stations and beach-ball plot that fit all polarities indicating efficient application of seismic network.

Lindung et al. (2018) presents a site-specific analysis of ground response during the Tarlay Earthquake on March 24, 2011 in Northern Thailand. In this study, NGA models were selected to predict ground motions due to earthquake. The equivalent linear and non-linear approaches were employed in one-dimensional ground response analysis. Furthermore, the spectral responses were produced by the equivalent linear and non-linear approaches, were compared with the seismic design code of Thailand. Peak ground acceleration at the ground surface obtained from both the equivalent linear and non-linear approaches certainly results in the high amplification factor showing the ground motion from the NGA models agree with strong motion parameters of Tarlay earthquake detected by a seismic network. (Fig. 2.10)

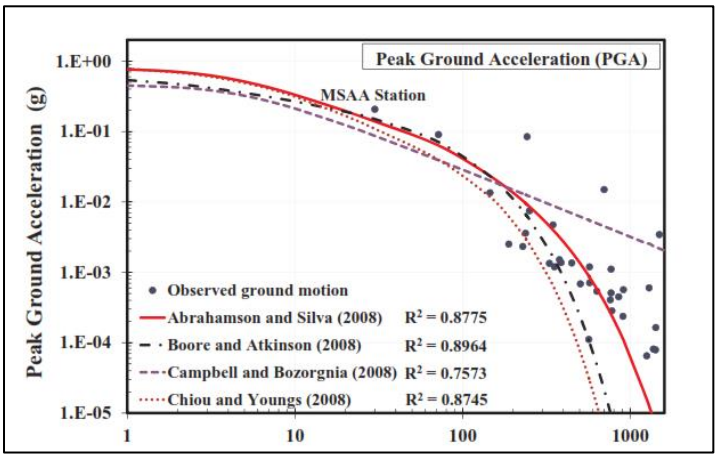

Fig. 2.10. NGA attenuation model compared to the ground motion or peak ground acceleration recorded by the seismic network during Tarlay Earthquake.

In attenuation analysis, the application of seismic network covering the earthquake source is the most important factor for determination of peak ground acceleration (PGA). In this study, BH-1 station was the closest site to Tarlay earthquake source and located at Mae Sai Station (MSAA), whereas BH-4 station was the farthest one. They found that the recorded ground motions obtained from surrounding stations deal with the predicted ground motions of the Boore and Atkinson model. The plotted value showed that Boore and Atkinson (2008) underestimated the recorded PGA. Based on the recorded PGA and the suitable attenuation model, the area surrounding the BH-1 station might have sustained serious damage due to the Tarlay earthquake where the liquefaction is possible when the PGA reaches 0.1 g.

CHAPTER III
DATA AND METHODOLOGY

3.1 Data

At present, TMD earthquake data consists of i) the seismic signals that are observed and recorded continuously including ground velocity and acceleration data, ii) the seismicity data that are analyzed and formally compiled. These data represent a performance of seismic network such as accuracy, precision, and limitation of seismic network as well as a seismic noise dominating the seismic network and the capability of seismic network for determining earthquake parameters. In this study, I analyzed the seismic network of Thai Meteorological Department (TMD) during January - June 2022 (Fig. 3.1) that are composed of capability of seismic network to detect ground velocity during earthquake for calculating focal mechanism and the capability of the seismic network to detect ground acceleration for evaluating ground motion attenuation during strong earthquakes in Thailand and adjacent areas. Although TMD has developed a seismic network by additional installation of seismic stations covering the earthquake source zones in Thailand, the telecommunication system is still not very well that it delays and has missing signals affecting the accuracy and precision of seismic network to determine the earthquake parameters. In this chapter, I compiled the seismic data and the earthquake events recorded by TMD seismic network and basically analyzed spatial and temporal variations of the seismic stations. In addition, the earthquake catalogue of TMD was also compared to other agencies, i.e. USGS, GEOFON, EMSC by analyzing number of events, earthquake magnitude, and the epicentral distribution. In this study, I applied the statistical method to analyze the TMD seismic network during January - June 2022. For example, the Complexity technique and Spectral Ratio method were applied to investigate the accuracy of seismic network. The Azimuthal Gap was employed to evaluate precision of seismic network, The Magnitude of Completeness (Mc) was utilized to determine limitation of seismic network, The Power Spectral Density (PSD) and Fourier Amplitude Spectra (FAS) were used to analyze ambient noise dominating seismic network, and the first motion polarities and Peak ground acceleration (PGA) data were applied to access capability of TMD seismic network.

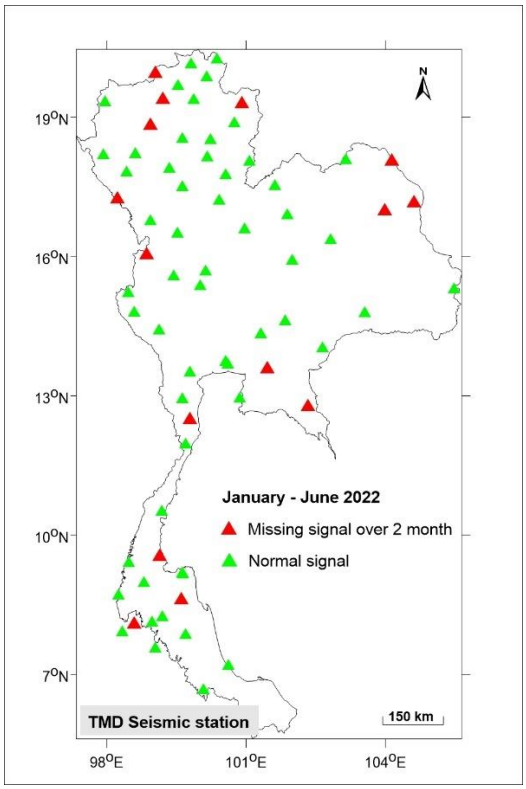

Fig. 3.1. The velocity seismic stations of TMD during January - June 2022 showing the distribution of seismic stations that signals were missing or discontinuous over 2 months (red triangle) and the stations with normal signals (black triangle).

The seismic data obtained from velocity seismic stations were utilized to determine the earthquake parameters, for example, the arrival times of P-waves were used to calculate earthquake epicenter, the amplitude of S-wave was used to calculate earthquake magnitude, and first-motion polarities of P-waves were used to calculate focal mechanism. The velocity seismic stations situated close to the earthquake sources, encourage the detection of micro earthquakes in the region and the velocity seismic stations surrounding earthquake epicenter can also be used to effectively calculate the focal mechanism. Therefore, the distribution of velocity seismic stations influences a performance of seismic network in the region. In this study, the velocity seismic stations of TMD during January - June 2022 indicate 15 stations with missing or discontinuous signals over 2 months from 71 whole velocity seismic stations, e.g., CHBT, CMMT, NAN, PANO, PASO, SKNT, and TSYB. These stations distributed mainly in the northern and southern parts of Thailand as shown in Fig. 3.1.

The seismic data recorded by the accelerograph stations can be used to estimate the ground shaking and ground motion attenuation from a strong earthquake. These parameters were calculated from maximum amplitudes of seismic waves observed and recorded at each accelerograph station for accessing the intensity of earthquake. The accelerograph stations near the earthquake sources contribute the detection of ground shaking representing the real severity of earthquake. Moreover, the distribution of accelerograph stations covering several areas serve to observe the attenuation of ground shaking and amplification of seismic waves in the region that may affect the buildings. In this study, the accelerograph stations of TMD during January - June 2022 indicate 17 stations with missing or discontinuous signals over 2 months from all of the 55 accelerograph stations. These missing data stations were mainly located close to the major cities in Thailand as shown in Fig. 3.2.

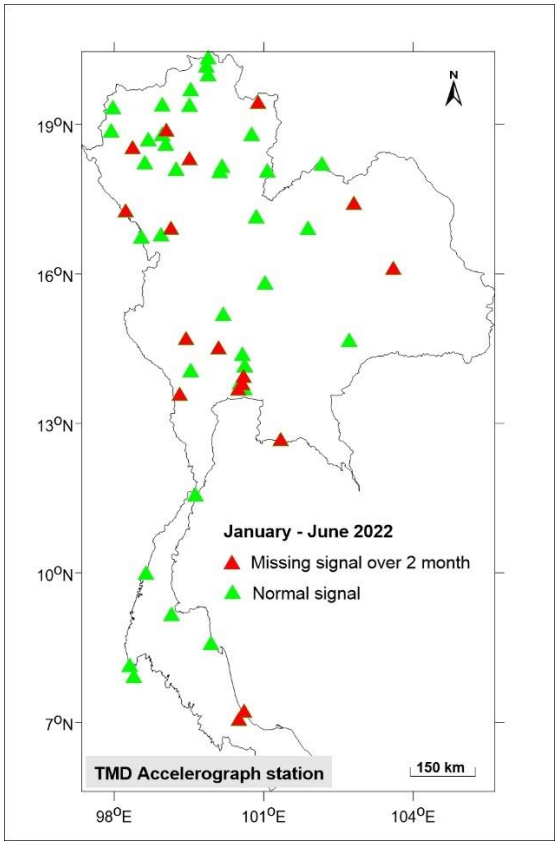

Fig. 3.2. The TMD accelerograph stations in January - June 2022 showing distribution of seismic stations that the signals were missing or discontinuous over 2 months and normal (red and black triangles, respectively).

The seismic signals from all of 126 seismic stations of TMD in January - June 2022 including the velocity seismic stations and accelerograph stations indicate that there were 32 seismic stations with missing signal over 2 months that distributed within the several areas. Most of them are due to telecommunication problem in remote areas. However, 94 seismic stations were still working effectively covering the active faults and seimic source zones in Thailand. Therefore, although some TMD stations have discontinuous and missing signals during January - June 2022, perfomance of TMD network was enough to observe and record significant earthquake events in Thailand and surrounding areas as shown in Fig. 3.3.

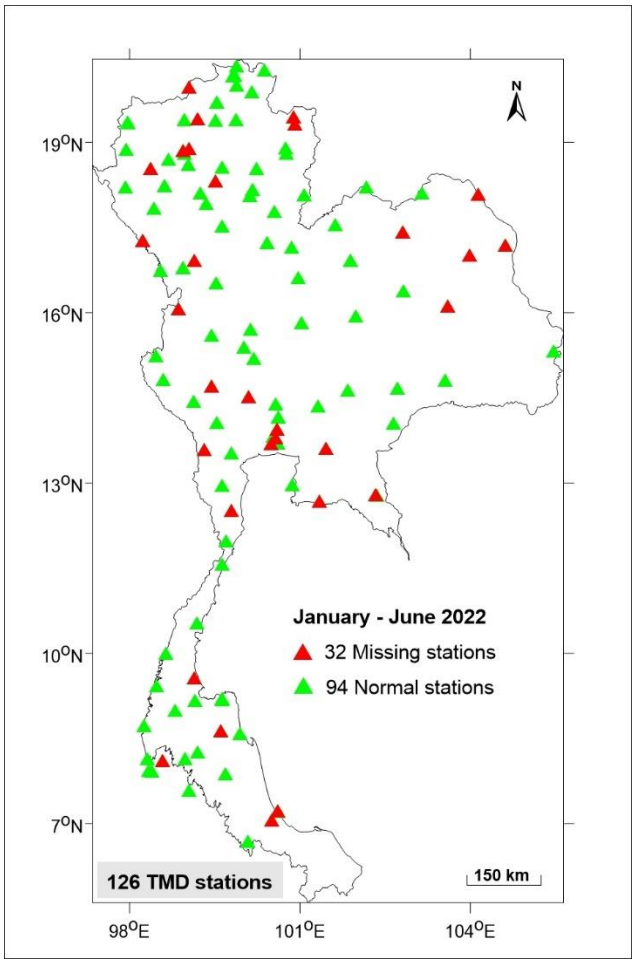

Fig. 3.3. Distribution of all TMD stations including velocity and accelerograph stations during January - June 2022 with missing or discontinuous signals and normal signals (red and black triangles, respectively).

The earthquake catalogue of TMD has recorded earthquake parameters that consist of origin time, magnitude, depth, latitude, longitude, and place of the earthquake as well as the number of phases used for calculation. TMD earthquake catalogue report all earthquake events in Thailand and adjacent areas (2-25°N, 92-110°E) that are detected and calculated by the seismic network of TMD. The earthquake epicenters are manually calculated and reported at the 3 digits of latitudes and longitudes (Table 3.1). Furthermore, the earthquake catalogue of TMD also record the felt reports of people who were affected the ground shaking. Meanwhile the earthquake catalogues of other agencies, i.e., EMSC, USGS, and GEOFON report the preliminary earthquake parameters that consist of origin time, magnitude, depth, latitude, longitude, and place of the earthquake as well as the additional information such as type of magnitude (mb, Ms, and Mw). The GEOFON is regarded as the agency that fastest report automatically earthquake events and report the status of earthquake calculation, i.e., Automatic (A), Manual (M), and Automatic that was confirmed (C) as demonstrated in Table 3.2. Meanwhile, USGS report parameters related to the precision of seismic network such as Azimuthal Gap, RMS, and closest epicentral distance (Table 3.3). At present, seismic network of EMSC is closest to Thailand (Compared to other network used in this study) that is able to detect and record micro earthquakes surrounding Thailand as illustrated in Table 3.4.

Table 3.1. Example of earthquake catalogue of TMD during January - June 2022.

Date	Mag	Lat	Lon	Depth	Phase	Region
2022-01-01 04:19:20	3.4	22.102	101.39	15	17	Yunnan, China
2022-01-02 04:52:58	1.6	20.317	100.24	3	7	Chiang Saen, Chiang Rai
2022-01-02 19:22:13	4.3	22.451	101.62	6	36	Laos - China Border
2022-01-02 19:35:34	3.9	22.234	101.55	5	29	Laos - China Border
2022-01-02 19:41:45	2.2	19.604	101.09	5	23	Laos
2022-01-02 20:59:13	1.7	19.621	101.13	5	16	Laos
2022-01-02 21:52:15	2.1	20.399	98.326	10	11	Myanmar
2022-01-03 18:59:46	3.9	4.403	97.503	172	13	Northern Sumatra
2022-01-04 15:02:45	4.2	11.978	93.768	110	32	Andaman Island, India
2022-01-04 18:23:45	4.6	15.054	108.44	30	11	Vietnam
2022-01-04 20:02:06	4.4	15.027	108.45	10	29	Vietnam

Table 3.2. Example of earthquake catalogue of GEOFON during January - June 2022.

Date	Mag	Type	Lat	Lon	Depth	Status	Region
2022-01-04 15:02:41	4.5	mb	11.88	93.71	140	M	Andaman Islands
2022-01-08 05:42:01	4.2	mb	11.03	93.26	84	M	Andaman Islands
2022-01-16 06:52:32	4.6	mb	3.5	96.47	61	M	Northern Sumatra
2022-01-18 02:22:14	4.6	mb	23.98	93.48	52	A	Myanmar-India Border
2022-01-21 10:12:32	5.3	mb	23.08	93.86	68	M	Myanmar-India Border
2022-03-01 11:04:11	5	mb	4.08	96.03	52	M	Northern Sumatra
2022-03-05 12:02:38	5.5	Mw	4.63	95.1	10	C	Northern Sumatra
2022-03-05 13:33:26	5	M	2.67	99.03	169	A	Northern Sumatra
2022-03-05 14:43:04	4.6	mb	22.12	101.62	10	A	Myanmar
2022-03-10 04:26:54	4.8	mb	3.89	95.95	52	A	Northern Sumatra
2022-03-13 01:11:03	4.7	mb	22.61	94.44	95	A	Myanmar
2022-03-14 02:22:38	4.5	mb	21.12	103.36	10	M	Vietnam
2022-03-15 09:08:50	4.7	mb	2.43	96.17	11	A	Northern Sumatra
2022-03-21 06:36:05	4.7	Mb	24.14	94.66	94	A	Myanmar-India Border

Table 3.3. Example of earthquake catalogue of USGS during January - June 2022.

Date	Mag	Type	Lat	Lon	Depth	Gap	DMIN	RMS	Region
2022-01-03	4.1	mb	4.3837	97.4417	191.56	134	0.973	0.81	Indonesia
2022-01-04	4.7	mb	13.0711	93.0237	35	109	1.433	0.55	India
2022-01-04	4.6	mb	11.9077	93.6061	131.6	53	5.913	0.61	India
2022-01-08	4.3	mb	11.0371	93.2253	88.26	90	0.775	0.75	India
2022-01-09	4.4	mb	6.8783	94.632	110.04	86	2.826	0.62	Indonesia
2022-01-11	4.6	mb	7.2609	94.2638	112.14	113	3.345	0.52	Indonesia
2022-01-11	4.2	mb	2.3287	109.7694	13.05	105	2.445	1.08	Malaysia
2022-01-12	4.6	mb	23.1568	94.6845	98.81	98	1.124	0.66	Myanmar
2022-01-12	4.1	mb	5.7034	94.115	55.39	140	2.858	0.67	Indonesia
2022-01-14	4.2	mb	24.3313	94.6403	89.01	102	4.179	0.89	Myanmar
2022-01-16	4.6	mb	3.5064	96.5606	68.91	59	1.753	0.63	Indonesia
2022-01-16	4.2	mb	23.8937	94.5597	73.01	118	3.862	0.75	Myanmar
2022-01-18	4.5	mb	24.0361	93.5196	60.79	69	2.192	0.48	India
2022-01-21	5.4	mww	23.0871	93.8172	58.96	22	2.046	0.48	Myanmar

Table 3.4. Example of earthquake catalogue of EMSC during January - June 2022.

Date	Mag	Type	Lat	Lon	Depth	Region
2022-01-02 21:35:40	3.1	M	4.4	96.5	10	NORTHERN SUMATRA
2022-01-02 15:20:05	3.4	M	24.86	95.14	18	MYANMAR
2022-01-02 12:23:06	3.7	M	24.75	95.1	57	MYANMAR
2022-01-03 20:30:34	2.7	M	24.1	94.21	10	MYANMAR-INDIA BORDER
2022-01-03 20:11:44	2.5	M	24.98	93.74	10	MANIPUR
2022-01-03 19:04:55	3.2	M	4.59	94.68	10	NORTHERN SUMATRA
2022-01-03 18:59:46	4	M	4.36	97.46	174	NORTHERN SUMATRA
2022-01-03 09:04:55	3.5	M	3.22	96.44	10	NORTHERN SUMATRA
2022-01-04 15:02:41	4.5	mb	11.83	93.65	137	ANDAMAN ISLANDS
2022-01-05 14:25:28	3.2	M	6.3	95.41	225	NICOBAR ISLANDS
2022-01-05 04:30:47	3.6	M	3.59	97.52	57	NORTHERN SUMATRA
2022-01-08 10:10:25	3.1	M	4.83	96.24	17	NORTHERN SUMATRA

The comparisons of earthquake catalogues of each agency indicate the earthquake catalogue of TMD can mostly detect and record the earthquake events during January - June 2022 (compared to other agencies) followed by the EMSC, USGS, and GEOFON, respectively because of most of these earthquakes have small magnitudes and occued near the seismic stations of TMD. Moreover, there were a lot of small earthquakes generated in Myanmar near the north of Thailand during June 2022, so these events can be better detected and recorded by TMD network (Fig. 3.4 and 3.5) whereas the earthquake catalogue of GEOFON recorded the number of events smaller than other agencies because of GEOFON is the global seismic network that seismic stations located away from Thailand but it can update global earthquake events faster than those of the other networks. For the earthquake catalogue of EMSC, there were a lot of small earthquakes recorded by this network. These events occurred surrounding Thailand especially in northern Sumatra Island away from local network of TMD. EMSC is the global network that is closer than other networks. Therefore, it can better detect and record these events. According to Fig. 3.5, the earthquake catalogue of TMD can record earthquake events with wide range of magnitudes, espectually micro earthquakes while other catalogues can mostly record only earthquake events with magnitudes more than 4.0.

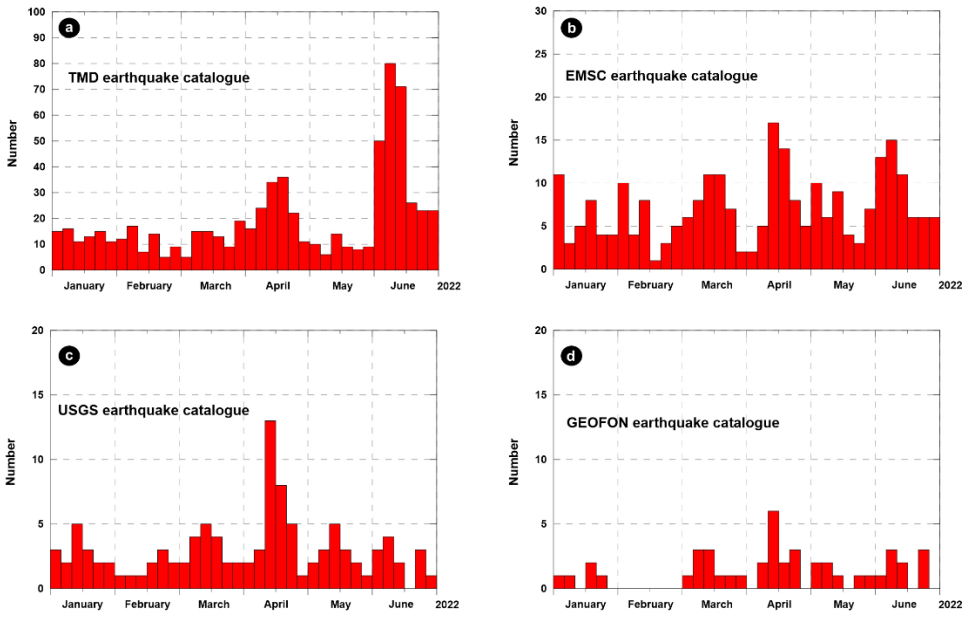

Fig. 3.4. Graphs showing the number of earthquakes in Thailand and adjacent areas with temporal variation during January - June 2022 that were recorded continuously by the earthquake catalogues of a) TMD, b) EMSC, c) USGS, and d) GEOFON.

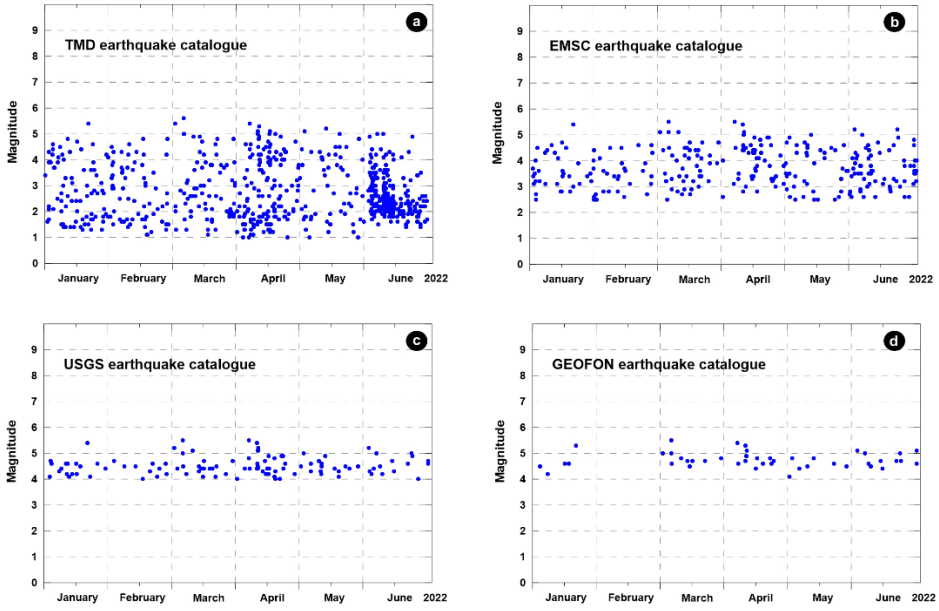

Fig. 3.5. Graphs showing earthquake magnitudes in Thailand and adjacent areas with temporal variation during January - June 2022 that were recorded continuously by the earthquake catalogues of a) TMD, b) EMSC, c) USGS, and d) GEOFON.

The spatial comparison of the earthquake catalogues of each agency indicate that during January - June 2022, TMD earthquake catalogue was able to record a large number of earthquakes in northern Thailand, Myanmar, Laos, and Vietnam while the earthquakes in the vicinity of Nicobar-Andaman and Northern Sumatra Islands surrounding Thailand, can be more detected and recoreded by the other agaencies, i.e., EMSC, USGS, and GEOFON. With respect to the spatial distribution of earthquake events deteced by seismic network of TMD, They demonstrated unregulated distribution with no pattern particularly in Myanmar because these earthquake events were detected incompletely by the local network of TMD with low accuracy of earthquake locations whereas the global networks are away from the earthquake therefore they cannot effectively detect and record these events as illustrated in Fig. 3.6.

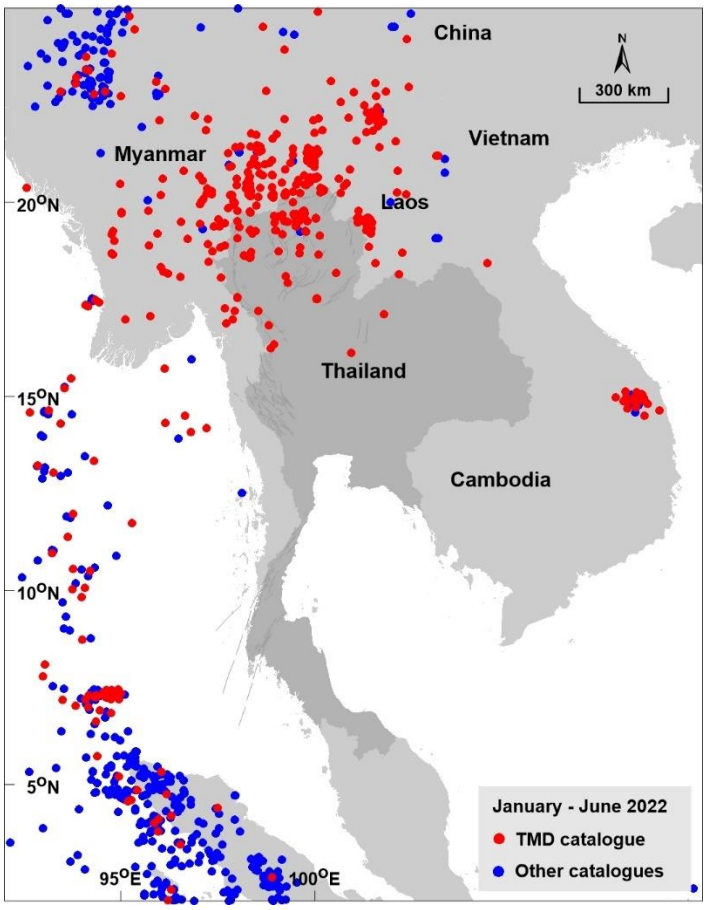

Fig. 3.6. Map showing the seismicity in Thailand and adjacent areas (2-25N, 92-110E) recorded during January - June 2022 from the earthquake catalogues of TMD (red circles) and other agencies (blue circles), i.e., EMSC, USGS, GEOFON.

Based on TMD earthquake catalogue during January - June 2022, there were both distant and local earthquakes (Fig. 3.7 and 3.8) occurred in Thailand and adjacent areas. For example, the distant earthquake of M5.4 occured in Myanmar that produced the seismic waves travelling to Thailand. They were detected and recorded obviously by seismic stations of TMD including CRMJ and SURI as the closest and furthest stations, respectively (up to 800 km) from the earthquake epicenter. The travel times of seismic waves from earthquake source in Myanmar to the northern part of Thailand were about 20 seconds. They took a long time enough for earthquake early warning from Myanmar before seimic waves with severe ground shaking arriving Thailand, particularly in major cities and Bangkok, the capital city of Thailand. Furthermore, the distant earthquakes can also produce long period ground motions that may be resonant with natural frequencies of tall buildings in Bangkok resulting stronger vibration.

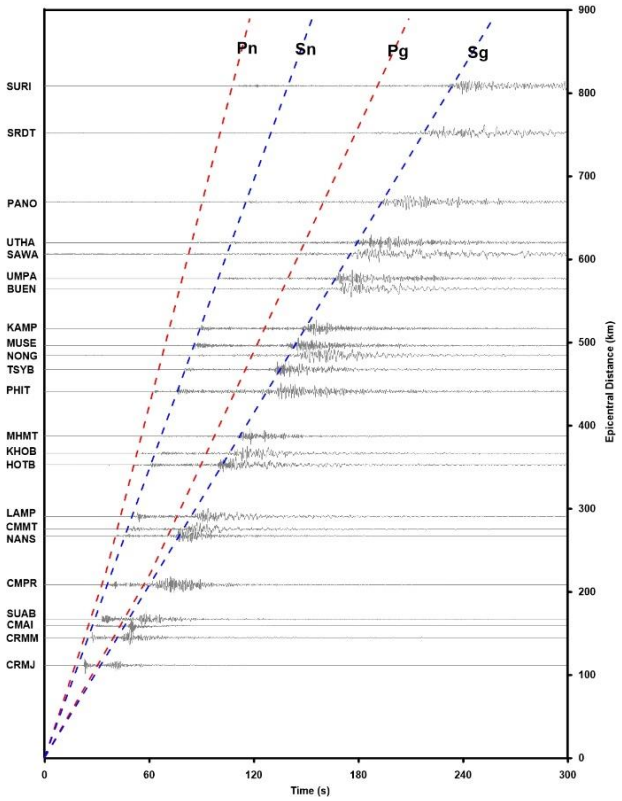

Fig. 3.7. Waveforms with the phase identification (dashed lines) of the M5.4 Myanmar (gray lines) were recorded by the velocity stations of TMD at the difference of epicentral distances in June 2022.

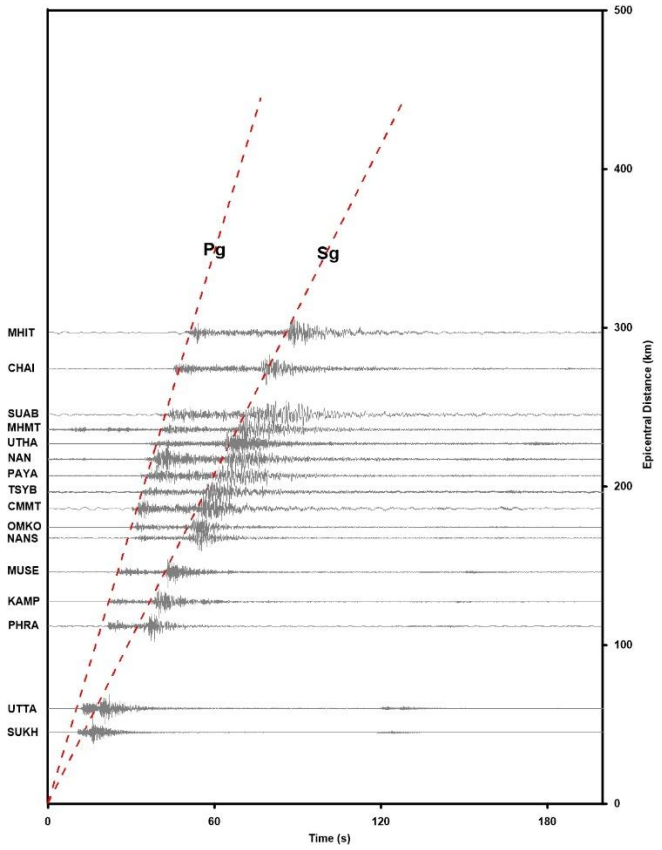

Fig. 3.8. Waveforms of M3.6 earthquake with the phase identification (dashed lines) in Uttaradit province, Thailand (gray lines), were recorded clearly by the velocity stations of TMD at the difference of epicentral distances in April 2022.

With respect to the local earthquake of M3.6 in Uttaradit province in the northern part of Thailand, the seismic waves traveled to the nearest station of TMD, i.e., SUKH within 10 seconds as illustrated in Fig. 3.8). This was difficult for early warning the local earthquake in Thailand. However, most of the earthquakes in Thailand, have small magnitudes with low level of ground shaking that no effect in the region. Previously, the micro to small earthquakes were not be detected and recorded completely by the seismic network of TMD because the small number of seismic stations that were not dense covering seismic sources in the region and they located far away from each other. So, it's possible to have earthquake sources in some areas that have not been discovered in Thailand. For example, although, there is no active fault published in the eastern part of Thailand, the small earthquakes were located in the area. This represents the capability of seismic network of TMD at the present.

3.2 Methodology

This procedure focuses on the analysis of seismic network accuracy of TMD during January - June 2022 according to the statistical methods for discrimination, i.e., Complexity (C) and Spectral Ratio (SR). Complexity technique is the ratio of integrated powers of the seismogram in the selected time windows while SR is ratio of integrated spectral amplitude of the seismogram in the selected frequency bands. These methods were employed in this study that suitable parameters for discrimination were determined using waveforms of seismic events of TMD with retrospective test. The obtained parameters were then used for classifying earthquake and blast in the region. The epicenters of probable blast were compared with the closest mine location for analyzing accuracy of TMD seismic network in Thailand (Fig. 3.9).

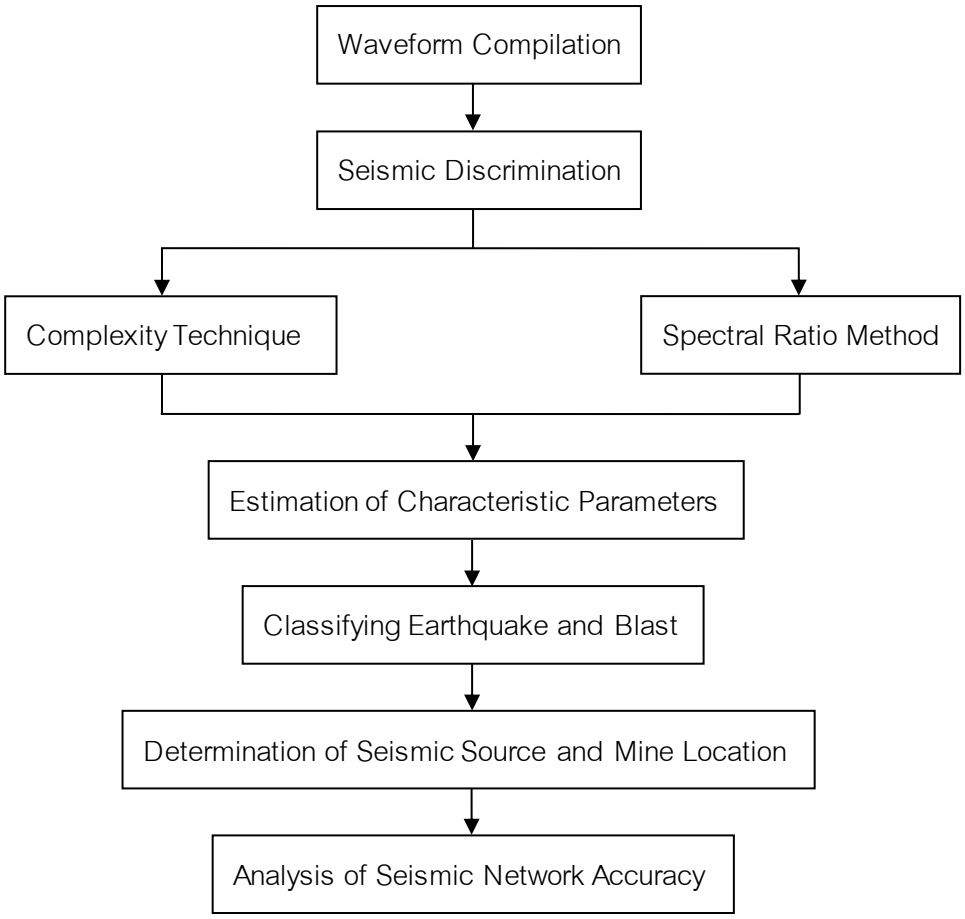

Fig. 3.9. Diagram showing the analysis of seismic network accuracy in January - June 2022 using waveform of the seismic events recorded by TMD seismic stations.

This flowchart displays analysis of seismic network precision of TMD during January - June 2022 based on the methods for investigating earthquake parameters, i.e., Root-Mean-Square (RMS) travel time residual and azimuthal gap. RMS were determined by comparison of the observed and calculated arrival times of seismic waves from an earthquake epicenter to each seismic station while Primary azimuthal gap is the largest gap between the azimuths of epicenter and stations representing the network geometry in a region. These parameters represent the precision of seismic network for calculating earthquake epicenter. In this study, seismic source zones that derivation of parameters characterizing the seismic activity, were identified in the study area for analyzing the spatial distributions of RMS and azimuthal gap. Moreover, both manual and automatic locations, were also compared together (Fig. 3.10).

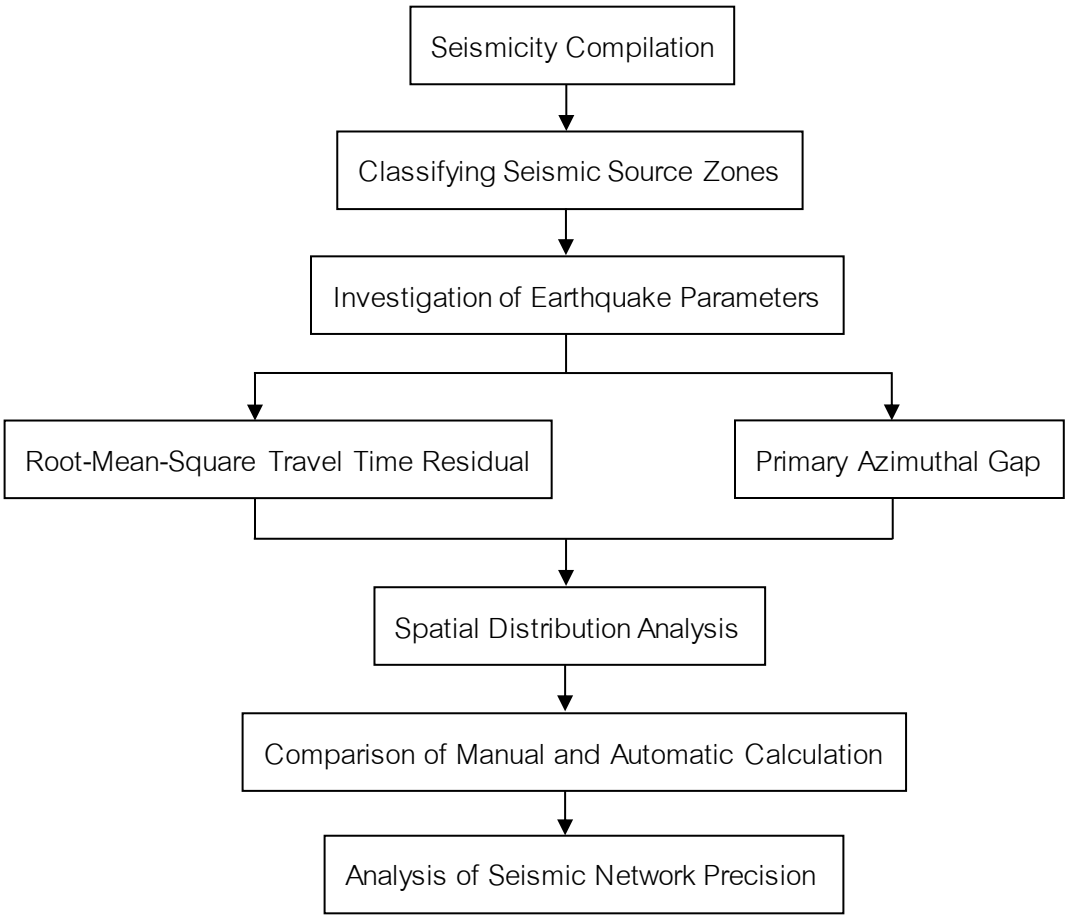

Fig. 3.10. Diagram showing the analysis of seismic network precision in January - June 2022 using earthquake parameters calculated from seismic network of TMD.

This step shows analysis of seismic network limitation of TMD during January - June 2022 with regard to methodology of improving TMD earthquake catalogue, i.e., Earthquake declustering and Investigation of man-made change. Earthquake declustering is the method for classifying main shock and aftershock applying statistical relationship of the magnitudes, origin times and locations of events. Theoretically, the magnitude of the main shock is larger than those of the subsequent aftershocks that these aftershocks typically are generated within the rupture area of main shock source. In this study, algorithm of Gardner and Knopoff (1974) was used to de-cluster and classify the events of main shocks in TMD earthquake catalogue. Then analyzing seismicity rate change in order to investigate events of man-made activities. Finally, the main shocks associated with tectonic activity were utilized to evaluate limitation of TMD network with magnitude of completeness (Mc) both spatially and temporally (Fig. 3.11).

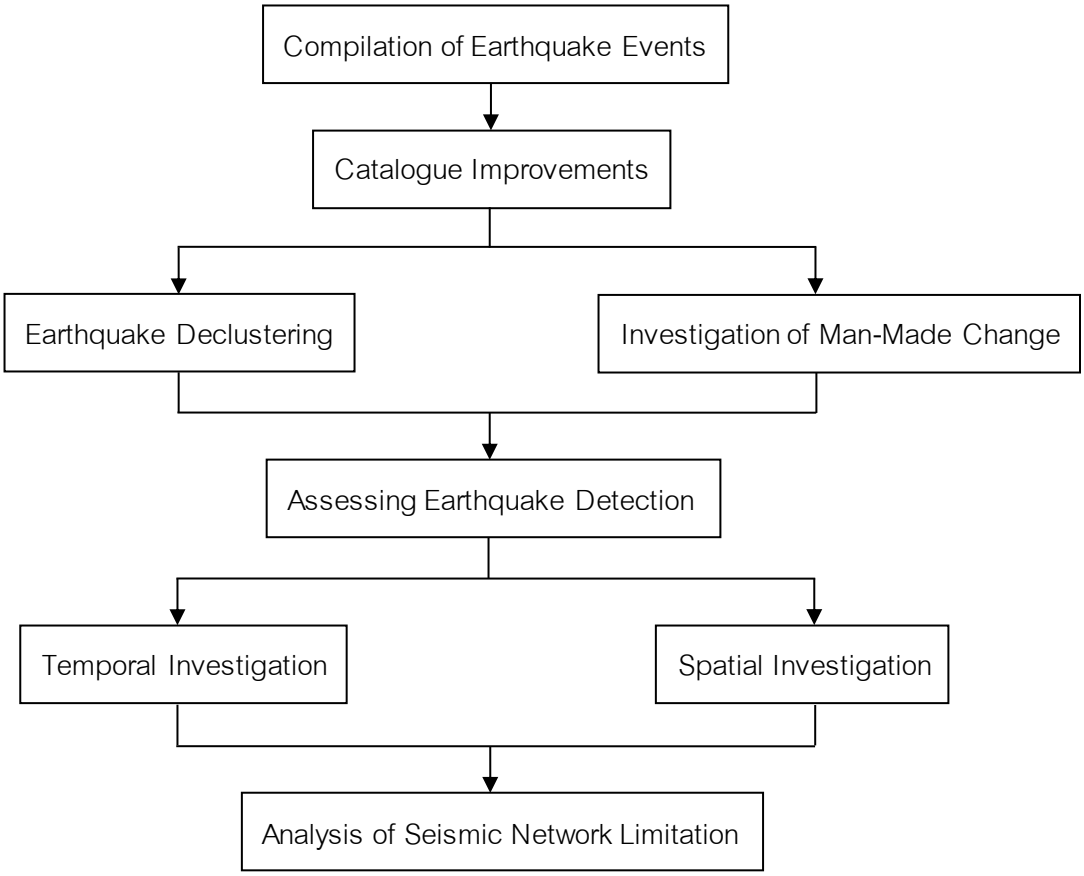

Fig. 3.11. Diagram showing the analysis of seismic network limitation in January - June 2022 using the seismicity obtained from the earthquake catalogue of TMD.

This procedure demonstrates the analysis of ambient noise around seismic stations that affecting TMD seismic network during January - June 2022. At first, the seismic signal recorded by TMD stations were employed to investigate noise levels using the methodology of Power Spectral Density (PSD) and Fourier Amplitude Spectra (FAS) including daily variation of ambient noise in the region representing Man-Made activities surrounding the sites that normally occur in day-time. Typically, the seismic signals at frequencies below 0.5 Hz indicate the ambient noise generated by oceanic and the large-scale meteorological sources while the waveforms with frequencies at 1 Hz and above 1 Hz mainly affected by wind and human activities surrounding seismic sites, respectively. The next step, characteristics of earthquake and noise were analyzed and compared for assessing the dominant frequencies representing the influence of seismic noise on the seismic network of TMD as illustrated in Fig. 3.12.

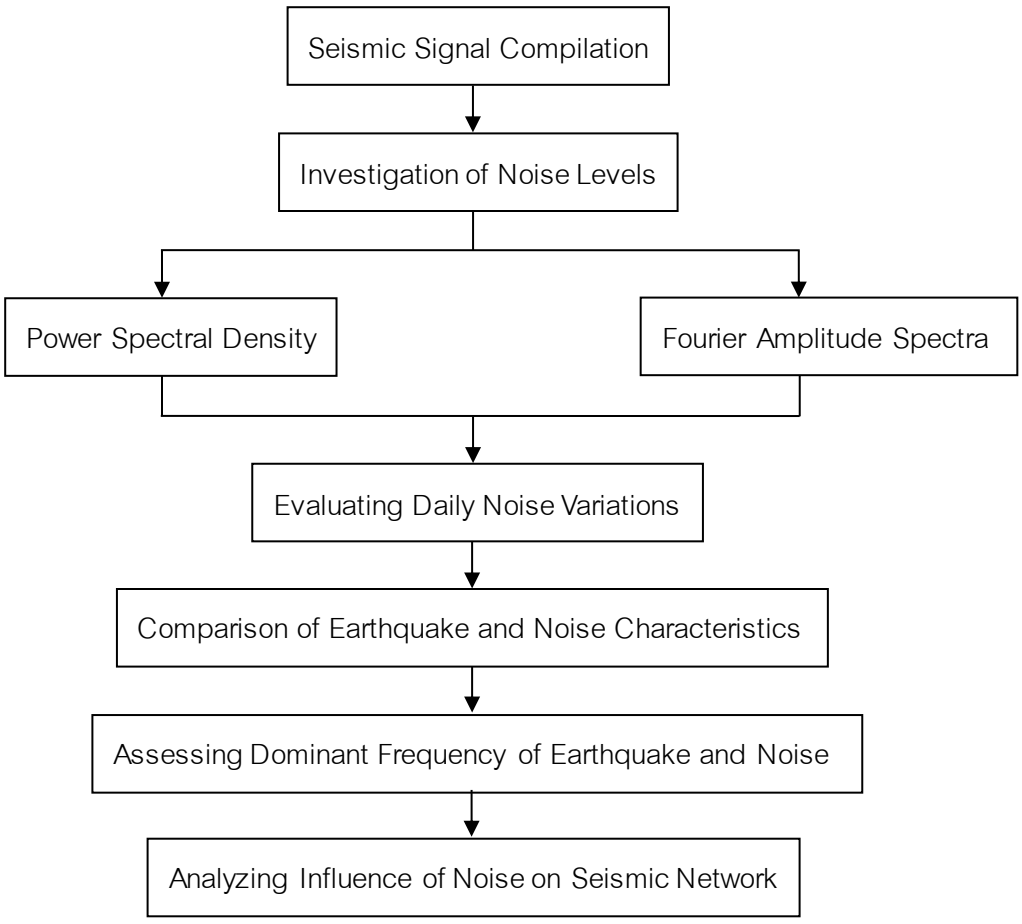

Fig. 3.12. Diagram showing the analysis of ambient noise that influence seismic network during January - June 2022 using seismic signals recorded by TMD stations.

This flowchart reveals analysis of the seismic network performance of TMD during January - June 2022. The earthquake parameters were determined for evaluating a capability of seismic network detection, i.e., peak ground acceleration (PGA) and first motion polarities. According to the earthquake events in Thailand and adjacent area, the waveforms detected by accelerograph stations and the velocity seismic stations of TMD were applied to determine the PGA and the first motion polarities, respectively. PGA at each seismic station demonstrate the attenuation of ground shaking normally depending on the epicentral distance from the seismic stations while the first motion polarities at each seismic station exhibit the direction of movement of active fault in the vicinity of earthquake epicenter known as Focal Mechanism. In this study, the PGA and first motion polarities were employed to calculate Shake Map and Beach Ball diagram, respectively in order to verify performance of TMD network (Fig. 3.13).

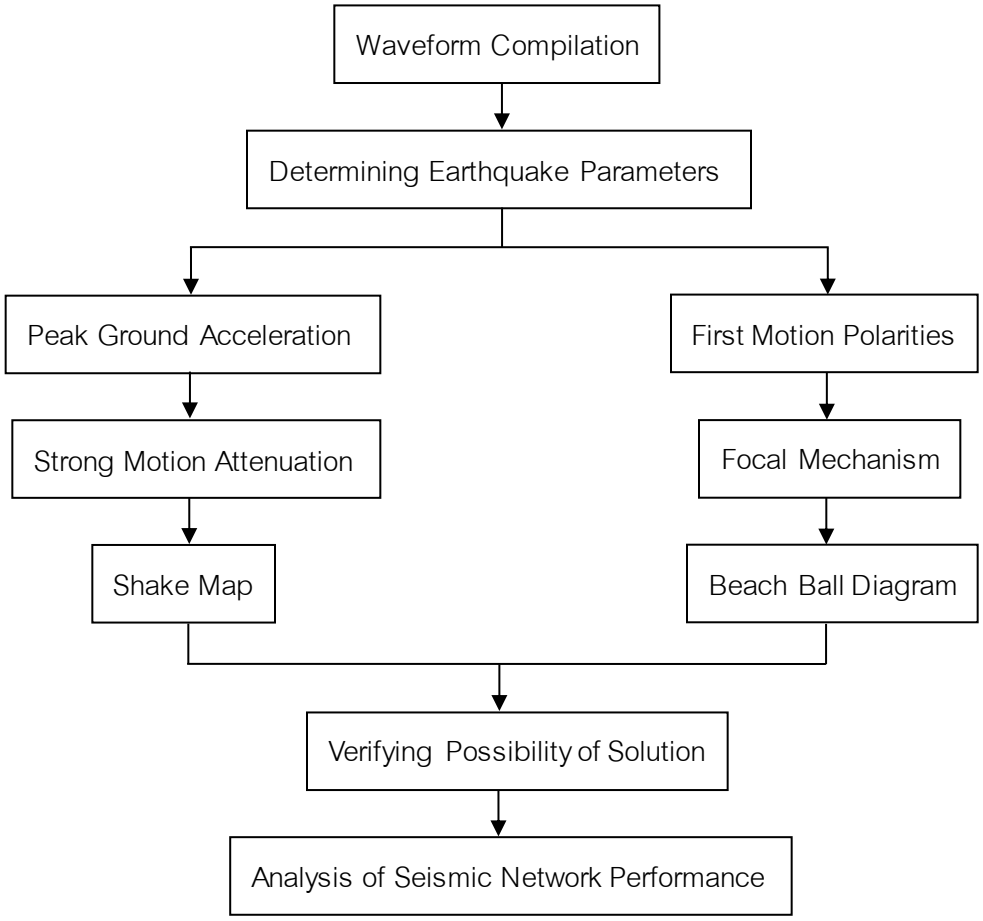

Fig. 3.13. Diagram showing analysis of seismic network performance in January - June 2022 using waveforms of earthquake events recorded by the stations of TMD.

CHAPTER IV
ANALYSIS OF TMD SEISMIC NETWORK

4.1 Accuracy of TMD seismic network

In this study, the 400 microseismic events with local magnitudes of 1.0-3.4 located in northern Thailand particularly around the Mining area were detected by TMD seismic network in the region during January - June 2022, were statistically discriminated between the mining blasts and the tectonic events by using the relationship between origin time and locations of the seismic events. A LAMP station of TMD network is closest a Mae Moh Mine approximately 30 km and is adjacent to the active faults in the region. Therefore, LAMP station was able to clearly detect both the waveforms generated by mining blasts and earthquakes whereas the other stations in study area, i.e., CMMT, LPSP, PHRS, and PHRA were not able to completely detect the events with magnitude less than 2.0 (Fig. 4.1).

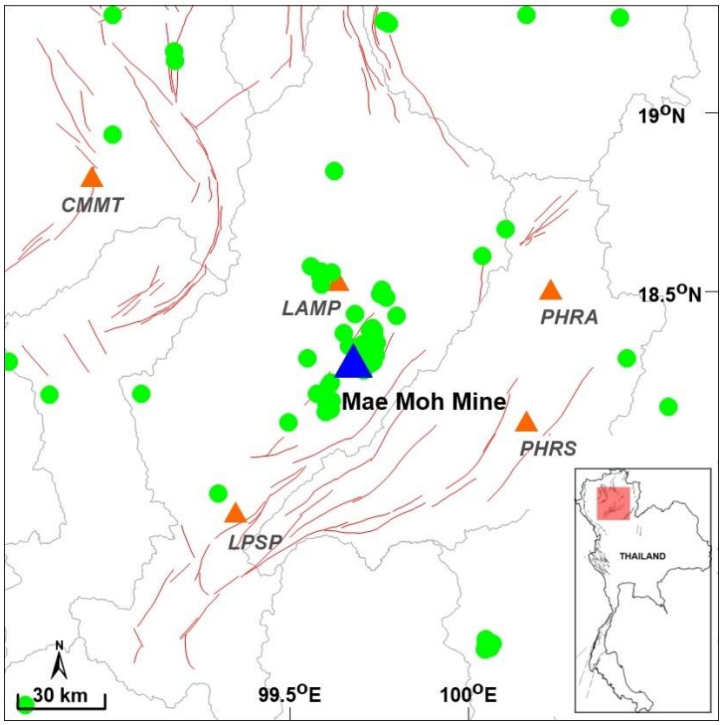

Fig. 4.1. Map showing microseismic events (green circles) with active faults (red lines) surrounding Mae Moh Mine (blue triangle) in Lampang province detected by the velocity stations (orange triangles) of TMD network in January - June 2022.

According to the locations of seismic events in this study, the depths of events were calculated manually using the software with the grid search method that the suitable depth resulting the travel time of seismic wave recorded by the seismic station is closest to the travel time obtained from the model. The calculated depths of events in this study are about 0 - 10 km below the ground surface (Fig. 4.2) associated with both intraplate seismic activity and geological structure in the region. However, the depths of seismic events that less than 1.0 are possible to generate by the mining blast in the area. Therefore, in this study, the seismic events with the depth less than 1.0 were investigated with the locations of mines in the area.

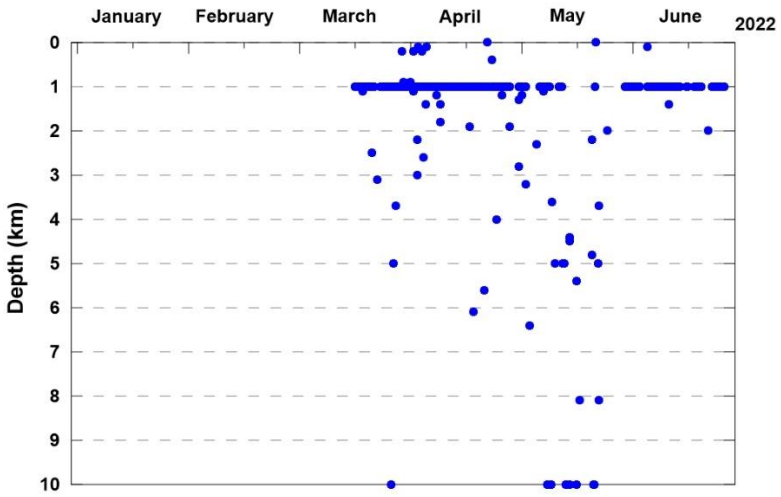

Fig. 4.2. Graph showing the depths of seismic events (blue circles) in the northern part of Thailand surrounding the mining area that detected by the seismic network of TMD during January - June 2022 and calculated manually by the software.

Furturemore, the waveforms of the seismic events recorded by TMD seismic stations, were also investigated with the waveform of the earthquake in the area. Theorotically, the waveform genearted by mining blast exhibit the dominant amplitude of P-wave comparing to the waveform generated by the earthquake event as demonstreated in Fig. 4.3. However, the seismic events in this study have small magnitudes that the P-wave of these events may not be created dominantly. Consequently, the locations, depths, origin time of the seismic events including characteristic of waveforms were utilized for discriminating between the earthquake events and seismic events generated by mining blast during January - June 2022.

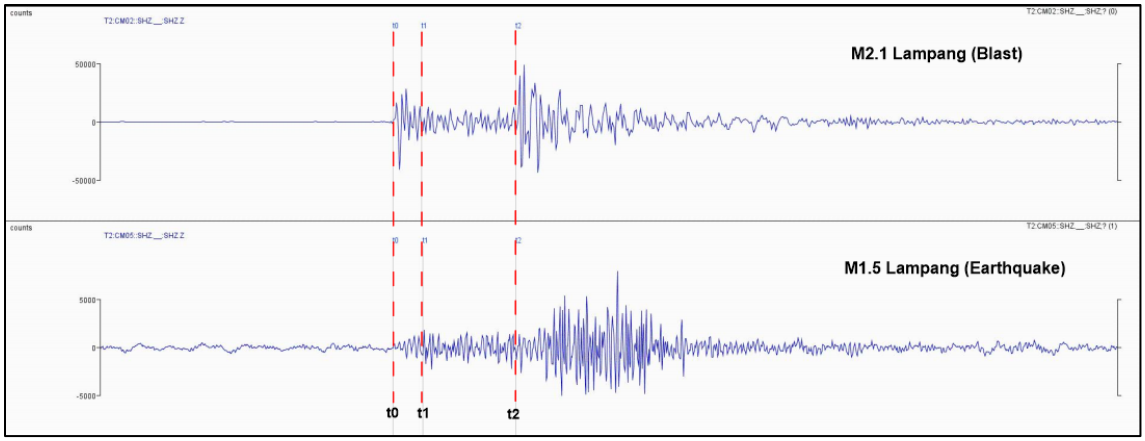

Fig. 4.3. Comparison of the characteristic of waveform generated by earthquake event (below) and miming blast (above) recorded by LAMP station of TMD network.

The results obtained from analyzing 400 seismic events recorded by a LAMP station of TMD network surrounding Mae Moh Mine in Lampang province during January - June 2022 indicate that the probable seismic events generated by the mining blast based on location, depth, origin time, and characteristic of the waveform, were located within approximately 7.5 km from the Mae-Moh mine. Generally, the locations of mining events should be close to the location of the mine. Therefore, in this study, locations of probable miming events calculated by seismic system of TMD, were compared with location of the Mae Moh Mine for determining the accuracy of TMD seismic network. This study found that locations of the probable mining events was closest at 3.1 km from the mining location (Table 4.1) representing the highest accuracy of seismic network of TMD during January - June 2022. However, there were some probable mining events located far away from the mining location, especially, at the distance more than 5 km. This indicates that the accuracy of TMD seismic network is low that may be caused by some of the seismic stations around the mining area have some problem that the waveforms cannot be detected by the seismic stations of TMD or the seismic signals are not clear resulting a small number of the seismic data was employed for calculating the location of mining events. However, most of probable mining events were still located at the distance less than 7.5 km form the mining location (Fig. 4.4) that is acceptable for determining seismic source and monitoring the earthquake hazard in Thailand and adjacent areas.

Table 4.1. Investigation of accuracy of TMD seismic network during January - June 2022 using the epicenters of mining events and location of Mae-Moh mine.

Events	Date	Time	Mag	Depth	Accuracy (km)
1	14-06-2022	04:19:55	1.4	1	3.087
2	23-03-2022	04:51:28	1.6	1	3.325
3	16-06-2022	04:13:31	1.4	1	3.472
4	15-06-2022	03:14:59	1.6	1	3.551
5	04-04-2022	03:34:27	1.8	1	3.563
6	07-06-2022	07:49:53	1.5	1	3.658
7	22-03-2022	07:52:05	1.6	1	3.705
8	13-06-2022	04:35:41	1.6	1	3.705
9	26-04-2022	09:57:24	1.5	1	3.711
10	18-03-2022	09:16:09	1.5	1	3.783

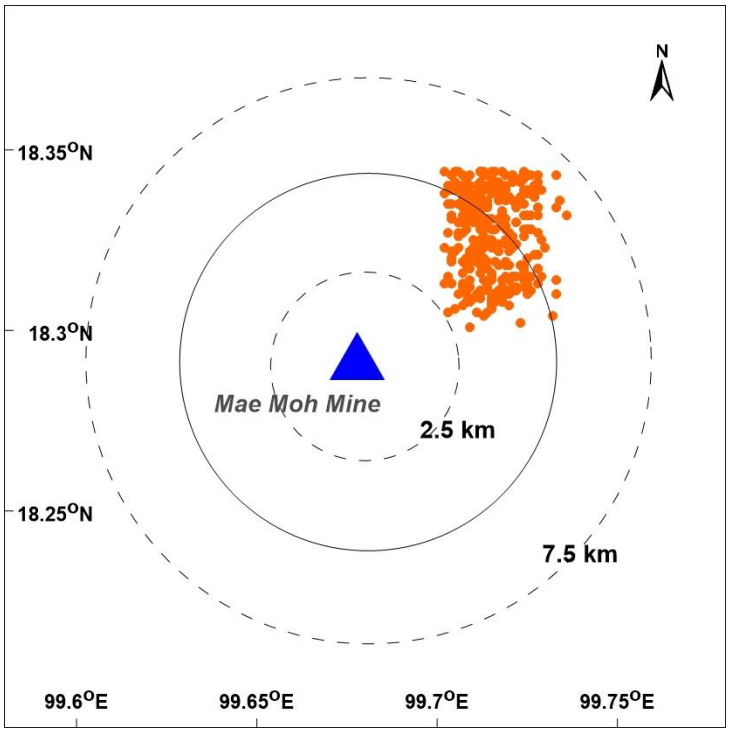

Fig. 4.4. Map showing a spatial distribution of blast epicenters (red circles) compared to the location of Mae-Moh mine (blue triangle) as the real source of those events representing accuracy of TMD seismic network during January - June 2022.

4.2 Precision of TMD seismic network

In this study, 8 seismic source zones in Thailand and adjacent areas were classified by tectonic activities in the region that consist of A) Northern Thailand, B) Western Thailand, C) Jinghong-Mengxing, D) Sagaing Fault Zone, E) Dein Bein Phu Fault Zone, F) Sumatra-Andaman Interplate, G) Red River Fault Zone, H) Sumatra Fault Zone. These events were located manually by seismic network of TMD during January - June 2022. Tectonically, the earthquake epicenters should be located systematically along the active faults in the region. However, the earthquake epicenters in study area were distributed uncertainly covering the seismic source zones (A-H) representing these events were not calculated precisely by TMD seismic network. Particularly, the earthquake events within the seismic source zones of F were recorded incompletely with a small number of earthquake events, that because these zones were away from Thailand and not covered by the seismic network of TMD (Fig. 4.5 and Table 4.2) affecting RMS residuals and azimuthal gaps of the events in a region.

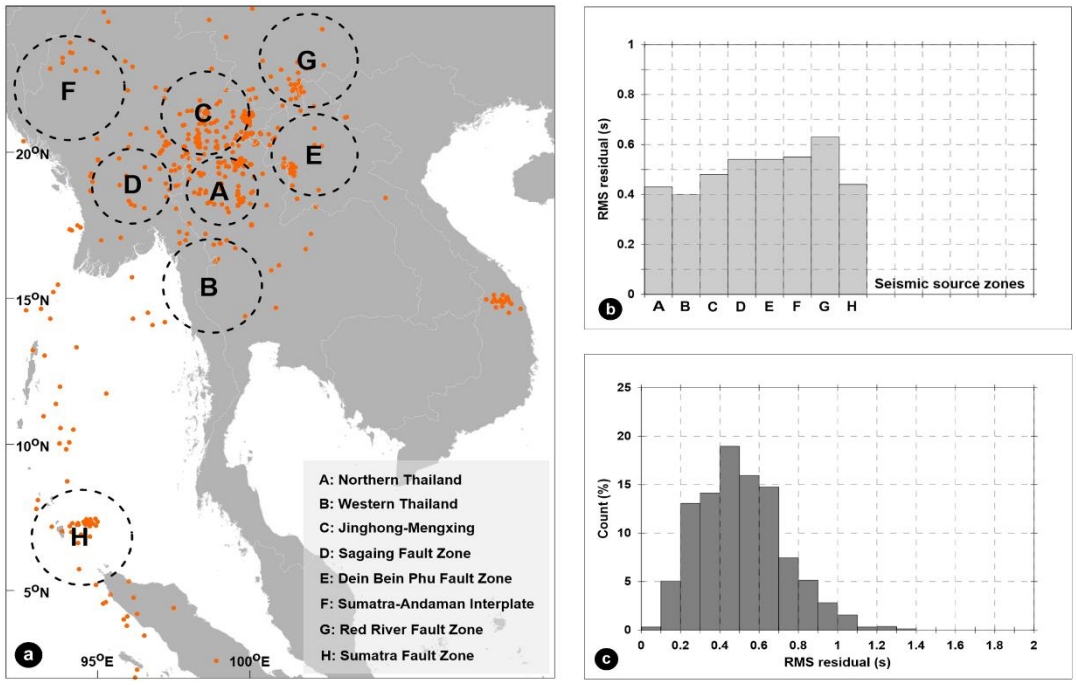

Fig. 4.5. a) Distribution of seismicity (orange circles) in the study area recorded by TMD network during January - June 2022 with b) the comparison of average RMS in 8 seismic source zones (dashed circles) and c) RMS counts of all events.

Table 4.2. The parameters indicate precision of TMD network within 8 seismic source zones.

Zone	Radius (km)	Number of Eq.	RMS (sec)	Azimuth Gap (Deg.)
A	Northern Thailand	905	0.43	123.21
B	Western Thailand	3	0.40	116.67
C	Jinghong-Mengxing	439	0.48	216.09
D	Sagaing Fault Zone	21	0.54	252.91
E	Dein Bein Phu Fault	42	0.54	224.55
F	Sumatra-Andaman	6	0.55	204.50
G	Red River Fault	31	0.63	266.32
H	Sumatra Fault Zone	32	0.44	270.81

According to the RMS residual in the region, the zone A and B of northern and western Thailand, respectively have the lowest RMS residual (0.4 sec) comparing to the other zones. This represents that the precision of TMD network in northern and western parts of Thailand is higher than those of the others. However, the RMS residuals of each zone during January - June 2022 are not different significantly in the range of 0.4-0.6 sec as demonstared in Fig. 4.5 and Table 4.2. With regard to the primary azimuthal gaps in this study area, the events located in northern and western parts have the low azimuthal gap of less than 130^{o} (compared to other source zones). This represents that the earthquake epicenters in these areas were surrounded appropriately by the seismic stations (Fig. 4.6) with high precision of the seismic network of TMD. However, there were several areas that the azimuthal gaps higher than 180^{o} particularly in the zones of the boundary of Thailand and outside Thailand. According to Fig. 4.7, there were also some areas in Thailand with high azimuthal gap (higher than 180^{o}), i.e., Nan. This indicates that the seismic stations was not cover sufficiently in these areas and may affect the precision of TMD network. According to the azimuthai gaps of seismic network of TMD in the zone of Chiang Rai province and the northern part of Lampang are less than 100^{o} as shown in the yellow zone in Fig. 4.7. This represents that the TMD seismic stations located satisfactory surrounding the earthquake sources in these areas that can be used for detecting earthquake events and determining earthquake parameters effectively.

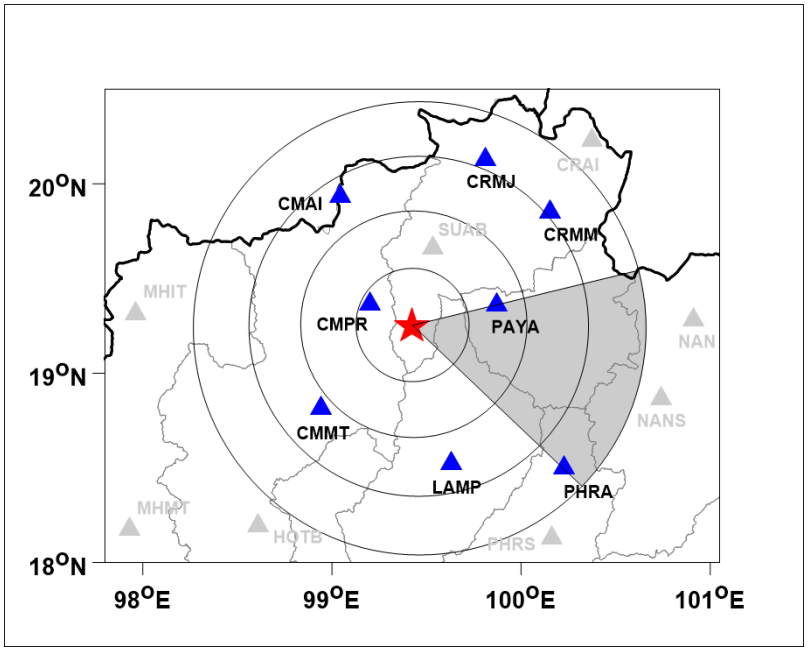

Fig. 4.6. Example of determining primary azimuthal gap (shaded area) of velocity seismic stations (blue triangles) of TMD network surrounding the earthquake epicenter (red star) recorded in the northern part of Thailand during January - June 2022.

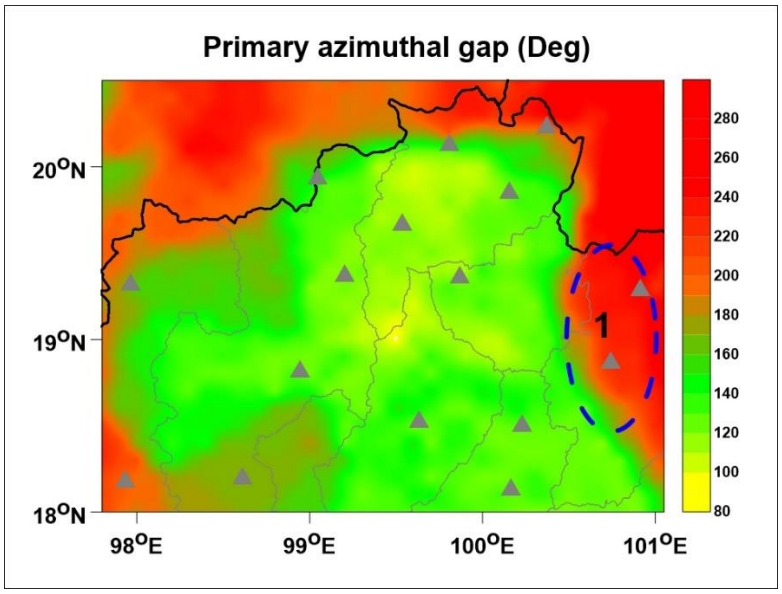

Fig. 4.7. Distribution of primary azimuthal gaps (colored zones) of TMD seismic network in northern Thailand in January - June 2022, indicated the areas of significant azimuthal gaps (dashed circles) representing precision of TMD seismic network.

In order to investigate precision of automatic analysis of TMD seismic network during January - June 2022, the waveforms of the earthquakes generated away from Thailand were identified automatically P-phases by the seismic network of TMD (Fig. 4.8). These waveforms were employed to compare the difference of P-phase picking by automatic and manual analysis. The results indicate that P-phases picked automatically and manually were different with travel time residuals of 0.1 - 3.2 seconds revealing dislocation of earthquake in the range of 0.7 - 25.2 km. Based on the stations used in this study, CMPR has the lowest precision for identifying P-phase automatically at the dislocation of 25.2 km while UTHA has the highest precision at the dislocations of 0.7 km as shown in Table 4.3.

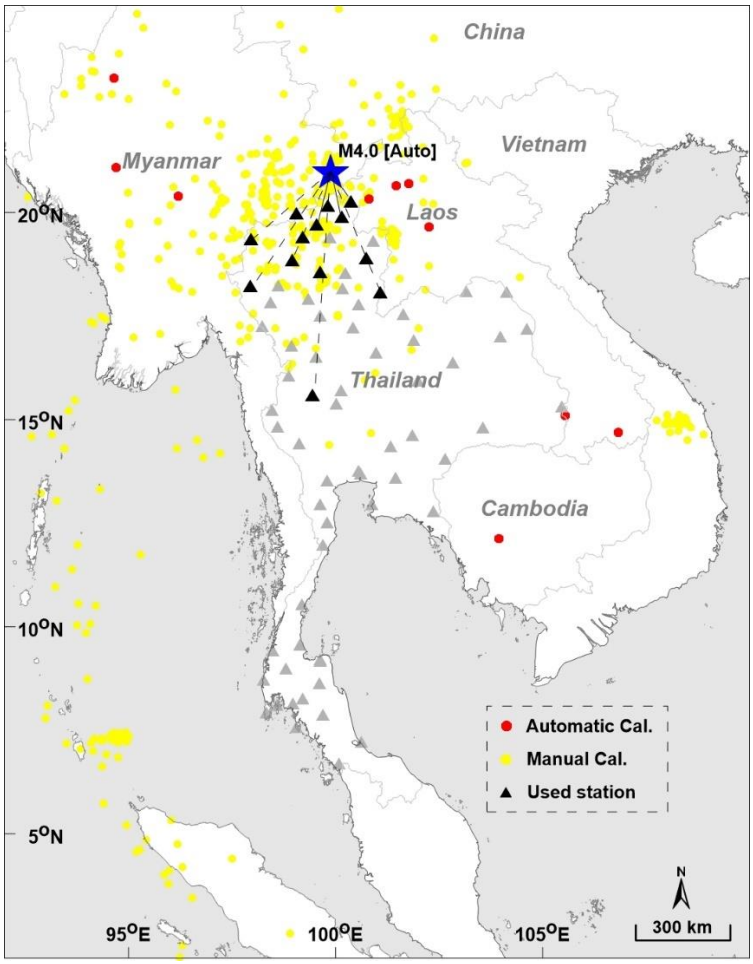

Fig. 4.8. Map showing locations of events automatically and manually calculated by TMD network during January - June 2022 (red and yellow circles, respectively). The blue star is automatically calculated events using TMD stations (black triangles).

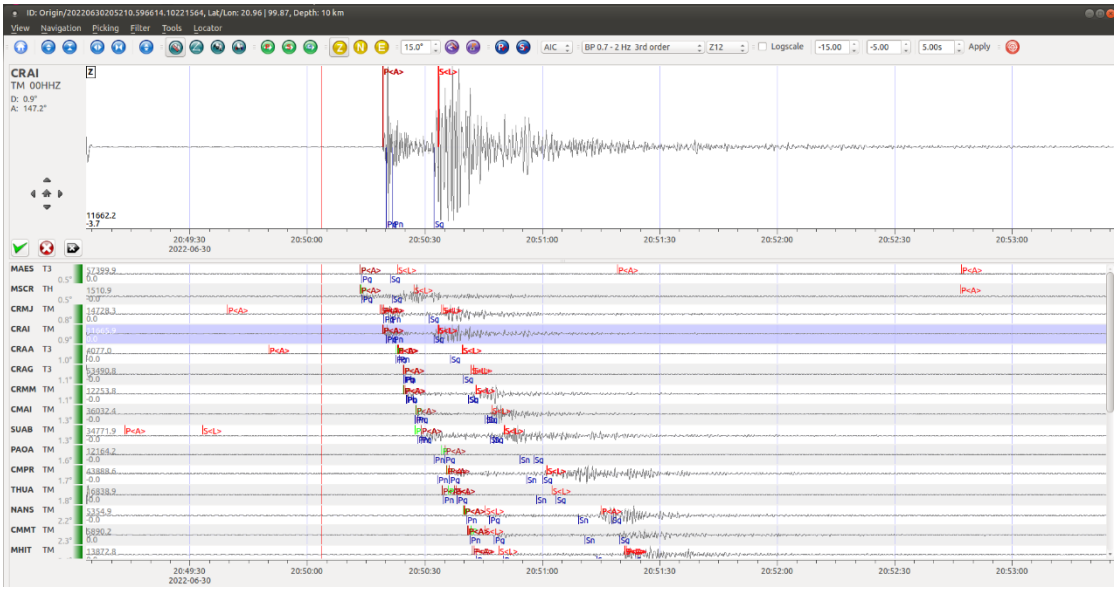

Fig. 4.9. Graph showing waveforms of event recorded at different epicentral distances with P-phase identified automatically (red lines) using SeisComP3 software.

Table 4.3. The parameters revealing precision of P-phase pickings identified automatically and manually by the seismic network of TMD during January - June 2022.

Station	Epicentral Dist. (°)	P-arrival time [Auto]	Travel time residual (s)	Azimuth (Deg.)	Dislocation (km)
CRMJ	0.83	20:50:19	0.54	184	4.3
CRAI	0.87	20:50:19	1.06	147	8.5
CRMM	1.14	20:50:25	0.02	166	0.2
CMAI	1.29	20:50:28	0.75	217	6.0
SUAB	1.34	20:50:29	1.39	193	11.1
CMPR	1.71	20:50:36	3.15	201	25.2
NANS	2.25	20:50:40	0.54	158	4.3
CMMT	2.32	20:50:41	0.63	202	5.0
MHIT	2.43	20:50:42	1.08	227	8.6
KHOB	3.14	20:50:53	0.30	158	2.4
MHMT	3.33	20:50:55	0.32	213	2.6
UTHA	5.42	20:51:24	0.09	184	0.7

4.3 Limitation of TMD seismic network

In this study, the seismicity in Thailand and adjacent areas detected by the velocity seismic stations of TMD from the past to December 2021 (Fig. 4.10) were employed to analyze the limitation of TMD seismic network. The completeness of earthquake events including both the magnitudes and numbers of earthquakes were recorded spatially indicating a capability of seismic network in the region. However, the seismicity used in this study consist of both main shocks and aftershocks that the increase of aftershocks in each area affecting the change of seismicity late associated with tectonic activity but were not able to represent a capability of earthquake detection of seismic network exactly. Therefore, the seismicity in the study area was decluttered using an algorithm proposed by Gardner and Knopoff (1974) for classifying main shocks and aftershocks in the region as illustrated in Fig. 4.11 and then the aftershocks events were be removed before evaluating limitation of TMD seismic network.

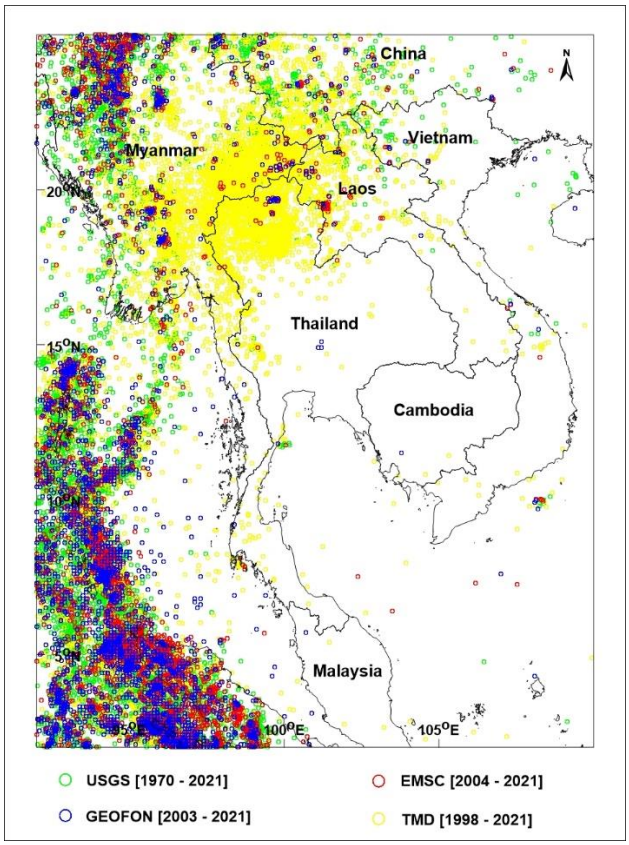

Fig. 4.10. Map showing the seismicity (circle symbols) in Thailand and adjacent areas recorded by various earthquake catalogues during 1970 - December 2021.

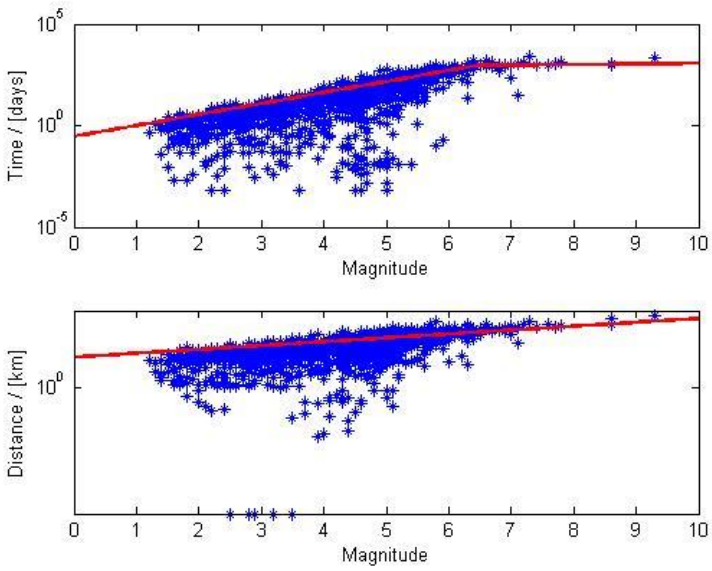

Fig. 4.11. Classification of earthquake events (blue symbols) consist of both main shocks and aftershocks by using the relationship of spatial distribution and temporal variation (red lines) of earthquakes in the study area.

Based on declustering of earthquake events in this study, the aftershock sequence normally generates in the specific region around the main shock epicenter and the number of aftershocks will decrease continuously in the limit of the time window. The relationship of aftershock distribution and temporal variation was utilized to decluster the earthquake events in Thailand and adjacent areas during 1970 - December 2021. The obtained results indicate that the 24,936 events were identified as the aftershocks or the same events from all of 30,079 earthquake events in this study. These aftershocks were removed from earthquake catalogue of TMD while 5.143 main shocks were employed to analyze limitation of TMD seismic network. This study found that the most of main shocks distributed in northern part of Thailand and the area of Thailand-Myanmar border representing a capability of earthquake detection of TMD seismic network in the region whereas there were a small number of earthquakes in the zones of western, eastern, and southern Thailand including Vietnam and Cambodia because there were a small number of active faults in the region. For a large number of earthquake events in Nicobar-Andaman and Sumatra Islands, they were mainly identified as aftershock events (Fig. 4.12). According to the earthquake magnitude variation, during 1970-1997, the most of

earthquakes were located with magnitudes in the range of 4.0-6.0 whereas the earthquakes during 1998-2021 were mainly detected with the magnitudes less than 4.0 (Fig. 4.13). This is because the TMD seismic network was installed in 1998 and has been operated continuously that were able to detect small earthquakes in the region. Furthermore, the microearthquakes with magnitudes less than 2.0 were recorded significantly after 2007 because the seismic network of TMD was upgraded from analog to digital system with an increased capability of earthquake detection. Consequently, the variation of earthquake magnitudes in Thailand and adjacent areas can represent the limitation of seismic network of TMD in each time period.

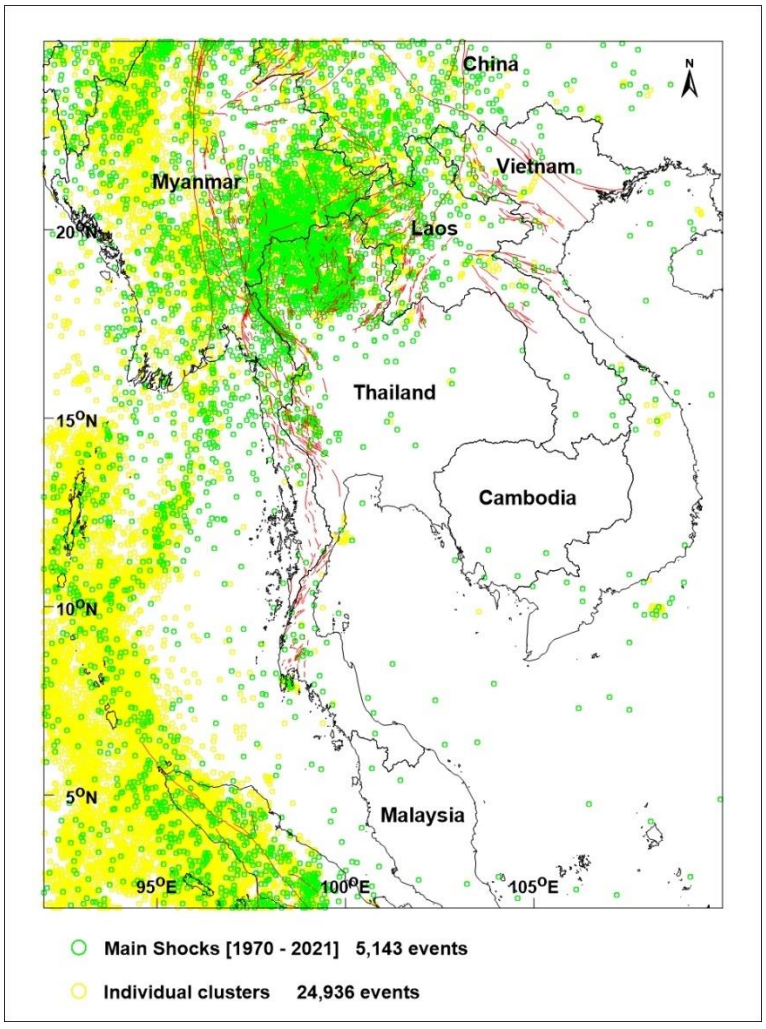

Fig. 4.12. Map showing distributions of main shocks and aftershocks (green and yellow circles, respectively) classified by algorithm mentioned above and recorded during 1970 - December 2021.

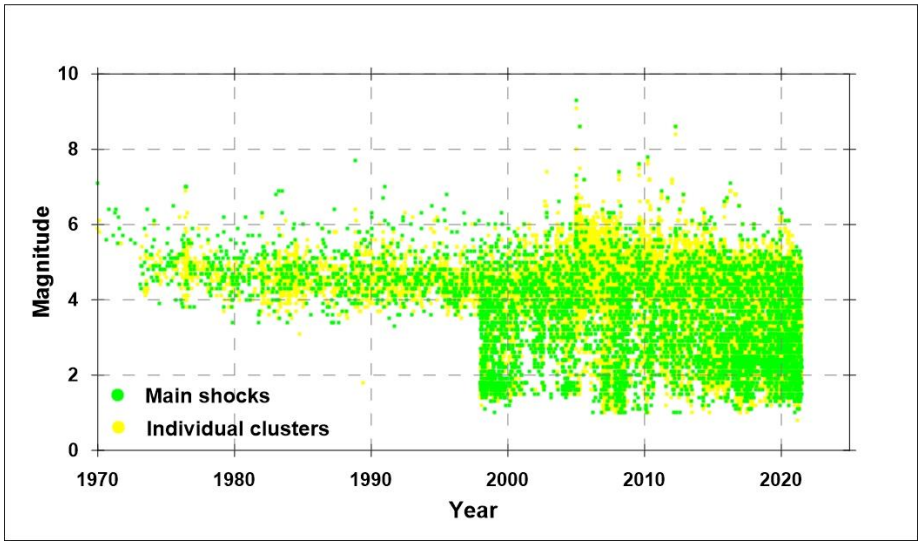

Fig. 4.13. Graph showing the temporal variations of earthquake magnitudes of both the main shocks and aftershocks (green and yellow circles, respectively) detected and recorded in the study area during 1970 - December 2021.

After removing aftershocks in earthquake catalogue of TMD, the cumulative number of main shock events against time should regularly increase as a straight line because the tectonic activities have gradually change for a long time. However, this study found that the line of cumulative number of main shocks was not straight exactly that was likely affected by man-made activities in the region such as increased and decreased seismic stations of TMD. This was able to be verified using the statistical method called Z-value indicating the change of seismicity rate in each time period. In order to avoid effect of human activities, the seismicity data within the time period that there was no change of seismicity rate, were employed in this study (Fig. 4.14). Finally, a cumulative number of main shocks that were not contaminated by man-made activities, looks like straight line (Fig. 4.15) representing tectonic activity exactly. Then, these seismicity as the completeness data with magnitudes larger than 4.0 since 2000, will be used to analyze limitation of TMD seismic network in this study. Although TMD seismic network can detect a lot of microearthquakes of magnitude less than 2.0 and record them for a long time, a number of these microearthquakes are sensitive with a capability of earthquake detection that depend on the increase or decrease of seismic stations in the region, especially the significant change of seismic network of TMD in 1998 as shown in Fig. 4.14 และ 4.15.

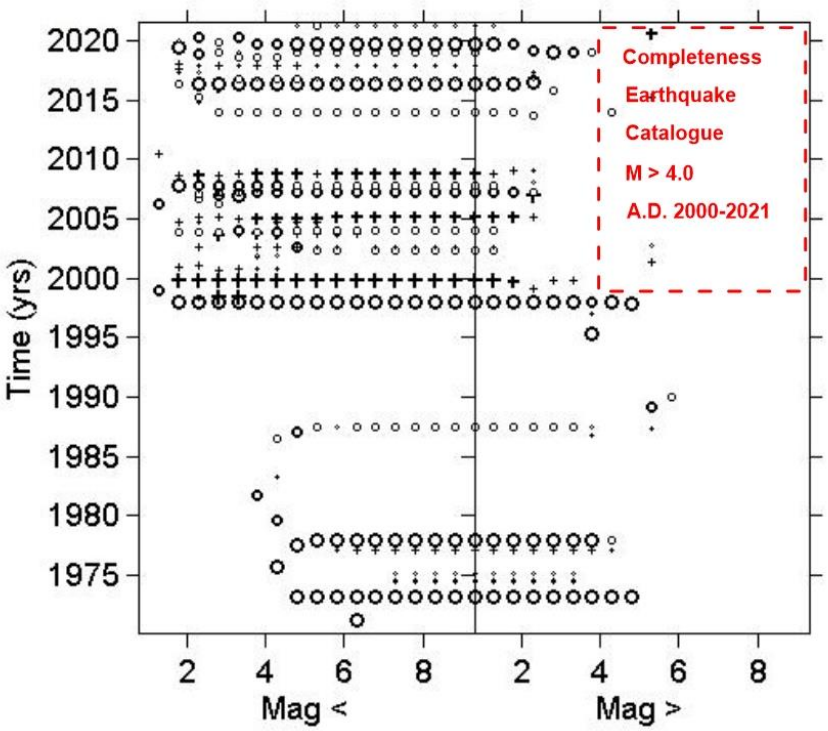

Fig. 4.14. Graph showing the seismicity rate changes against magnitudes both increase (plus) and decrease (circle) in study area during 1970 - 2021 with the zone of completeness for the earthquake catalogue of TMD (red square).

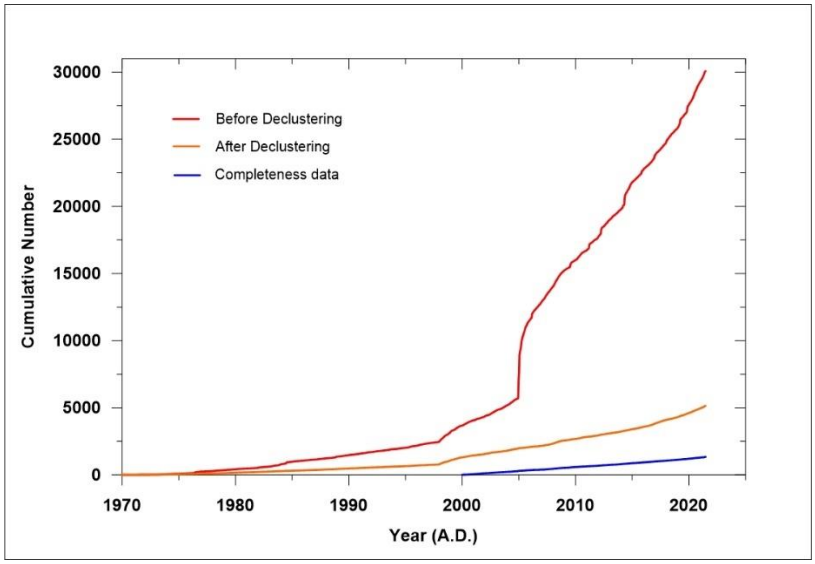

Fig. 4.15. Comparison of cumulative number of the events before and after declustering (red and orange lines, respectively) and cutting the events affected by man-made activity (blue line) in the study area during 1970-2021.

After improving the earthquake catalogue of TMD, the obtained main shock events were employed to evaluate spatially limitation of TMD seismic network during July - December 2021. In this study, the seismic source zones in Thailand and adjacent areas consist of A: Northern Thailand, B: Western Thailand, C: Jinghong-Mengxing, D: Sagaing Fault Zone, E: Dein Bein Phu Fault Zone, F: Sumatra-Andaman Interplate, G: Red River Fault Zone, H: Sumatra Fault Zone as demonstrated in Fig. 4.16. A number of earthquake events within each zone represented the tectonic activity in the region. In this study indicates that the zones of Thailand-Myanmar border in the northern part (zones I and J) have high seismicity that TMD seismic network was able to detect and record satisfactory during July - December 2021.

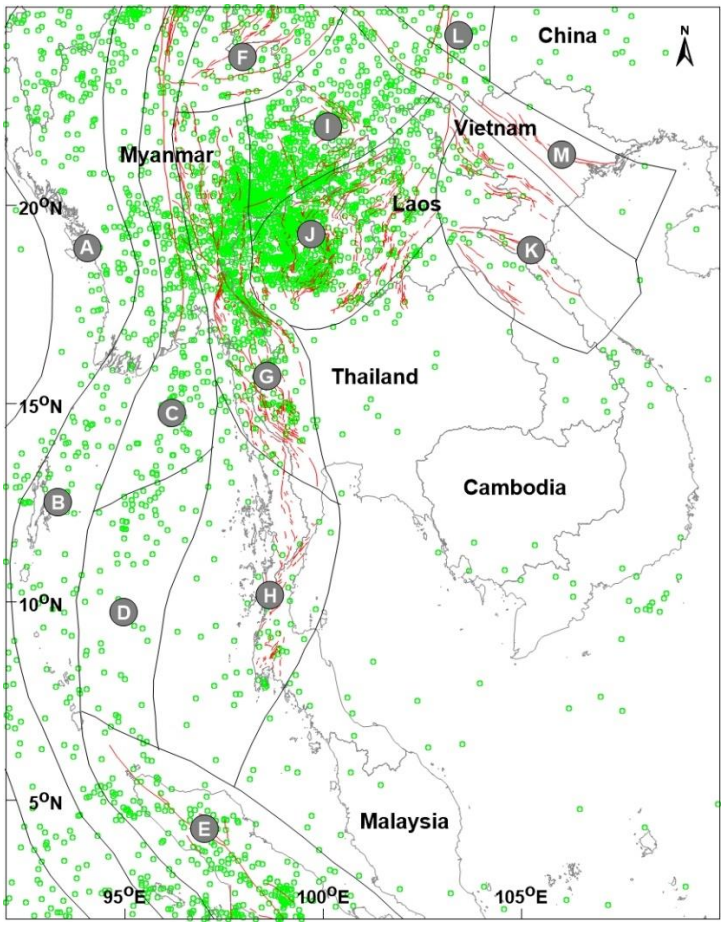

Fig. 4.16. Map showing the spatial distribution of the main shock events (green circles) that were detected and recorded during 2000 - December 2021 within the 13 seismic source zones (zones of A-M) covering Thailand and adjacent areas.

In order to analyze the limitation of TMD seismic network, the main shocks within 8 seismic source zones (zones A-H) were statistically investigated magnitude of completeness (Mc) according to relationship between cumulative number and magnitude of 40 main shocks detected within the area of 150 km-radius from the seismic source zone. The results indicated the seismic network of TMD had the highest efficiency with the Mc of 2.3 for detecting the earthquake events in northern Thailand that represent earthquake with the lowest magnitude of 2.3 detected and recorded completely. The results also illustrate the TMD seismic network was able to completely detect small earthquakes with magnitude of 4.8 in Sumatra-Andaman subduction zone known as the one of significant tsunami source of the world. Therefore, large earthquakes in this zone are also detected completely by the seismic network of TMD that accommodate for monitoring and warning tsunami generated by large earthquakes in the region. Moreover, the seismic source zones that are away from the TMD seismic network such as the Song Da - Song Ma fault (zone K) and Red River fault (zone M), have the Mc of 4.4 and 4.1, respectively indicating the seismic network of TMD can detect small earthquakes in distant areas (approximately 300 km from Thailand) as shown in Table 4.4 and Fig. 4.17.

Table 4.4. Magnitude of completeness (Mc) and a, b parameters calculated from number of earthquake events within the constrained radius of seismic source zones A-M.

Zone	Seismic Source	Events	Mc	a	b
A	Sumatra-Andaman Interplate	128	4.8	5.47	0.759 ± 0.08
B	Sumatra-Andaman Intraslab	164	4.4	4.94	0.665 ± 0.07
C	Sagaing Fault Zone	223	4.6	4.47	0.895 ± 0.10
D	Andaman Basin	55	4.7	6.45	1.040 ± 0.20
E	Sumatra Fault Zone	83	5.0	5.97	0.911 ± 0.20
F	Hsenwi-Nanting Fault Zones	91	4.5	5.85	0.921 ± 0.10
G	Western Thailand	698	2.8	4.07	0.548 ± 0.02
H	Southern Thailand	57	2.7	2.91	0.458 ± 0.06
I	Jinghong-Mengxing Fault Zones	630	3.1	4.11	0.495 ± 0.02
J	Northern Thailand – Dein Bein Phu	1176	2.3	3.98	0.532 ± 0.02
K	Song Da - Song Ma fault Zones	42	4.4	5.74	1.010 ± 0.20
L	Xianshuihe Fault Zone	17	NaN	NaN	NaN
M	Red River Fault Zone	33	4.1	4.26	0.693 ± 0.10

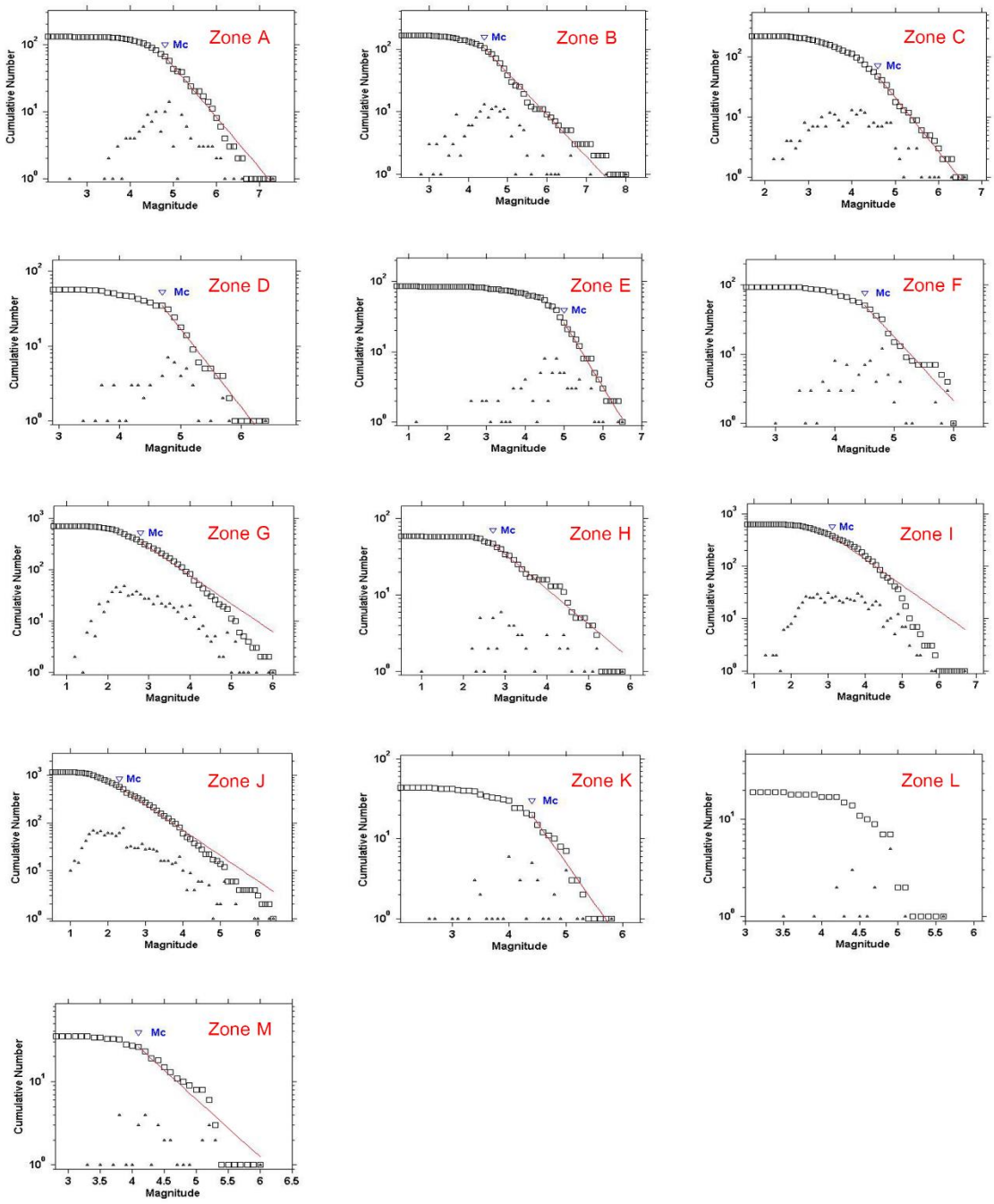

Fig. 4.17. Relationships of cumulative numbers and earthquake magnitudes (red line) indicating magnitude of completeness (Mc) of events recorded by TMD seismic network during 2000 - December 2021 within 13 seismic source zones (A-M).

According to the improved earthquake catalogue of TMD, main shocks during 2000 - 2021 were regarded as completeness of earthquake events representing exactly the tectonic activities in the region. Temporal variation of these events indicate the earthquakes detected continuously by seismic network of TMD since 2000 that the number of earthquakes were not different significantly in each time period excluding the events recorded in 2008 and after 2017. The increased events significantly in 2008 were possible to occur from the selection of algorithm for earthquake declustering that aftershocks are remained in this study whereas the increased events after 2017 were because the seismic network of TMD were improved and upgraded during this time period that can more detect earthquakes in the region (Fig. 4.18).

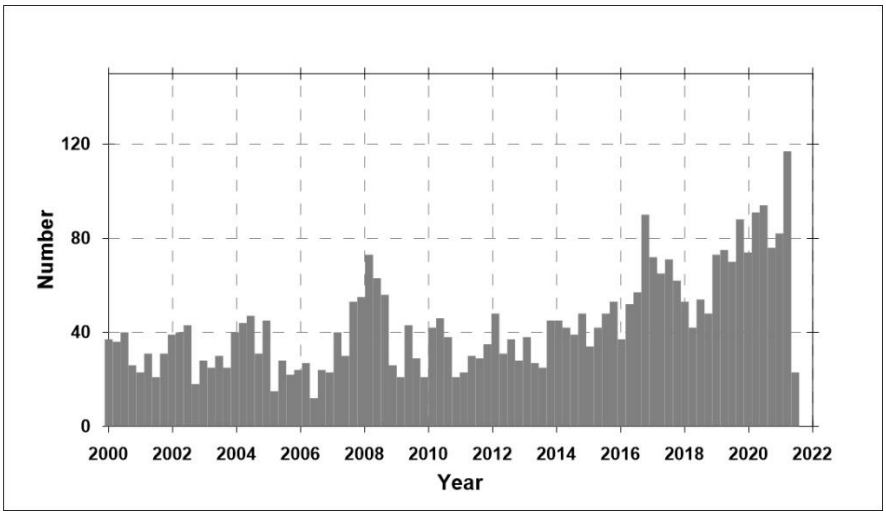

Fig. 4.18. Temporal variation of main shock events passing improvement of earthquake catalogue of TMD during 2000 - 2021.

As the Mc-value mentioned above were temporally calculated utilizing the whole of earthquake data in study area, this was interpreted as the efficiency of TMD seismic network for entirely detecting earthquake events in Thailand and adjacent areas that not constrained a specific area. Consequently, in order to intensively investigated limitation of TMD seismic network of each specific area, main shocks located within an area of 150-km radius from each grid node, were employed to calculate magnitude of completeness spatially with the grid size of 0.25 degrees covering the whole of study area. In this study, the regions were away from the seismic source zones with the number of main shocks were less than 30 events, were not

used to calculate the Mc-values because of obtained results were unreasonable representing the limitation of TMD network in the region. The results indicated the area of northern Thailand was able to completely detect events with lowest magnitudes of approximately 1.6 indicating the highest efficiency of seismic network of TMD during July - December 2021 in the region while the main areas of northern and western Thailand have Mc-values in the range of 2.0-2.5 (zones J and G) that the local magnitudes were larger than 2.5 can be completely detected covering the whole of northern and western Thailand. With regard to capability of earthquake detection in southern Thailand, the Mc-values were in the range of 3.5-4.5 (zone H) revealing efficiency of TMD network in southern part was lower than those of northern and western parts of Thailand because of a number of seismic stations installed in southern part were not dense (compared to the northern part of Thailand). Mc-map demonstrated the lowest efficiency of TMD seismic network within the Sumatra-Andaman subduction zone (zones A and B) that can completely detect only events with magnitudes lager than 5.0 as shown in Fig. 4.19.

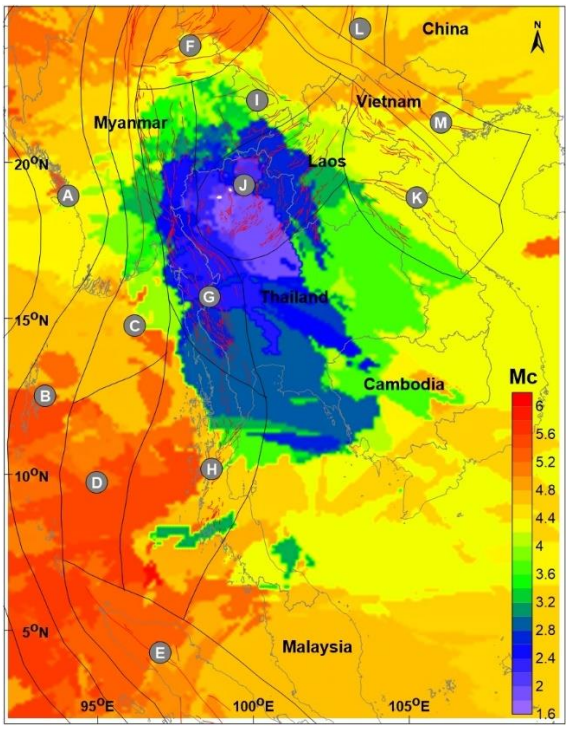

Fig. 4.19. Map showing spatial distribution of Mc-values representing limitation of seismic network of TMD during 2000 - December 2021 that red and blue zones indicate the high and low efficiencies of earthquake detection, respectively.

4.4 Ambient noise in TMD seismic network

In this study, the background noise around seismic stations of TMD during January - June 2022, were analyzed Power Spectral Density (PSD) for evaluating ambient noise levels around the sites. According to PSD analysis, broadband seismic stations throughout Thailand as shown in Fig. 4.20 were used to analyze the Power Spectral Density for assessing seismic noise levels around the sites. The obtained results illustrate that most of broadband stations have PSD variation of ground noise within the range of global noise model boundary defined by Peterson (1993) throughout the period of 0.1-100 seconds representing the suitable level of background noise that not affected seismic stations of TMD.

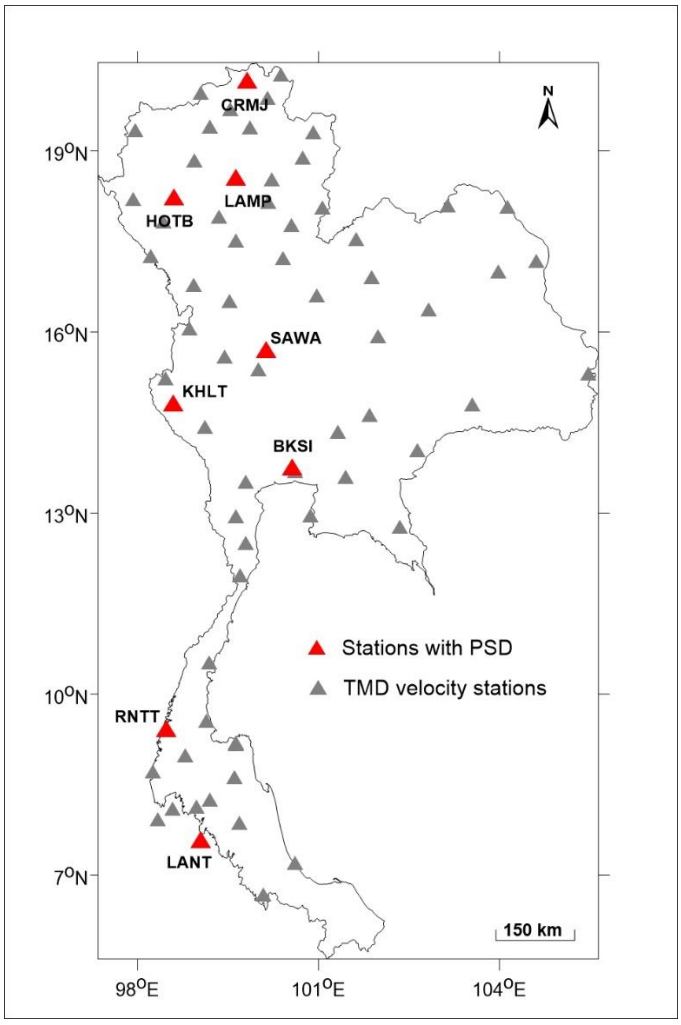

Fig. 4.20. Map showing velocity seismic stations of TMD (gray triangles) with broadband stations were investigated levels of background noise (red triangles).

However, there were some broadband stations of TMD that the PSD of ambient noise exceed the boundary of global noise model, i.e., BKSI and HOTB. Both of them located in the populated areas in the major city, indicating the waveforms of earthquakes recorded by these stations, may be affected by the background noise in the region. Typically, strong signals of noise lead to low efficiency of seismic network for detecting and recording earthquake events. According to PSD analysis in this study, the background noise with the highest PSD were found in short period of 0.1 - 1 sec (Fig. 4.21) representing human activities around the sites. Meanwhile, ambient noise generated from natural forces (generally around 1 - 10 sec) were not dominant in this study. Practically, the ambient noise can be filtered with the frequency of 1 -5 Hz for local earthquake making the waveform more clear to analyze effectively. However, the strong ambient noise in the frequency range of earthquake cannot be filtered causing the determination of earthquake parameters may be low efficiency.

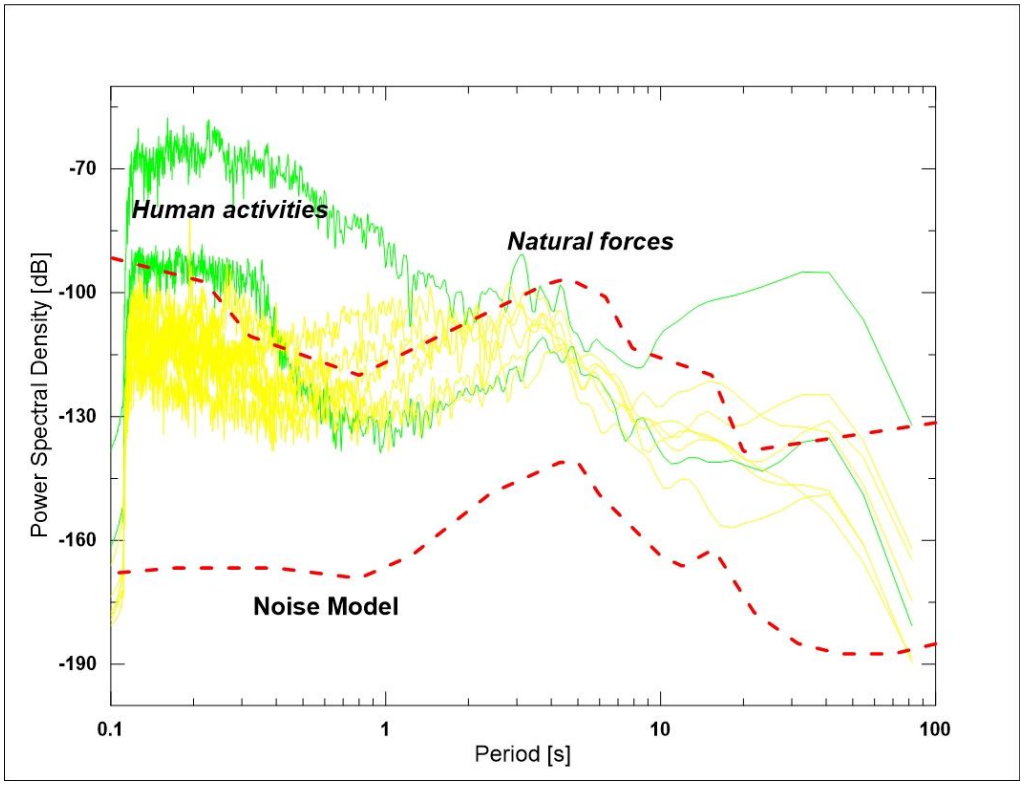

Fig. 4.21. Graph showing Power Spectral Density of ambient noise around broadband stations of TMD were displayed within (yellow lines) and over (green lines) the boundary of global noise model (dashed lines) defined by Peterson (1993).

4.5 Application of TMD seismic network

According to the previous work, many large earthquakes of magnitude more than 6.0 in the study area, were able to be detected and recorded by a seismic network of TMD, e.g., M6.0 in Laos (2007) and M6.8 in Myanmar (2011). However, these earthquake sources were located mainly outside Thailand away from the seismic stations of TMD. So, the applications of TMD seismic network have a low efficiency to determine the earthquake parameters, i.e., the location and magnitude of earthquake, focal mechanism, as well as the ground shaking attenuation in the region. Regarding a development of TMD seismic network with increasing of many seismic stations at present, the applications of TMD seismic network for determining the earthquake parameters in Thailand and adjacent area during January - June 2022, were carefully investigated in this study. The earthquake with M5.4 in Myanmar regarded as the largest event surrounding Thailand during the first 6 months of 2022 and M3.6 at Uttaradit as the event affecting Thailand, were employed to analyze the capability of application of TMD seismic network for determining earthquake parameters (Fig 4.22).

- The earthquake with magnitude 3.6 in Myanmar

The waveforms of the main shock events were able to be recorded clearly by the TMD velocity stations. The phases of waveforms of each station used in this study, can be identified conveniently by manual phase picking corresponding to the global velocity model (Fig. 4.23) Although this event has small magnitude with weak motion, the seismic waves of earthquake can be detected obviously around the earthquake source (within the radius of 300 km). The first phases of P-waves can be observed as first motions revealing polarities of the waveforms that were then utilized to calculate focal mechanism of this event. In this study, the first motion polarities were detected obviously by 16 seismic stations of TMD surrounding the earthquake epicenter, i.e., SRDT, UTHA, UMPA, SAWA, RATC, KAMP, MUSE, PHET, PBKT, TSYB, PATY, KRDT, CHAI, UTTA, SRAK, and MHMT stations. Based on locations of this event and velocity stations used in this study, the azimuth and the take-off angle of each station were calculated theoretically as shown in Table 4.5. These parameters were utilized together with first motion polarities (up and down) obtained earlier for calculating focal mechanism of M3.6 earthquake in the pattern of beachball diagram as demonstrated in Fig. 4.24.

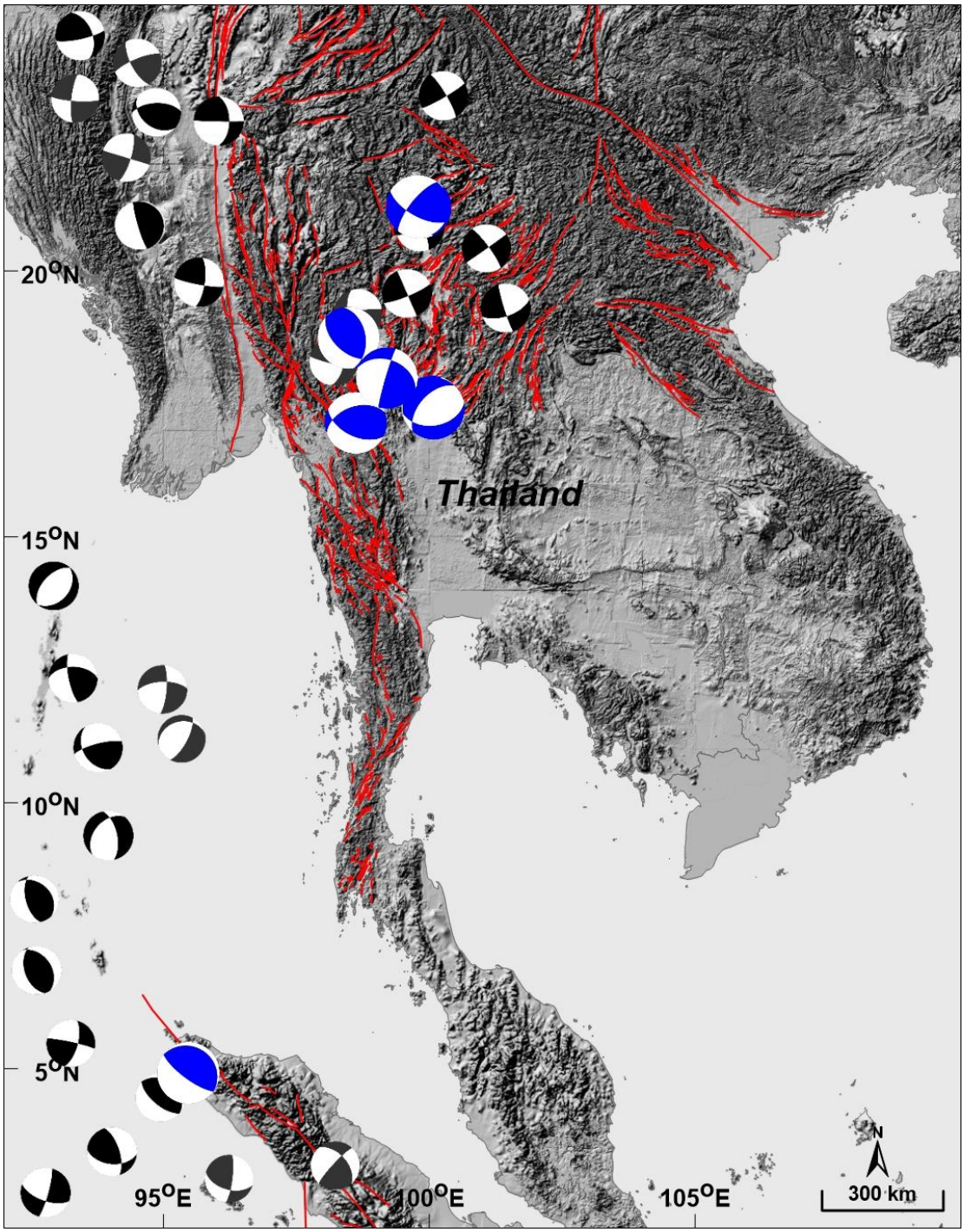

Fig. 4.22. Map showing epicenters and focal mechanisms (circle symbols) of earthquake events, particularly M3.6 and M5.4 calculated by the seismic network of TMD during January - June 2022. The red lines indicate active faults in the region.

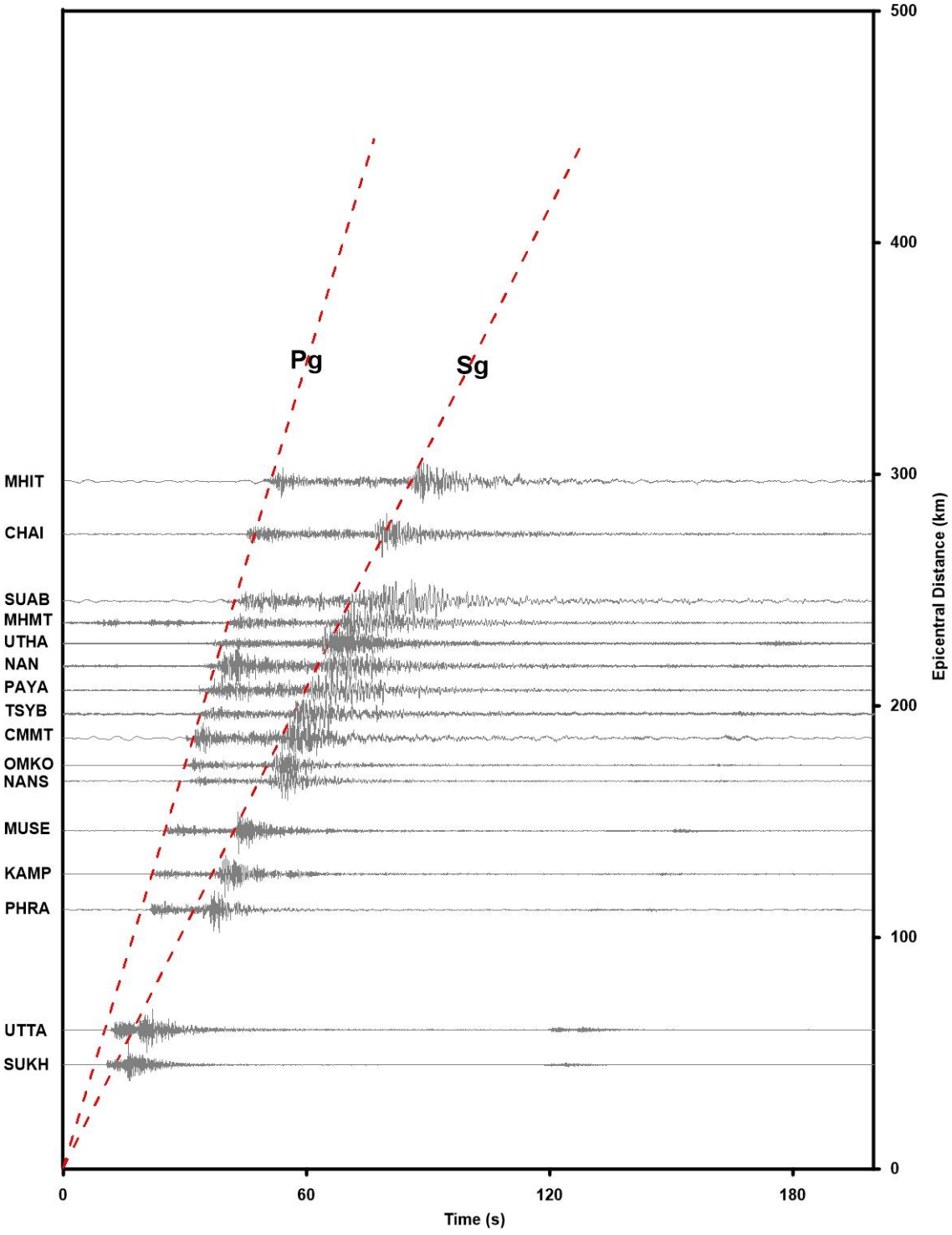

Fig. 4.23. Graph showing the waveforms of M3.6 earthquake in April 2022 detected by TMD velocity stations at differences of epicentral distances.

Table 4.5. The parameters used for determining a focal mechanism of M3.6 earthquake.

No	Station	Network	Epicentral Dist. (km)	Azimuth (°)	Take-off angle (°)
1	SUKH	TM	44.346	265.769	66.5
2	PHIT	TM	53.080	132.483	66.0
3	UTTA	TM	59.526	64.211	65.7
4	LPSP	TM	84.605	298.635	63.5
5	PHRA	TM	111.402	9.883	60.7
6	LAMP	TM	120.663	338.700	59.5
7	KHOB	TM	122.305	61.956	59.5
8	KAMP	TM	126.785	205.992	58.6
9	PBKT	TM	143.092	136.704	54.6
10	MUSE	TM	145.326	234.622	54.6
11	LOEI	TM	167.165	89.867	49.5
12	NANS	TM	167.207	25.888	49.5
13	HOTB	TM	169.929	296.650	48.8

In this study, focal mechanism of M3.6 Uttaradit earthquake was determined using first motion polarity technique together with the waveforms recorded by TMD seismic stations surrounding earthquake epicenter for evaluating movement of fault rupture in all directions, 13 velocity seismic stations of TMD were able to clearly detect waveforms of this event that the obtained parameters were sufficient to calculate the focal mechanism in this study. The results reveal various solutions of strike, dip, and rake directions representing Normal, Normal right-lateral oblique, and Normal left-lateral oblique faulting in beachball diagram (Fig. 4.24 and Table 4.6). In order to constrain focal mechanism solution, the lying of seismogenic faults in the region was compared to the possible solutions indicating Normal right-lateral oblique with direction of strike 222.22, dip 52.84 and rake -115.41 was the most reasonable solution. Consequently, seismic data recorded surrounding earthquake epicenter were necessary in order to constrain focal mechanism solutions and represent exactly the tectonic activity and movements of active faults in the region.

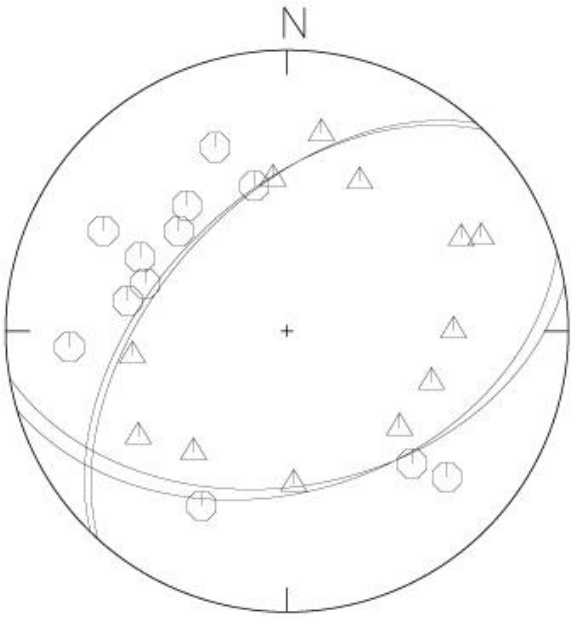

Fig. 4.24. Diagram showing all of probable solutions (black lines) of focal mechanisms of the M3.6 earthquake was analyzed with up and down polarities of waveforms (circle and triangle symbols, respectively) detected by TMD seismic network.

Table 4.6. Example of probable parameters revealing directions of fault rupture movements and types of focal mechanism of M3.6 Uttaradit earthquake in this study.

No.	Strike (°)	Dip (°)	Rake (°)	Fault type
1	73.71	42.27	-67.37	Normal left-lateral oblique
2	224.32	51.62	-109.28	Normal
3	80.41	43.96	-60.48	Normal left-lateral oblique
4	222.22	52.84	-115.41	Normal right-lateral oblique

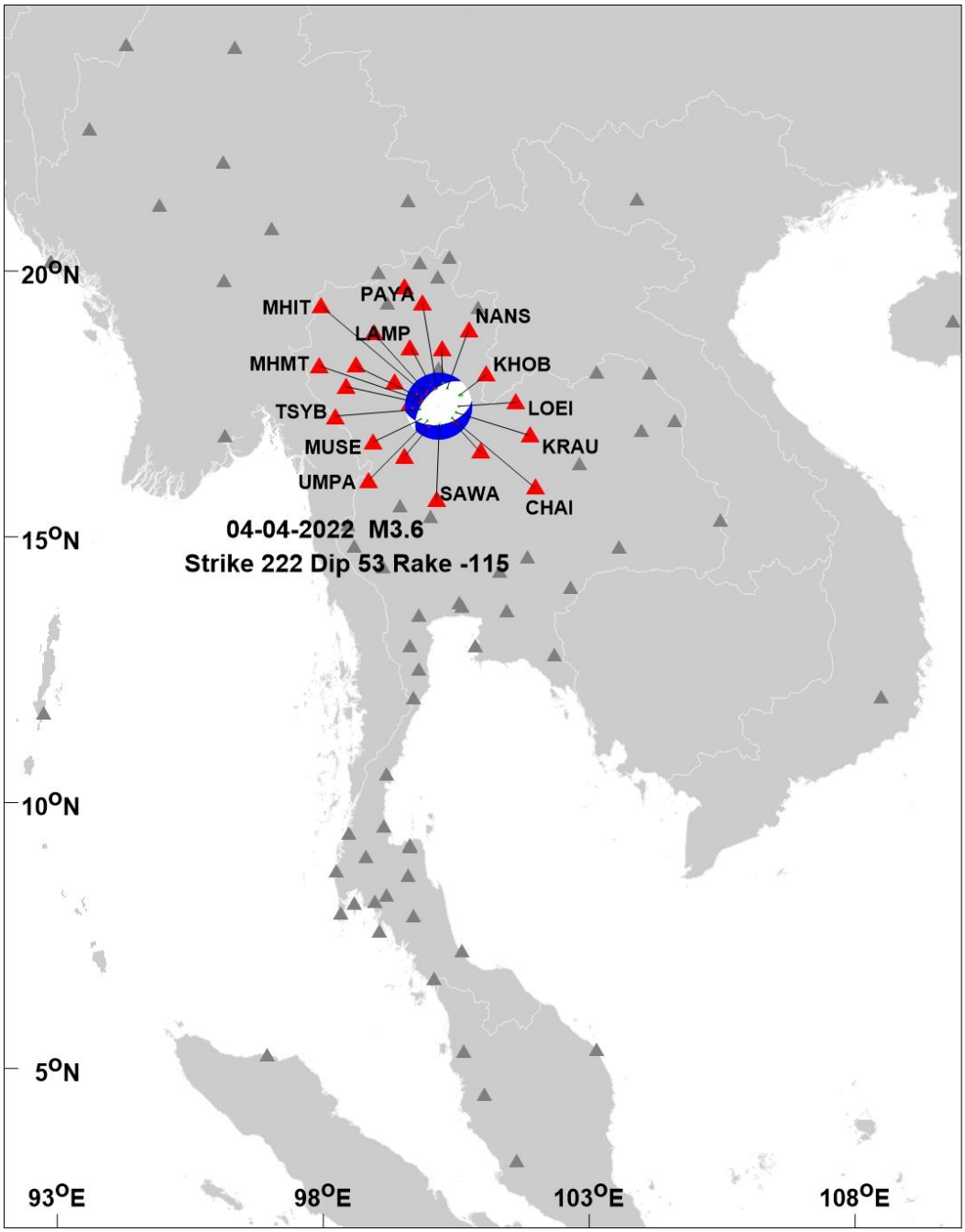

Fig. 4.25. Map showing determination of focal mechanism of M3.6 earthquake according to the first motion polarities of up and down (blue and white zones, respectively) obtained from the velocity seismic stations of TMD (red triangles).

With regard to the application of TMD seismic network, the peak ground acceleration (PGA) of the earthquake with magnitude of 3.6 in Thailand were determined in this study that the nearest accelerograph station of TMD is away from earthquake epicenter approximately 44 km that can clearly detect the waveforms of this event with PGA of 0.02%g revealing the highest shaking level recorded in Thailand. However, the PGA data closer than 40 km from the earthquake epicenter, were not able to be recorded by the accelerograph stations of TMD leading to insufficient data for estimating the attenuation of ground shaking within the close distance from the earthquake epicenter. Therefore, the attenuation model needs to be used for estimating the earthquake shaking level covering all of the areas (Fig. 4.26). According to M3.6 earthquake in Thailand, the acceleration data recorded by TMD stations were compared statistically with the 5 attenuation models. The results indicated that the observed data were mostly corelated with the attenuation model of Chiou and Youngs (2008) at the RMS = 1.11 (Fig. 4.27 and Table 4.7) and this attenuation model also associated with the felt reports form the earthquake event in Thailand (Fig. 4.26).

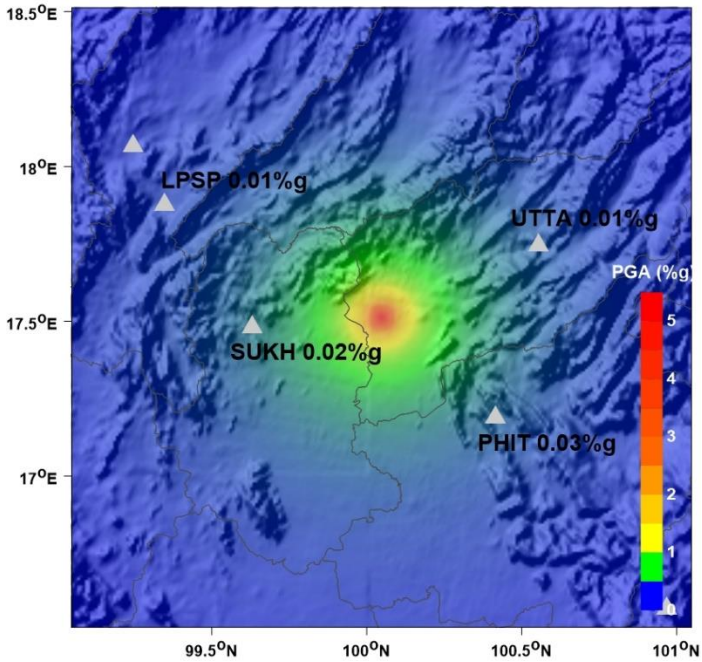

Fig. 4.26. Map showing the shaking levels of M3.6 earthquake in Thailand calculated from attenuation model of Chiou and Youngs (2008) compared with the observed data from TMD seismic stations (white triangle) in the areas.

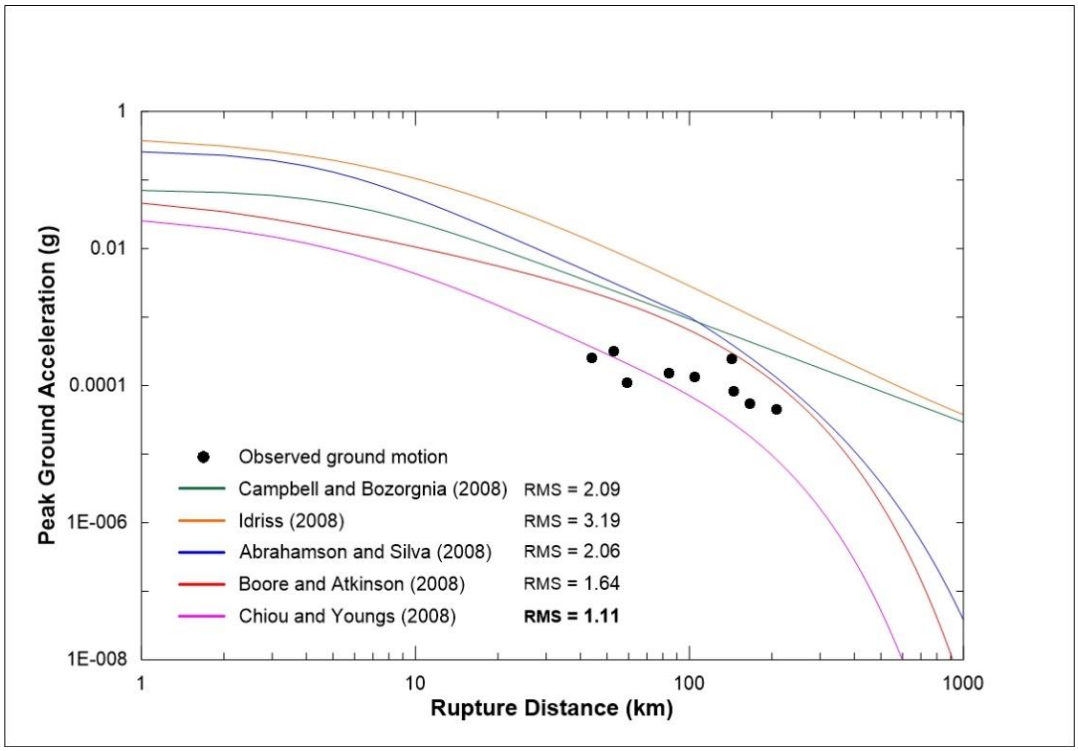

Fig. 4.27. Graph showing the attenuation of peak ground accelerations (PGA) of M3.6 earthquake in Thailand calculated from 5 attenuation models (colored lines) that were compared with the observed PGA (black circles) from TMD stations.

Table 4.7 The peak ground acceleration (PGA) data recorded by seismic stations of TMD from the earthquake event of M3.6 in Thailand.

No.	Stn.	Lon. (°)	Lat. (°)	Type	Dist. (km)	PGA (cm/s^2)		
						EW	NS	V
1	SUKH	99.631	17.482	Surface	44.27	0.2452	0.2612	0.1957
2	PHIT	100.417	17.189	Surface	53.01	0.2987	0.3076	0.2882
3	UTTA	100.554	17.744	Surface	59.38	0.0939	0.0671	0.1092
4	LPSP	99.346	17.875	Borehole	84.39	-	0.1486	0.0623
5	SOEA	99.246	18.066	Surface	104.57	0.1723	0.1296	0.1210
6	PBKT	100.969	16.574	Surface	143.00	0.2425	0.2089	0.0888
7	MUSE	98.935	16.752	Borehole	145.27	0.0814	0.0613	0.0513
8	LOEI	101.624	17.509	Surface	166.87	0.0449	0.0534	0.0308
9	UMPA	98.860	16.026	Surface	208.02	0.0443	0.0357	0.0164

- The earthquake with magnitude 5.4 in Myanmar

In order to investigate the application of seismic network of TMD for determining focal mechanism of the earthquake outside Thailand, M5.4 earthquake in Myanmar was employed in this study. The waveforms were detected by seismic stations of TMD only in the southern parts of the earthquake epicenter where are the areas of Thailand while the northern, western and eastern parts are the areas outside the country that there are only the stations from other networks (Fig. 4.28 and 4.29). Therefore, using only the data from TMD stations to determine focal mechanism by polarity technique, may cause the missing data in the northern, western and eastern parts of epicenter leading to misinterpretation of tectonic activity in the areas.

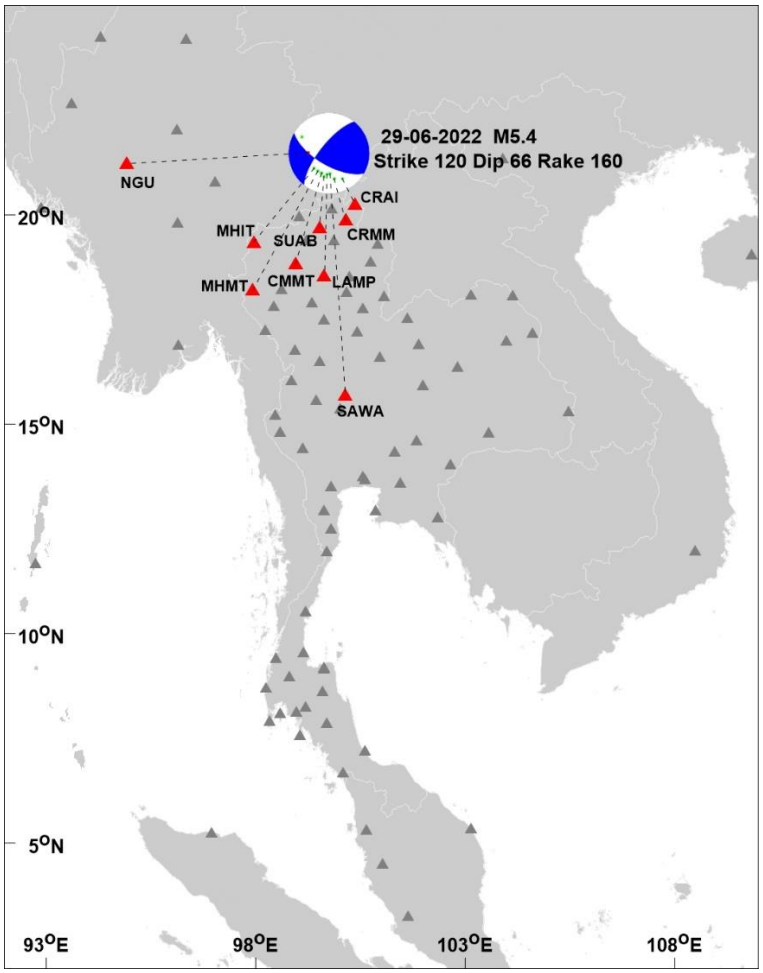

Fig. 4.28. Map showing determination of focal mechanism of M5.4 in Myanmar according to the first motion polarities of up and down (blue and white zones, respectively) obtained from the velocity seismic stations of TMD (red triangles).

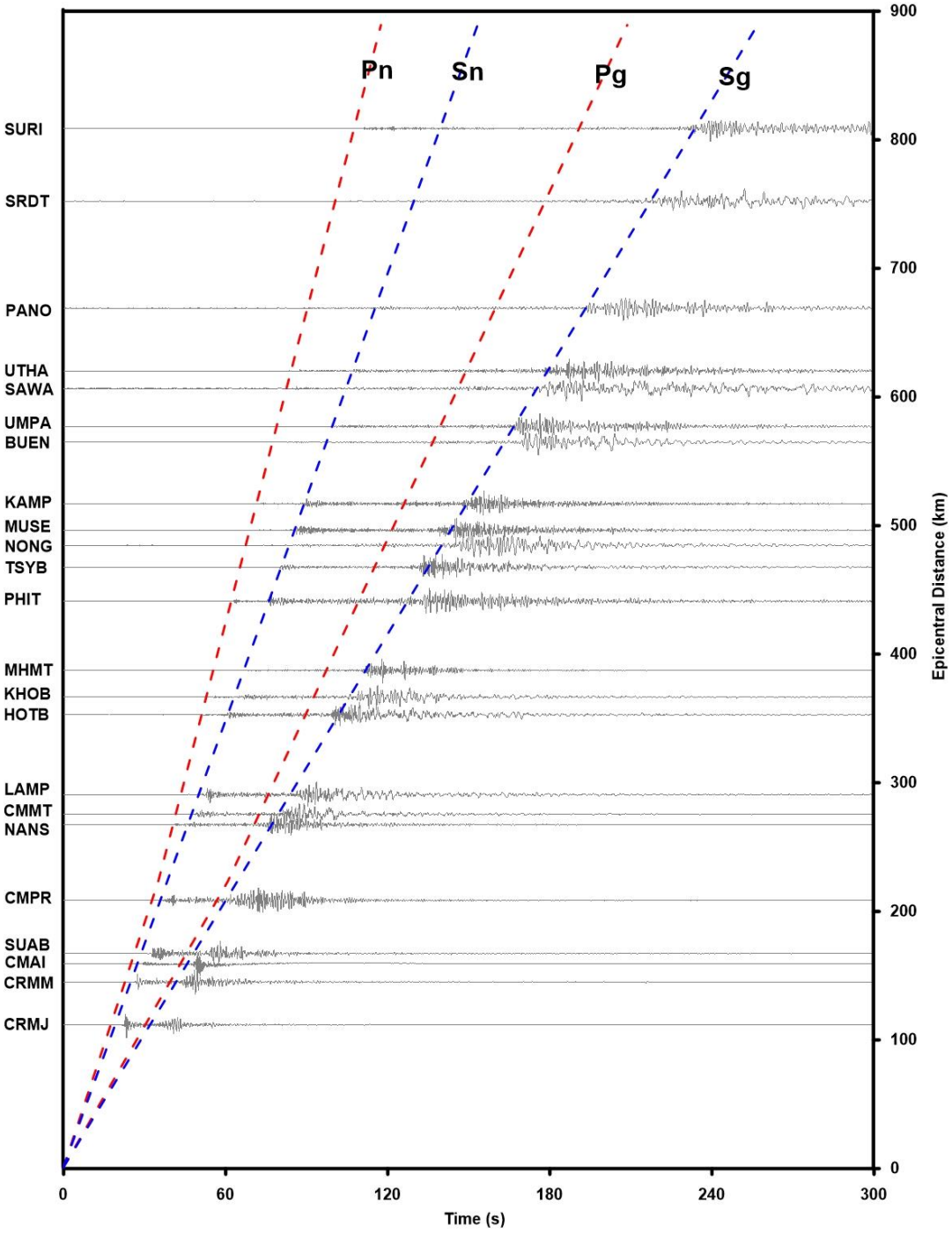

Fig. 4.29. Graph showing the waveforms of M5.4 earthquake in Myanmar detected by TMD seismic stations at the differences of epicentral distances with the phase identification obtained from the global velocity model (dash line).

At present, although the accelerograph stations of TMD cover the whole of seismic source zones in Thailand, the stations were so far from each other resulting a distribution of observed PGA were not dense covering the area of earthquake epicenter. Consequently, the attenuation models of earthquake ground shaking were necessary for analyzing spatially the shaking level of the earthquake event. In this study, the acceleration data recorded by seismic station of TMD, were compared with the 5 attenuation models, i.e., i) Campbell and Bozorgnia (2008), ii) Idriss (2008), iii) Abrahamson and Silva (2008), iv) Boore and Atkinson (2008), and v) Chiou and Youngs (2008) as demonstrated in Fig 4.30. Theoretically, the calculated PGA data mainly depend on magnitude, epicentral distance and focal mechanism of earthquake. In this study, the calculated PGA from attenuation model were statistically compared with the observed PGA from TMD accelerograph stations (Table 4.8) in order to determine attenuation model was most appropriate to the observed PGA in the region. This study indicated that the PGA obtained from attenuation model of Abrahamson and Silva (2008) were mostly correlated with the observed PGA from accelerograph stations of TMD at Root Mean Square Error (RMS) of 0.96 (compared to the other attenuation models). So, this attenuation model was regarded as a suitable model for the 5.4 Myanmar earthquake in this study.

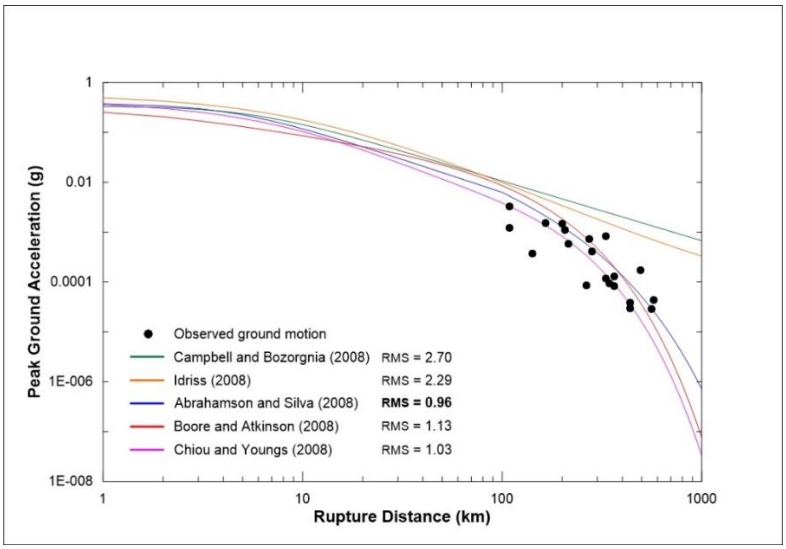

Fig. 4.30. Graph showing the attenuation of peak ground accelerations (PGA) of M5.4 Myanmar calculated from 5 various attenuation models (colored lines) that were compared with the observed PGA (black circles) from TMD stations.

Table 4.8 The peak ground acceleration (PGA) data recorded by seismic stations of TMD from the earthquake event of M5.4 in Myanmar.

No.	Stn.	Lon. (°)	Lat. (°)	Type	Dist. (km)	PGA (cm/s^2)		
						EW	NS	V
1	CRMJ	99.809	20.127	Borehole	110.43	1.0624	0.8596	1.2070
2	CRAI	100.373	20.229	Surface	111.22	3.2358	2.7743	0.8174
3	CRMM	100.154	19.849	Borehole	143.74	0.3628	0.2550	0.2358
4	SUAI	99.535	19.661	Surface	165.89	1.5098	1.6395	0.7972
5	PAOA	99.507	19.347	Surface	200.59	1.4472	1.3493	0.5269
6	CMPR	99.202	19.366	Borehole	207.23	1.0496	1.0790	0.5626
7	THUA	100.883	19.408	Surface	216.79	0.5763	0.5578	0.3972
8	NANS	100.742	18.864	Borehole	266.11	0.0548	0.0669	0.0844
9	CMMT	98.944	18.814	Surface	274.23	0.6583	0.4676	0.7074
10	MHIT	97.963	19.315	Surface	283.81	0.5130	0.3957	0.2258
11	MAEC	98.373	18.497	Surface	331.61	0.6603	0.8085	0.3278
12	PHRS	100.162	18.129	Borehole	333.21	0.1138	0.0953	0.0543
13	SOEA	99.246	18.066	Surface	345.48	0.1301	0.0933	0.0927
14	LPSP	99.346	17.875	Borehole	364.48	-	0.1265	0.1001
15	KHOK	101.069	18.026	Surface	365.38	0.1125	0.0812	0.0620
16	PHIT	100.417	17.189	Surface	439.85	0.0245	0.0290	0.0250
17	LOEI	101.624	17.509	Surface	441.05	0.0365	0.0376	0.0241
18	MUSE	98.935	16.752	Borehole	495.07	0.1686	0.0888	0.0334
19	BUEN	104.131	18.045	Borehole	563.43	0.0331	0.0278	0.0185
20	UMPA	98.860	16.026	Surface	575.79	0.0429	0.0375	0.0263

Based on the suitable attenuation model of Abrahamson and Silva (2008), the PGA were calculated at each grid node with grid spacing of 0.25 degerees covering approximately 300 km from the earthquake epicenter that a focal mechanism solution obtained earlier was also employed in this study. The result indicate the intensity of erathquake ground shaking with PGA values over than 1 %g (weak level) within the area of 200 km-radius from epicenter including some areas in the northern part of Thailand corresponding to the felt report in the area as demonstrated in Fig. 4.31.

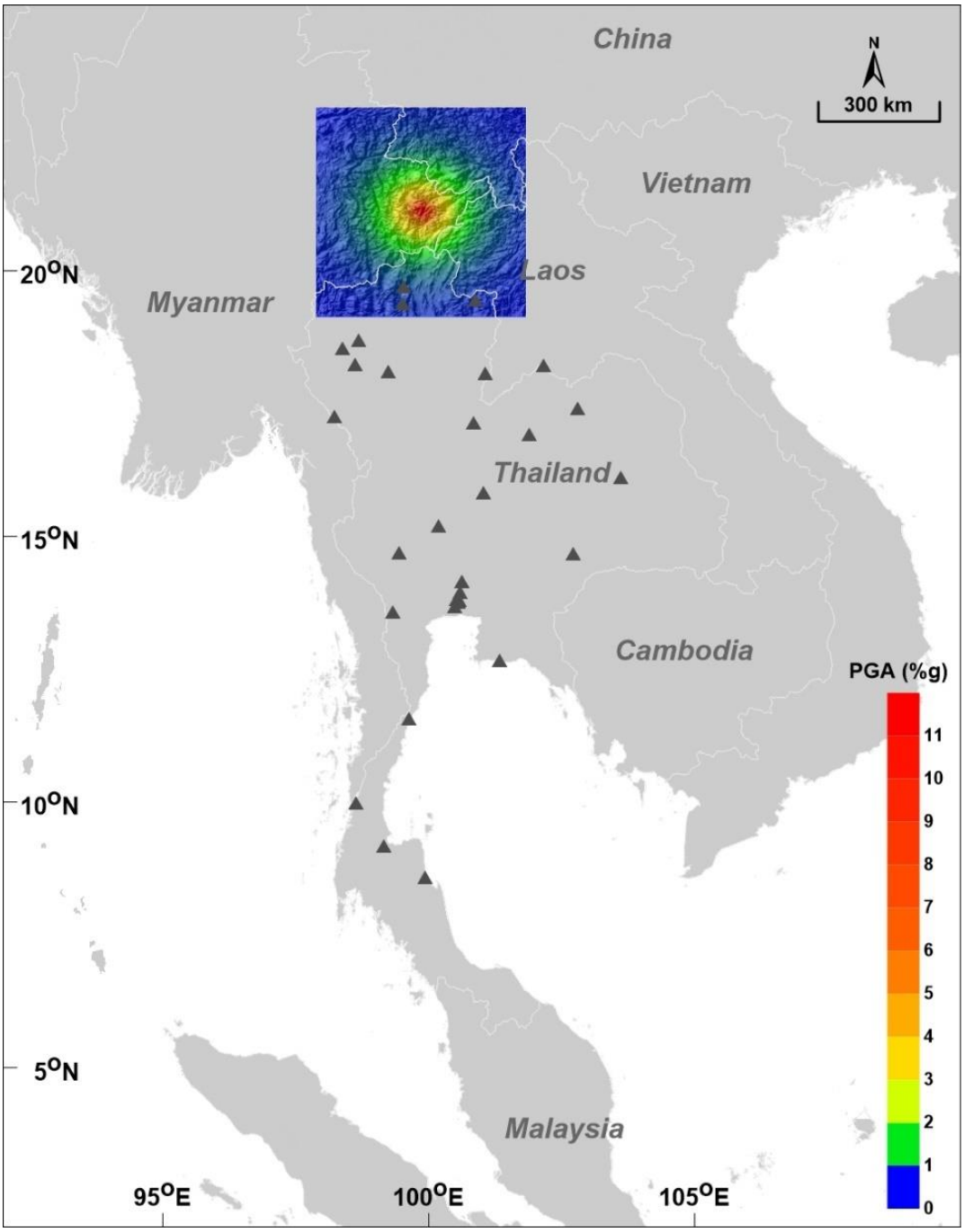

Fig. 4.31. Map showing spatial distribution of PGA (colored zones) obtained from model with the shaking levels surrounding the epicenter of M5.4 earthquake.

With regard to the application of TMD seismic network, the peak ground acceleration (PGA) of the M5.4 Myanmar was determined in this study that nearest accelerograph station of TMD is away from earthquake epicenter approximately 110 km, was able to clearly detect waveforms of this event with PGA of 0.12%g revealing the highest ground shaking recorded in Thailand. However, PGA data closer than 110 km from the earthquake epicenter, were not able to be recorded by the accelerograph stations of TMD leading to the insufficient data for estimating the attenuation of ground shaking within the close distance from the epicenter. So, the attenuation model should be used in this study (Table 4.9). Although this event located outside Thailand, the earthquake has a large magnitude, the ground shaking can be detected obviously in several areas in Thailand by seismic stations of TMD as illustrated in Fig. 4.32.

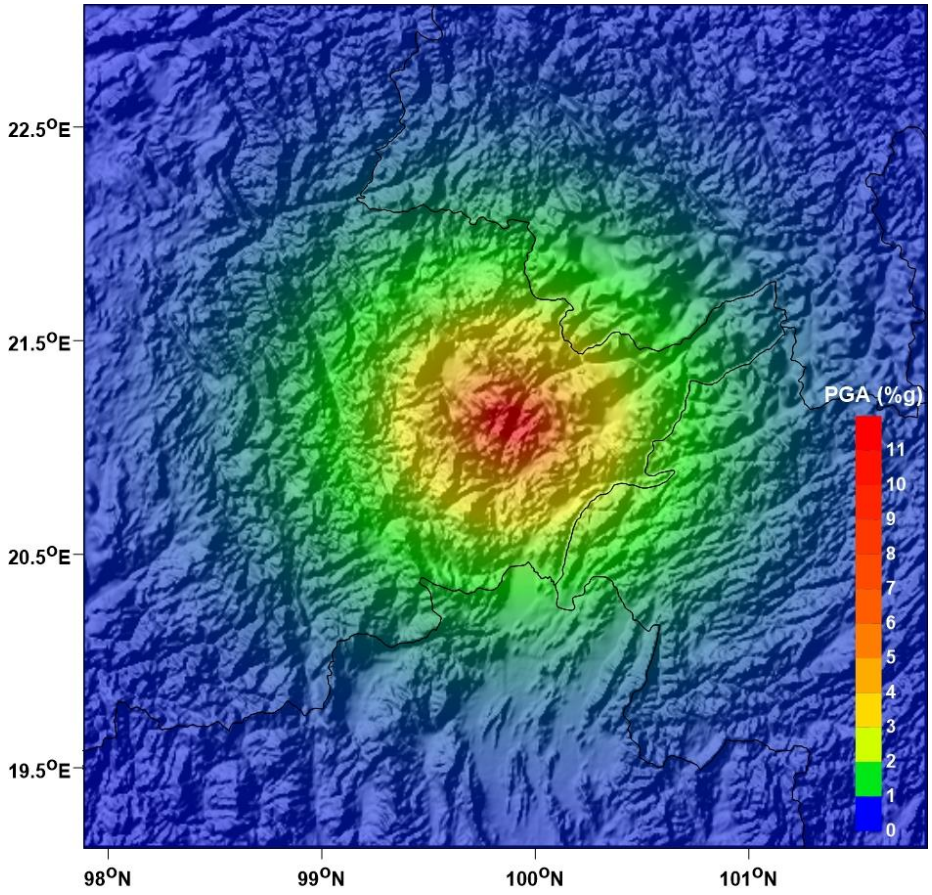

Fig. 4.32. Map showing the distribution of earthquake ground shaking of M5.4 earthquake with intensity levels (colored zones) simulated from suitable attenuation model of Abrahamson and Silva (2008).

Table 4.9. Peak ground accelerations (PGA) of M5.4 Myanmar earthquake calculated from 5 attenuation models varied with the rupture distance.

Rupture Dist. (km)	Peak Ground Acceleration (g)				
	Model I	Model II	Model III	Model IV	Model V
1	0.371821	0.332415	0.36371	0.49429	0.253538
2	0.340653	0.315193	0.303814	0.425772	0.205804
3	0.300843	0.291145	0.257169	0.371176	0.171655
4	0.260954	0.264502	0.220203	0.326901	0.14795
5	0.225277	0.238281	0.190463	0.290452	0.130694
6	0.195014	0.214104	0.166216	0.260052	0.11753
7	0.169904	0.192592	0.146216	0.234406	0.1071
8	0.149195	0.173795	0.129545	0.212554	0.098588
9	0.132079	0.157502	0.115521	0.193766	0.091476
10	0.117847	0.143407	0.103622	0.177484	0.085421
20	0.051411	0.070261	0.044284	0.08877	0.052121
30	0.030577	0.044272	0.02484	0.054372	0.037158
40	0.021015	0.031626	0.016218	0.037213	0.028258
50	0.01568	0.024297	0.011605	0.027323	0.022266
60	0.012333	0.019567	0.008797	0.021057	0.017945
70	0.010063	0.016284	0.006924	0.016814	0.014688
80	0.008435	0.013885	0.005591	0.013795	0.01216
90	0.007219	0.012063	0.004595	0.011562	0.010155
100	0.00628	0.010634	0.003825	0.00986	0.008539
150	0.002626	0.006544	0.001699	0.005298	0.003838
200	0.001283	0.004635	0.00082	0.003398	0.001841
250	0.000683	0.003547	0.000411	0.002409	0.000915
300	0.000384	0.00285	0.00021	0.001822	0.000466

CHAPTER V
CONCLUSION

According to analysis of TMD seismic network during January - June 2022, the obtained results lead to the conclusion as follows;

1. The Most accuracy of TMD seismic network for locating the seismic events in Thailand was approximately 3.1 km from the seismic source.
2. The highest precision covered zone of northern and western parts of Thailand with the comparatively least RMS residual of approximately 0.4 sec.
3. The zones of Red river fault indicate the comparatively low precisions of TMD seismic network with RMS residual approximately 0.63 sec.
4. The seismic network of TMD covered appropriately in the northern part, particularly in Chiang Rai and Lampang provinces with best azimuthal gap less than 100 degrees.
5. The zone of Nan province reveals the bad covering of TMD seismic network with the azimuthal gap over 200 degrees.
6. The automatic phase picking of TMD seismic network indicates the residual of 0 -3.2 sec with the dislocations of events up to 25.2 km.
7. The limitation of TMD network indicates the earthquakes within Thailand, particularly northern and western parts were detected completely with the magnitude over 2.8.
8. The earthquakes outside Thailand with the magnitudes below 4.8 were not detected and recorded completely by the seismic network of TMD.
9. The most of seismic stations of TMD illustrate ambient noise levels within boundary of the global noise model representing waveforms recorded by TMD seismic network were not affected by background noise around the sites.
10. Application of TMD network indicate that the epicenter of M3.6 Uttaradit earthquake was surrounded by the seismic stations of TMD. Therefore, focal mechanism of this event can be calculated effectively in this study.

11. M3.6 Uttaradit earthquake was located away from the accelerograph stations of TMD resulting the data of ground shaking cannot be recorded within 40 km from epicenter.
12. An attenuation model of Chiou and Youngs (2008) was suitable for simulating ground shaking of M3.6 Uttaradit earthquake that the model correlated with observed data significantly at the lowest RMS of 1.11 (Compared to other models in this study).
13. An attenuation model of Abrahamson and Silva (2008) was suitable for simulating the ground shaking of M5.4 Myanmar earthquake that the model correlated with observed data significantly at the lowest RMS of 0.96 (Compared to other models in this study).
14. The seismic events in northern Thailand can be discriminated between mining blast and earthquake reasonably using location, depth and characteristic of the waveform.
15. According to the results obtained from this study, the earthquakes affected Thailand with M>4.0 were still detected and recorded effectively by the seismic network of TMD during January - June 2022.

REFERENCES

Abrahamson, N.A. and Silva, W.J., 2008. Summary of the Abrahamson & Silva NGA ground-motion relations. Earthquake Spectra, 24(S1), 67-97.

Arai, N. and Yosida, Y., 2004. Discrimination by short-period seismogram. International Institute of Seismology and Earthquake Engineering, Building Research Institute (IISEE), Lecture Note, Global Course, Tsukuba, 10p.

Asten, M.W. and Henstridge, J.D., 1984. Array estimators and the use of microseisms for reconnaissance of sedimentary basins. Geophysics, 49(11), 1828-2078.

Bard, P.Y., Bonnefoy-Claudet, S., and Cotton, F., 2003. SESAME: Site effects assessment using ambient excitations. Final report, WP08, Nature of noise wavefield. European Commission.

Belinic, T. and Markusic, S., 2017. Empirical criteria for the accuracy of earthquake locations on the Croatian territory. Geofizika, 34.

Bondar, I., Myers, S.C., Engdahl, E.R., Bergman, E.A., 2004. Epicentre accuracy based on seismic network criteria. Geophysical Journal International, 156, 483-496.

Boore, D.M. and Atkinson, G.M., 2008. Ground motion prediction equations for the average horizontal component of PGA, PGV, PGD, and 5%-damped PSA at spectral periods between 0.01 and 10.0 s. Earthquake spectra, 24(S1), 99-138.

Burtin, A., Bollinger, L., Vergne, J., Cattin, R., and Nabelek, J.L., 2008. Spectral analysis of seismic noise induced by rivers: A new tool to monitor spatiotemporal changes in stream hydrodynamics. Journal of Geophysical Research: Solid Earth, 113.

Campbell, K.W. and Bozorgnia, Y., 2008. NGA ground motion model for the geometric mean horizontal component of PGA, PGV, PGD, and 5%-damped linear elastic response spectra for periods ranging from 0.01 to 10 s. Earthquake Spectra, 24(S1), 139-171.

Charusiri, P., Rhodes, B.P., Saithong, P., Kosuwan, S., Pailoplee, S., Wiwegwin, W., Doarerk, V., Hinthong, C., and Klaipongpan, S., 2007. Regional tectonic setting and seismicity of Thailand with reference to reservoir construction. International

Conference on Geology of Thailand: Towards Sustainable Development and Sufficiency Economy.

Chatelain, J.L., Roecker, S.W., Hatzfeld, D., and Molnar, P., 1980. Microearthquake seismicity and fault plane solutions in the Hindu Kush Region and their tectonic implications. Journal of Geophysical Research: Solid Earth, 85(B3).

Chiou, B.S. and Youngs, R.R., 2008. An NGA model for the average horizontal component of peak ground motion and response spectra. Earthquake spectra, 24(S1), 173-215.

Dahle, A., Climent, A., Taylor, W., Bungum, H., Santos, P., Ciudad Real, M., Lindholm, C., Strauch, W., and Segura, F., 1995. New spectral strong motion attenuation models for Central America. Proceedings of the fifth International Conference on Seismic Zonation, October 17-19, Nice, France.

Fisher, R.A., 1936. The use of multiple measurements in Taxonomic problems. Annals of Eugenics, 7(2), 179-188.

Gardner, J.K. and Knopoff, L., 1974. Is the sequence of earthquakes in Southern California, with aftershocks removed, Poissonian?. Bulletin of the Seismological Society of America, 64(1), 363-367.

Geiger, L., 1912. Probability method for the determination of earthquake epicenters from the arrival time only. Bulletin of Saint Louis University, 8, 60-71.

Gitterman, Y. and Shapira, A., 1993. Spectral discrimination of underwater explosions. Israel Journal Earth Science, 42, 37-44.

Gupta, I.D., 2002. The state of the art in seismic hazard analysis. ISET Journal of Earthquake Technology, 39(428), 311-346.

Gutenberg, B., 1958. Caustics produced by waves through the earth's core. Geophysical Journal International, 1(3), 238-248.

Gutenberg, B. and Richter, C.F., 1944. Frequency of earthquakes in California. Bulletin of Seismological Society of America, 34, 185-188.

Habermann, R. E., 1987. Man-made changes of Seismicity rates. Bulletin of the Seismological Society of America, 77, 141-159.

Hsiao, N.C., Lin, T.W., Hsu, S.K., Kuo, K.W., Shin, T.C., Leu, P.L., 2013. Improvement of

earthquake locations with the Marine Cable Hosted Observatory (MACHO) offshore NE Taiwan. Marine Geophysical Research, DOI 10.1007/s11001-013-9207-3.

Hwang, H. and Huo, J.R., 1997. Attenuation relations of ground motion for rock and soil sites in eastern United States. Soil Dynamics and Earthquake Engineering, 16(6), 363-373.

Idriss, I.M., 2008. An NGA empirical model for estimating the horizontal spectral values generated by shallow crustal earthquake. Earthquake Spectra, 24, 217-242.

Ishimoto, M. and Iida, K., 1939. Observations sur les seismes enregistres Par le microsismographe construit dernierement. Bulletin of the Earthquake Research Institute, University of Tokyo, 17, 443-478.

Kazmer, M., Sanittham, K., Charusiri, P., and Pailoplee, S., 2011. Archaeoseismology of the AD 1545 earthquake in Chiang Mai, Northern Thailand. In: 2nd INQUA-IGCP-567 International Workshop on Active Tectonics, Earthquake Geology, Archaeology and Engineering, Corinth, Greece, 1-4.

Kekovali, K., Kalafat, D., and Deniz, P. 2012. Spectral discrimination between mining blasts and natural earthquake: Application to the vicinity of Tuncbilek mining area, Western Turkey. Journal of the Physical Sciences, 7(35), 5339-5352.

Kissling, E., 1988. Geotomography with local earthquake data. Review of Geophysics, 26(4).

Konstantinou, K.I., 2018. Estimation of optimum velocity model and precise earthquake locations in NE Aegean: Implications for seismotectonics and seismic hazard. Journal of Geodynamics, 121, 143-154.

Lindung, Z.M., Suched, L., and Tetsuo, T., 2018. Analysis of seismic ground response caused during strong earthquake in Northern Thailand. Soil Dynamics and Earthquake Engineering, 114, 113-126.

Marsan, D., 2003. Triggering of seismicity at short timescales following Californian earthquakes. Journal of Geophysical Research: Solid Earth, 108.

McNamara, D.E. and Buland, R.P., 2004. Ambient noise levels in the Continental United States. Bulletin of the Seismological Society of America, 94(4), 1517-1527.

Milne, J., 1886. Earthquake and other earth movements. Appelton, New York.

Pailoplee, S., 2014. Earthquake activities along the strike-slip fault system on the Thailand-Myanmar border. Terrestrial, Atmospheric and Oceanic Sciences, 25(4), 483-490.

Pailoplee, S., Pantarak, C., and Vichai, C., 2013. Earthquake activities in the Thailand-Laos-Myanmar border region: A statistical approach. Terrestrial, Atmospheric and Oceanic Sciences, 24(4), 721-730.

Pailoplee, S., Sugiyama, Y., and Charusiri, P., 2009. Deterministic and probabilistic seismic hazard analyses in Thailand and adjacent areas using active fault data. Earth Planets Space, 61, 1313-1325.

Pavlis, G., 1986. Appraising earthquake hypocenter location errors: A complete, practical approach for single-event locations. Bulletin of the Seismological Society of America, 76(6), 1699-1717.

Peterson, J., 1980. Preliminary observations of noise spectra at the SRO and ASRO stations. U.S. department of interior geological survey, open-file report, 80-992.

Peterson, J., 1993. Observations and modeling of seismic background noise. U.S. department of interior geological survey, open-file report, 93-322.

Reid, H.F., 1910. The Mechanics of the Earthquake, The California Earthquake of April 18, 1906. Report of the State Investigation Commission 2, Carnegie Institution of Washington, Washington, D.C.

Rocca, M.L. and Galluzzo, D., 2019. Focal mechanisms of recent seismicity at Campi Flegrei, Italy. Journal of Volcanology and Geothermal Research, 388.

Rydelek, P.A. and Sacks, I.S., 1989. Testing the completeness of earthquake catalogues and the hypothesis of self-similarity. Nature, 337, 251-253.

Snoke, J.A., Munsey, J.W., Teague, A.G., and Bollinger, G.A., 1984. A program for focal mechanism determination by combined use of polarity and SV-P amplitude ratio data. Earthquake Notes, 55(3), 15.

Sukrungsri, S. and Pailoplee, S., 2016. Precursory seismic quiescence along the Sumatra-Andaman Subduction Zone: Past and present. Journal of seismology, DOI 10.1007/s10950-016-9602.

Sukrungsri, S., Promsuk, C., Kamjudpai, C., and Kirtsaeng, S., 2019. Discrimination of Seismic Events in Lampang Province: A Complexity Approach. Proceeding on the 5th EnvironmentAsia International Conference, 13-15 June 2019, The Empress Hotel, Chiang Mai, Thailand, P. 85.

Taylor, D. A., Snoke, J.A., Sacks, I.S., and Takanami, T., 1990. Nonlinear frequency magnitude relationship for the Hokkaido corner, Japan. Bulletin of the Seismological Society of America, 80, 340-353.

Toro, G.R., Abrahamson, N.A., and Schneider, J.F., 1997. Model of strong ground motions from earthquake in Central and Eastern North America: Best estimates and uncertainties. Seismological Research Letters. 68(1), 41-57.

Trnkoczy, A., Bormann, P., Hanka, W., Holcomb, L.G., and Nigbor, R.L., 2002. Site selection, preparation and installation of seismic station, in IASPEI New Manual of Seismological Observatory Practice, 1(7), 1-106.

Weber, B., Becker, J., Hanka, W., Heinloo, A., Hoffmann, M., Kraft, T, Pahlke, D., Reinhardt, J., Saul, J., Thoms, H., 2007. SeisComP3 - automatic and interactive real time data processing. Geophysical Research Abstracts, 9, 09219.

Wiemer, S. and Wyss, M., 2000. Minimum magnitude of complete reporting in earthquake catalogs: Examples from Alaska, the Western United States, and Japan. Bulletin of the Seismological Society of America, 90, 859-869.

Willmore, P.L., 1979. Manual of seismological observatory practice, Report SE-20, World Data Center A for Solid Earth Geophysics, US Dep. Of Commerce, NOAA. Boulder, Colorado.

Wilson, D., Leon, J., Aster, R., Ni, J., Schlue, J, Grand, S., Semken, S., Baldridge, S., and Geo, W., 2002. Broadband seismic background noise at temporary seismic stations observed on a regional scale in the southwestern united states. Bulletin of the Seismological Society of America, 92(8), 3335-3342.

Woessner, J. and Wiemer, S. 2005. Assessing the quality of earthquake catalogues: Estimating the magnitude of completeness and its uncertainty. Bulletin of the Seismological Society of America, 95, 684-698.

Yilmaz, S., Bayrak, Y., and Cinar, H., 2012. Discrimination of earthquake and quarry blasts in the eastern Black Sea region of Turkey. Journal of Seismology, 17: 721-734.

Young, C.J., Chael, E.P., Withers, M.M., and Aster, R.C., 1996. A comparison of the high-frequency (>1Hz) surface and subsurface noise environment at three sites in the United States. Bulletin of the Seismological Society of America, 86(5), 1516-1528.